博士論文

A Study of Image Sensors with In-Pixel Selective-Signal Detection

（画素回路内信号選択機能を有するイメージセンサに関する研究）

A Dissertation
Submitted to the Department of
Electrical Engineering and Information Systems,
the University of Tokyo
in Partial Fulfillment of the Requirements
for the Degree of Doctor of Philosophy

Supervisor: Professor Makoto Ikeda

37-137066
金 雄鉉

DEPARTMENT OF
ELECTRICAL ENGINEERING AND INFORMATION SYSTEMS,
THE UNIVERSITY OF TOKYO

Nov 30th, 2018

Abstract

Active sensing using image sensors are widely used in various applications, including three dimensional range-finding for mobile devices and automobiles. Traditional image sensors for active sensing have mainly four challenges: temporal resolution, spatial resolution, dynamic range, and power consumption. Moreover, in recent applications using active sensing, the instrument security has been a big issue with the security of the measurement system. Many studies and researches have shown remote attacks on active sensing based system such as LiDAR and ToF, and proposed software and hardware countermeasures that improve resilience against these attacks. These studies and researches mainly have aimed at system-level or software-level solutions. However, these options require additional space, demand additional processing capacities, and increase cost, which is problematic in low cost-driven applications. The sensor-level approaches and solutions are required in these applications. The image sensors with selective-signal detection can be one of the solutions to the problems. The requirements for the image sensors are wide modulation frequency range and wide dynamic range considering various applications under strong background light.

This thesis presents a new approach for an image sensor that can detect the selective signal while suppressing the background light for specific applications such as 3-D range-finding with modulated and coded light. This thesis focuses on the implementation of selective-signal detection imaging systems. Two types of image sensors are proposed and implemented to

improve the reliability of the measurement while suppressing the background light. And, active optical sensing with the coded light is proposed.

First, we propose an image sensor with in-pixel selective-charge-subtraction circuits for selective light detection under strong background light. For the detection of selective-signal light from incident light, an in-pixel demodulation pixel is employed. And Adaptive Charge Unit (ACU) in the pixel circuit is introduced to prevent the saturation problem by the background light. Demodulation pixel and a charge injection mode suppression circuit using floating diffusion (FD) level sensing circuit for background light realize high signal selectivity and wide dynamic range. The image sensor has been designed, fabricated, and successfully measured. The signal selectivity of the image sensor is confirmed from the measurement. The minimum signal to background light ratio (SBR), the dynamic range, and the maximum modulation frequency of the image sensor are -18.8 dB, 89.3 dB, 50 kHz respectively in measurement. The image sensor achieved wider modulation frequency range than previous works.

Second, we propose an image sensor with compensation of background light using a current mirror under strong background light. To achieve selective-light detection, an in-pixel demodulation pixel are employed. Current mirror circuit in pixel circuit is introduced to duplicate the background light induced photocurrent, and to prevent the saturation problem by compensation of background light induced photocurrent during integration time. Demodulation pixel and a charge injection mode suppression circuit using current mirror circuit realize high signal selectivity and wide dynamic range with less number of transistors in a pixel. Two types of current-duplication-error-reduced pixel circuit are proposed further. The image

sensor has been designed. The signal to background light ratio of dummy-added type, and V_B-separated type are -38.8 dB, and -30.7 dB respectively with dynamic range 94.6 and 92.4 dB in the measurement. The number of transistors in a pixel of dummy-added type, and V_B-separated type are 19, and 15 respectively. All types of pixel circuits achieved better SBR and DR and less number of transistors in a pixel circuit than previous works.

For enhancing instrumental security on the stage of collecting information using an image sensor, active optical sensing with the coded light is proposed. The requirements for the image sensor with coded light are mentioned: (1) constant integration time and (2) unpredictability. The method of bit conversion to generate coded light is proposed. Active optical sensing with coded light is evaluated and the signal selectivity with coded light is obtained as SNR 2.5 dB in same integration time at the case using modulation light. However, the SNR of signal-selectivity decreases by 57.6% from the case using modulated light. It is confirmed that the effect to an image sensor from the coded light is similar to the case using higher modulation frequency than base modulation frequency that is used to generate the coded light.

As can be seen from the above results, the image sensors and active optical sensing schemes with modulated light and coded light realize wide modulation frequency range, wide dynamic range and robust image acquisition systems. We are sure that these results in this thesis, such as two types of image sensors and active optical sensing with modulated light and coded light, can be used for the instrumental security and contribute to the active optical sensing performance and reliability improvements.

Acknowledgments

During my times in the University of Tokyo, I had a great time in my life. I had experienced many things and had learned a lot, and importantly I had an exciting time with my colleagues and friends.

First of all, I would like to thanks the dissertation supervisor, Prof. Makoto Ikeda for his supports, enduring guidance, and encouragement throughout my undergraduate and graduate studies. His passion and knowledge have greatly advanced my knowledge, attitude and philosophy about research. And I have always had his constant support, productive discussion, and many great opportunities. I feel very fortunate to have taken him as my supervisor. And I will forever cherish this experience for my lifetime.

I would like to acknowledge my dissertation committee, Prof. Hiroyuki Morikawa, Prof. Kiyoharu Aizawa, Prof. Masahiro Fujita, Prof. Makoto Takamiya, and Prof. Tetsuya Iizuka, for their invaluable suggestions and comments.

I am grateful to all the current and past members in Asada-Ikeda-Nakura-Iizuka laboratory for their helpful advices, heartful encouragement, comfortable research circumstances and pleasant time.: in particular, Dr. Hiroaki Yoshida, who is currently in Fujitsu Corp., for his valuable advices originated in his exceptional research talent, and indispensable encouragement during my undergraduate year in the laboratory; Prof. Yunkyung Kim, who is currently in Dong-A University, Pusan, Korea, for his friendly talk and many essential advices on my

laboratory life; Dr. Jinmyeong Kim, who is currently in Samsung Electronics Corp., Korea, for his kind advices on my laboratory life and many other activities in the laboratory; Dr. Hiromitsu Awano, who is currently in Osaka University, for his generous support and constructive advices on my research; Dr. Toshiyuki Kikkawa, who is currently in the University of Tokyo, for his generous support and advices on my research and many other activities in the laboratory; Mrs. Uetsuki, for their helpful assistance for my research activities in the laboratory.

I wish to thank all the members of VLSI Design and Education Center (VDEC), the University of Tokyo, for their support in CAD environment and VLSI process technologies. The CAD tools and process technologies used in this study have been provided by Synopsys, Inc., Cadence Design Systems, Inc., Mentor Graphics, Corp., Rohm Corp., and LAPIS with Tohoku University through VDEC.

I also wish to thank the Global Ph.D. Sponsorship from LG Electronics Corp. for the financial support.

I would like to thank my greatest appreciation to my parents, Kyoyang Kim and Youngsoon Kim, to my parent-in-law, Soonok Lee, and to my eldest uncle, Kyocheol Kim, for their constant support and encouragement throughout my life.

Finally, I would like to give my thanks with all my heart and love to my family, Jaeeun(aka LJ), Kwanrok, and Kwanho.

Contents

List of Figures

List of Tables

Chapter 1

Introduction

1.1 Applications based on active optical sensing

Active optical sensing has been widely used in various applications, including 3-D range finding for clinical [16, 17], scientific, and industrial applications [18–20]. In such applications, a non-contact measurement technique suitable for estimating the target distance uses microwave, ultrasonic wave or light wave as shown in Fig. 1.1. However, only with light-wave technology, it is possible to obtain good resolution with compact measurement settings required for 3-D range finding.

In applications for active optical sensing, four main challenges in image sensors have been found as shown in Fig. 1.2. The first challenge is frame rate, or high temporal resolution. Commercial or conventional image sensors have various frame rate from 15 to 120 frames per second (fps). In order to suppress the motion-blur from fast moving targets, some sensors have high-speed and high frame rate over 1000 fps [21–25]. The second challenge is high spatial resolution. the typical image sensors have the number of pixels larger than 4,096 (64$\times$ 64 pixels). and the pixel digitized signal has 8-bit bit-depth in gray-scale or 10-bit bit-depth or more in color mode. Therefore the image sensor need to transmit 4,096 bytes per one frame.

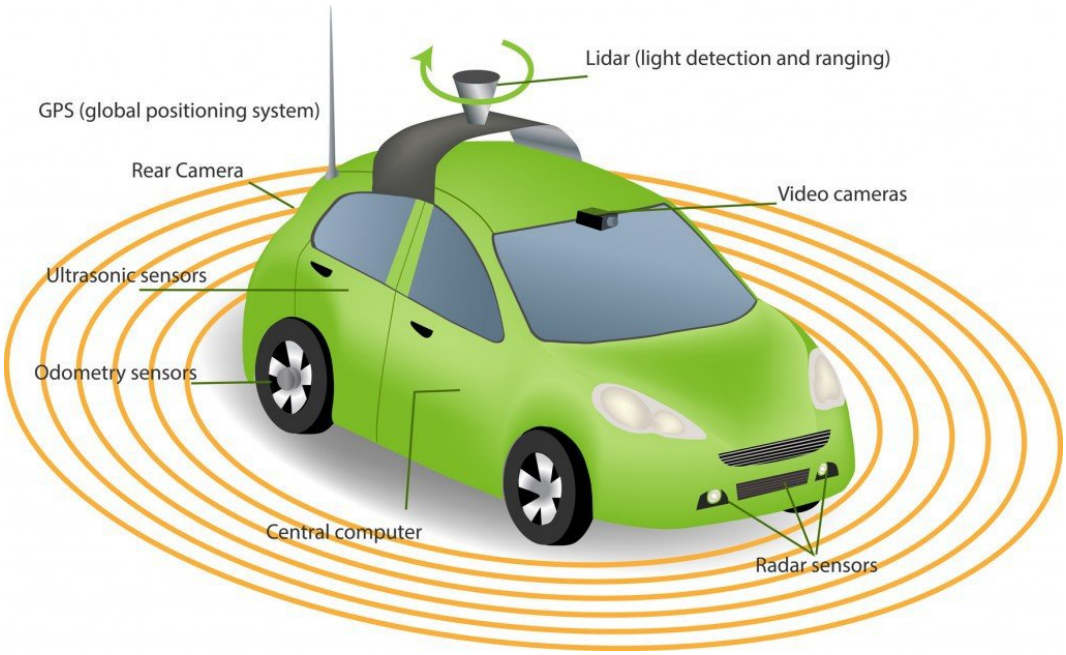

Figure 1.1 Application using active optical sensing: Active sensors in Google's driverless car [1].

It can be a problem in resource-limited applications. Some image sensor [26] archives high spatial resolution. However, the image sensor [26] requires power-consuming circuit. The third challenge is wide dynamic range. In outdoor applications, ambient illumination varies from dark to bright. And strong ambient illumination severely degrades the performance of image sensors. Fig. 1.3 (a) is an object placed outdoors on a clear day. Fig. 1.3 (b) is an image of the sky at 9am. Ambient illumination increases 2,000 lux, 24,000 lux and 90,000 lux, respectively and the reconstruction quality degrades as shown in Fig. 1.3 (c-e). Therefore, the sensitivity and the dynamic range of image sensors should be high for reliable sensing [27]. The last challenge is power consumption. The low power consumption is good for various applications with limited ever sources such as battery or energy harvesting from the environment [28]. However, because the voltage scaling influences the SNR which effects the image quality, the scaling down of the power consumption of image sensors is difficult

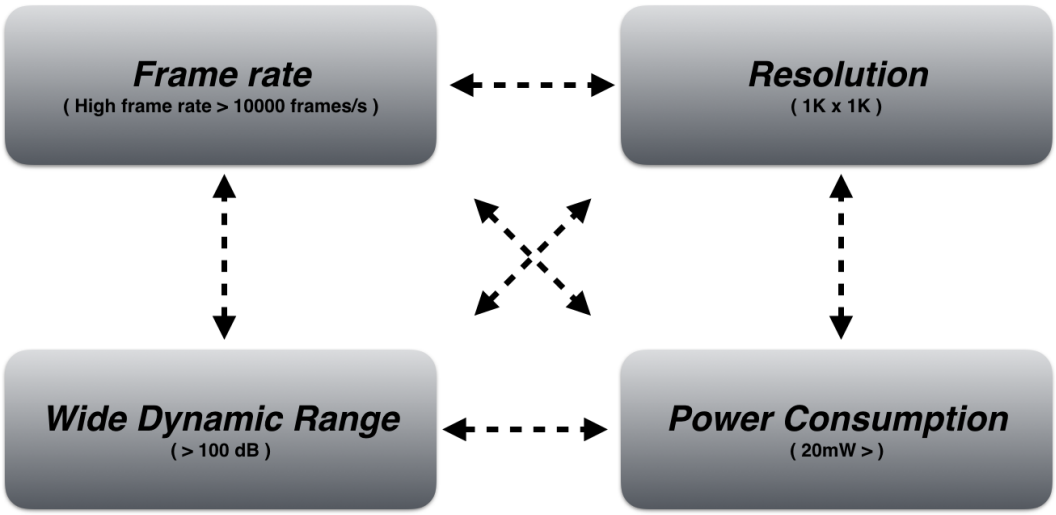

Figure 1.2 Four main challenges in image sensors for active optical sensing.

and limited.

Because above four challenges have trade-off relationships each other, it is a tough work to optimize or balance for the four main challenges. Widening dynamic range induces increase of power consumption. High spatial resolution also induces increase of power consumption. High temporal resolution decreases spatial resolution with limited power consumption. Therefore, according to a specific application, optimization are performed with consideration for these four challenge: temporal resolution, spatial resolution, dynamic range, and power consumption.

1.2 New Challenges of Image sensors

IoT (Internet of Things) system and CPS (Cyber Physical System) are rapidly spreading to industrial or social applications in recent years. These systems collect, analyze and utilize real world information by active sensing technique using image sensor in some applications. They are made on the assumption that the measured values by the measuring instruments are

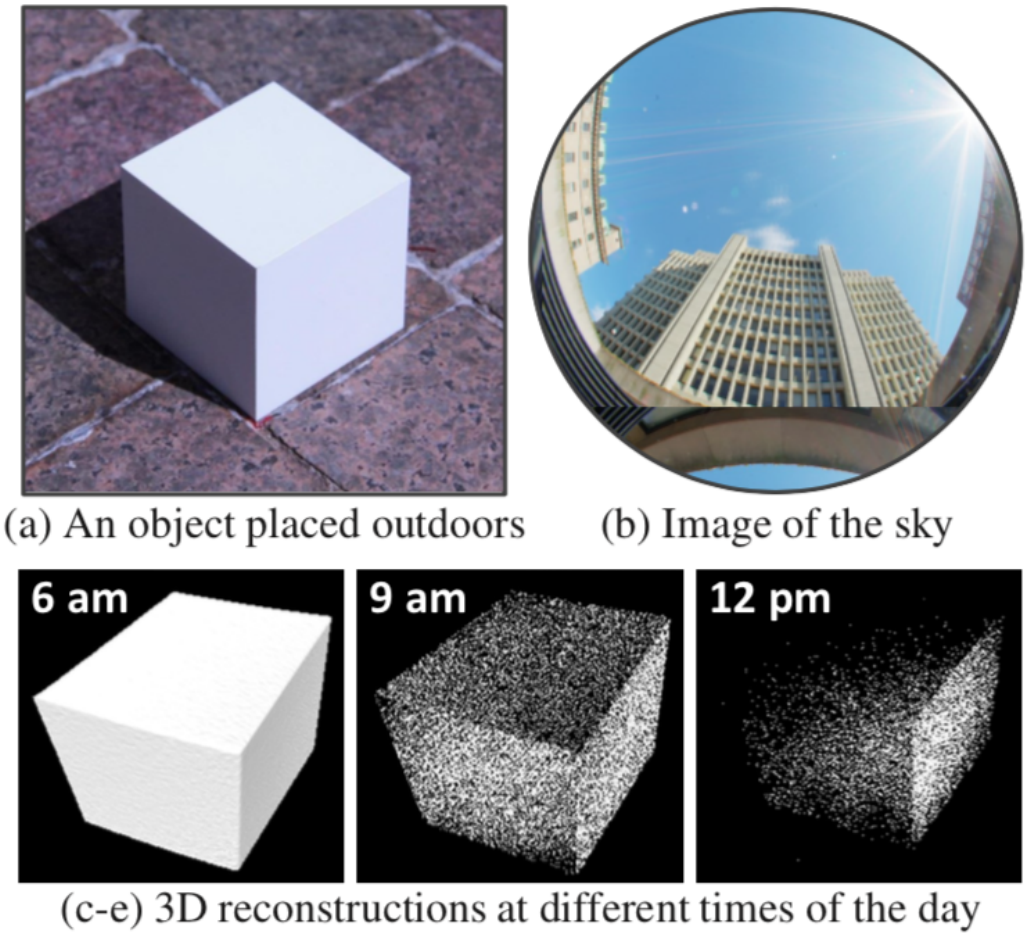

Figure 1.3 Effect of ambient illumination on active optical sensing [2].

correct. Even if it is impossible to directly attack the inside of the system, there is a risk that the system can be attacked by manipulating the measurement result. As an example, there is AEB (Automatic Emergency Braking) of a car to prevent and reduce a traffic accident in recent years. AEB measures the distance to the surrounding obstacles, detects the danger from the change of distance with an active sensing technique such as LIDAR (LIght Detection And Ranging) installed in a car and a stereo camera etc. AEB also works on the assumption that the output of the active sensing technique is correct. If the output of the active sensing technique is manipulated, AEB induces an accident. Therefore, the instrumental security is

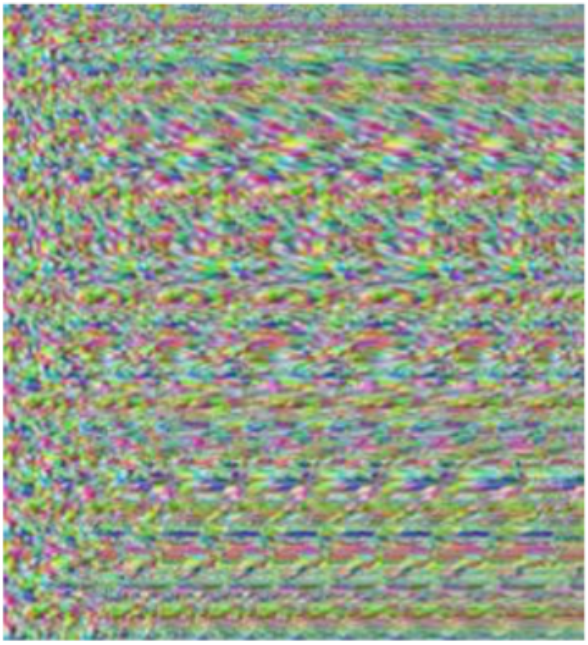

Figure 1.4 Stereogram image for spoofing attack to stereo technique [3].

required for safety assurance on applications.

There are previous works about the attack against stereo technique and LIDAR systems that measure the distance to the object using ToF method . In [3], the DoS attack on stereo camera and the measurement distance camouflage attack have been reported. [3] shows that DoS attack can make the measurement abnormal by irradiating strong illumination to one side of the stereo camera system. And [3] also shows that distance spoofing attack makes the object appears farther than the actual distance by the projection of the induced stereogram image as shown in Fig. 1.4. As shown in Fig. 1.5, the target object is a picture on flat plane. But the image from measurement has various distance from 2 meters to 256 meters like a real view scene of a tunnel.

In [29], the case of attack to the LIDAR mounted on the actual vehicle has been reported. It is performed by irradiating a laser pointer of a wavelength different from the target LIDAR.

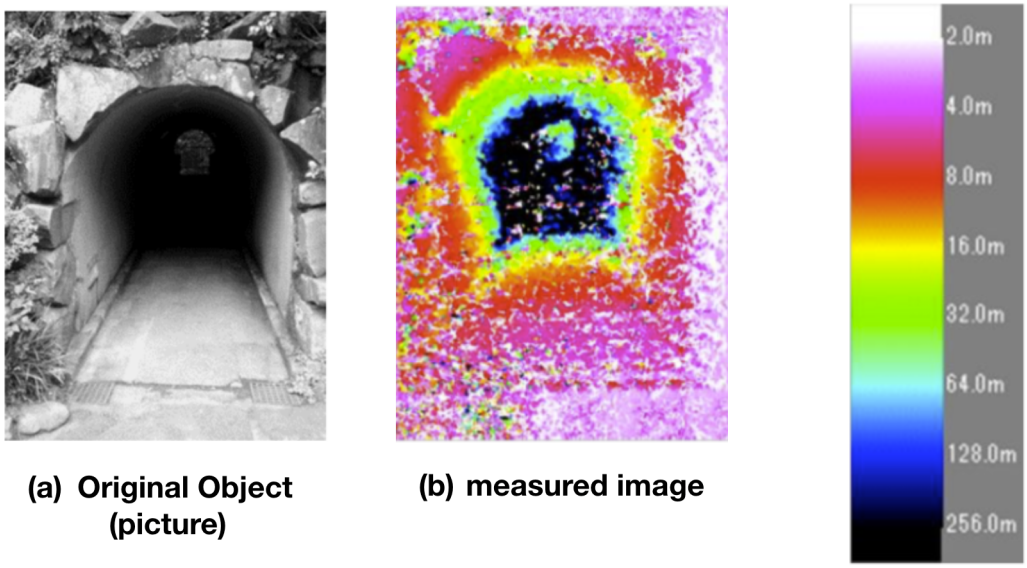

Figure 1.5 Result of attack using stereogram image [3].

[4] presents remote attacks on camera-based system and LiDAR. The attacks, such as blinding, jamming, replay, relay, and spoofing, are performed effectively in laboratory experiments. In [4], the attacker creates counterfeit signal that duplicates the pattern after analyzing the pulse pattern out from the LIDAR to be attacked. And the attacker aims at injecting copies to target LiDAR. The delay, number of pulses, number of copies, pulse width and pulse period are the variables that can be controlled. Fig. 1.6 shows an example how the trigger delay and the number of copies affect the counterfeit signal, shows that the counterfeit signal makes the object appears nearer than the actual distance, and shows that the counterfeit signal makes the object disappears from the actual position.

The other case [5] of attack to LIDAR is that the measured value can be manipulated by irradiating light impersonating as measuring light emitted by the camera as shown in Fig. 1.7.

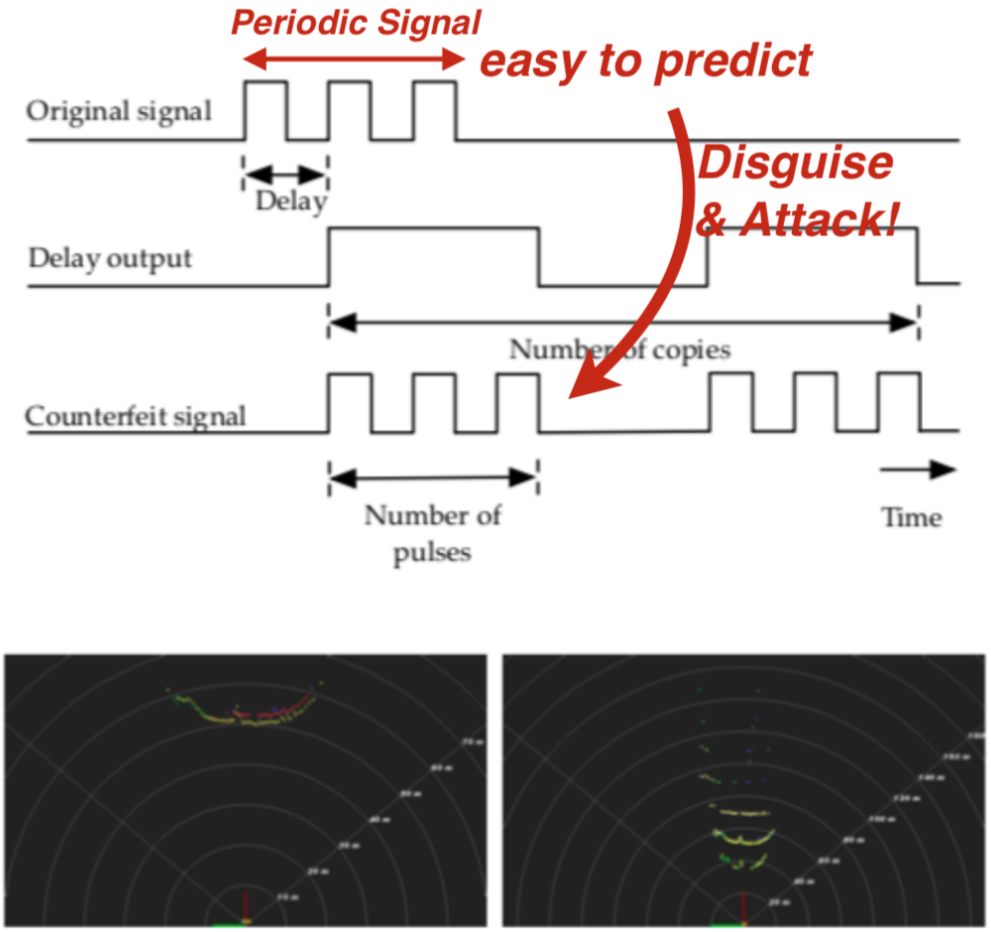

Figure 1.6 Remote Attacks to LIDAR [4].

Normal operation of Time of Flight is presented as below:

$$t = \frac{Q_2}{Q_1 + Q_2} \times l_p \tag{1.1}$$

Where, t means the time of flight. l_p means pulse width of projection light. Q_1 and Q_2 mean the charge of photo-electron in floating diffusions FD_1 and FD_2 respectively in pixel circuit. Based on it, attack light (spoofing light) is generated and irradiated to the measurement

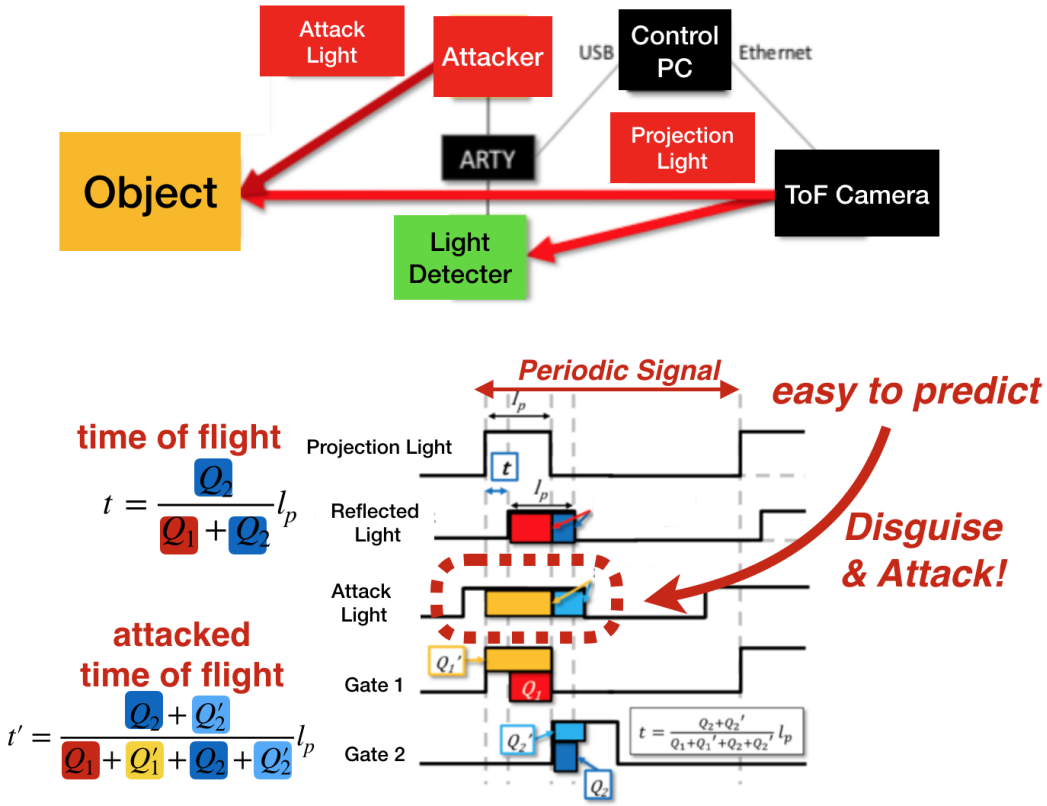

Figure 1.7 Pulse-Light Spoofing against ToF Camera [5].

object. Tampering with measured values has been operated as below:

$$t' = \frac{Q_2 + Q_2'}{Q_1 + Q_1' + Q_2 + Q_2'} \times l_p \tag{1.2}$$

Where, t' means the attacked time of flight. Q_1' and Q_2' mean the additional charge of photo-electron in floating diffusions FD_1 and FD_2 respectively in pixel circuit by spoofing light. In comparison between Eq. 1.1 and Eq. 1.2, the spoofing light induces the additional charge into two floating diffusion FD_1 and FD_2. And the mount of Q_1' and Q_2' can be controlled by the delay or the width of pulse of the spoofing light. It means that [5] can control or change the measured value of time of flight arbitrarily.

There is also a report of a previous study on weakpoint when using fixed frequency as

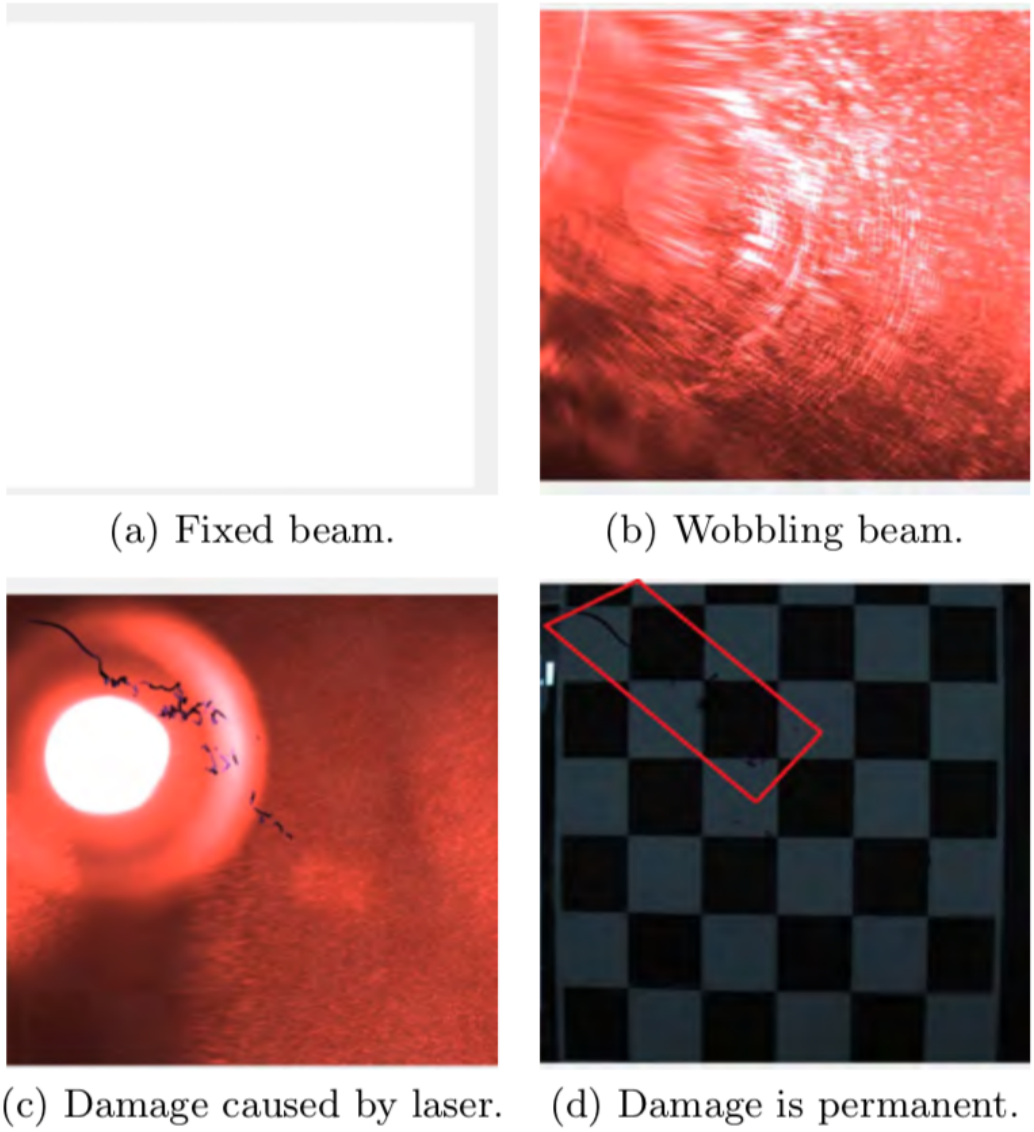

Figure 1.8 Blinding sensor with confronted laser [6].

modulation frequency. The actual attack experiment against the ToF camera is shown in Fig. 1.10 (a). Light emitted from the TOF camera is measured and analyzed using the light receiver circuit. From the analysis result as shown on Fig. 1.10 (b), informations such as the frame interval, the light emission pattern per one frame, the frequency of the measurement light pulse, and so on are obtained. Using these analysis results, the original measurement light is duplicated in the light emitter circuit to interfere. As shown in Fig. 1.10 (c), attack

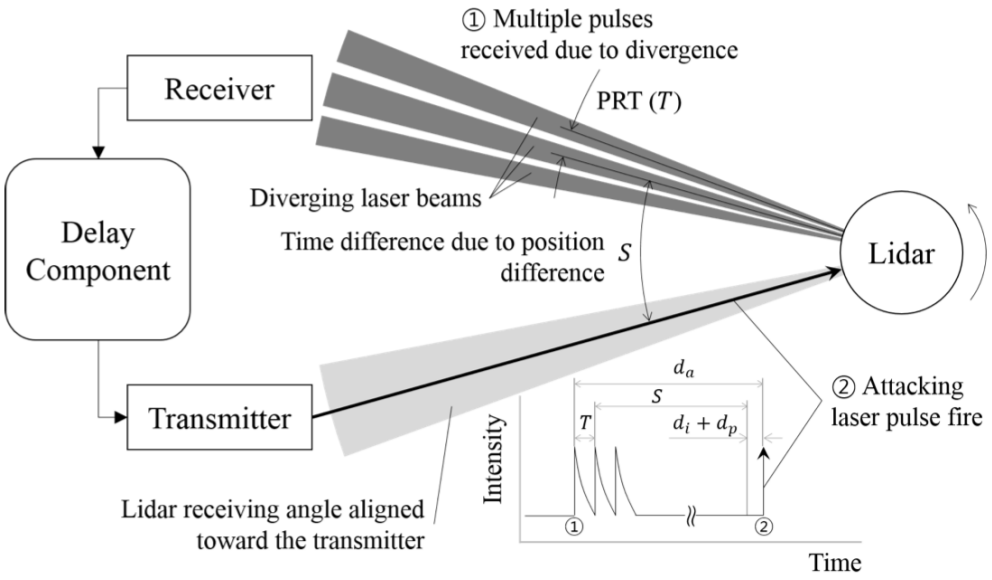

Figure 1.9 Spoofing LiDAR with delay(d_a) injection [7].

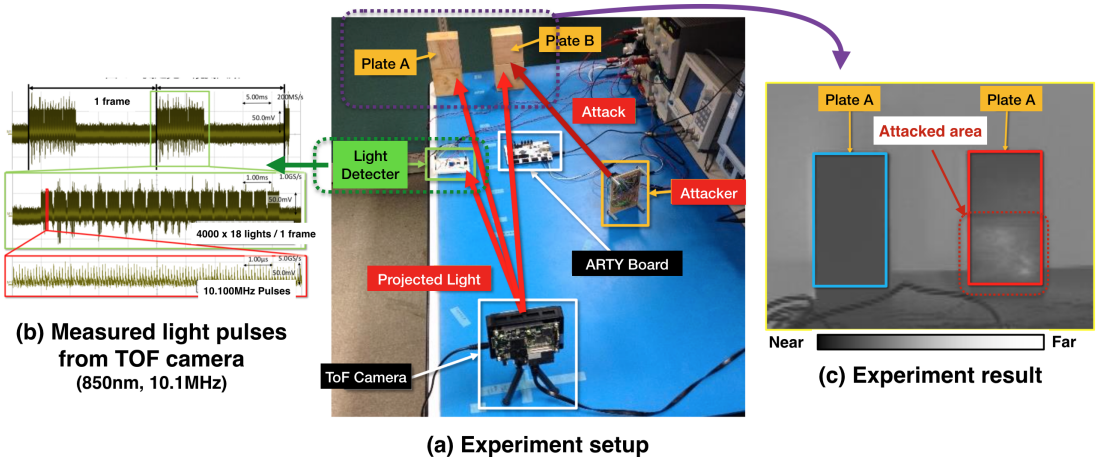

Figure 1.10 Easy to attack against modulated light based method [5, 8].

on only the right plate in two plates that are equidistant. The attack brings the error data of distance. From this result [5, 8], it is necessary to consider a solution that do not use modulated light easy to predict and duplicate.

Previous works are reported based on software or sensing system level [4,6,7,30,31]. These researches [4, 6, 7, 30, 31] are studied for the attack types: Blinding by saturation as shown in

Table 1.1 Comparision of software- or system-based solutions against attack to sensor.

Previous works	Attack types	Countermeasure	Limitation
[6]	Blinding	Multiple sensors	System cost
[30]	Spoofing	Challenge response authentication (CRA) algorithm	slow response
[4]	Blinding Spoofing	Multiple or random probing	low framerate
[7]	Blinding Spoofing	Multiple sensors and random-direction pinging	System cost reliability issue on moving parts
[31]	Spoofing	Multiple sensors	At least one sensor should serve as the reference sensor

Fig. 1.8, and spoofing by delay injection as shown in Fig. 1.9. Each of the previous works presented their respective countermeasures for the attack. The attack types, countermeasures, and the limitations are summarized and compared in Table 1.1. Most of methods is processing with the algorithm that assumes that at least one sensor should serve normally within multiple sensors. So, there are limitations such as a large amount of calculation, slow response, low frame-rate, and high system cost .

1.3 Research goal

In almost applications using active optical sensing, image sensors are required to have high instrumental security in addition to traditional challenges such as frame rate, resolution, wide dynamic range, and power consumption. Fig. 1.11 illustrates the active optical sens-

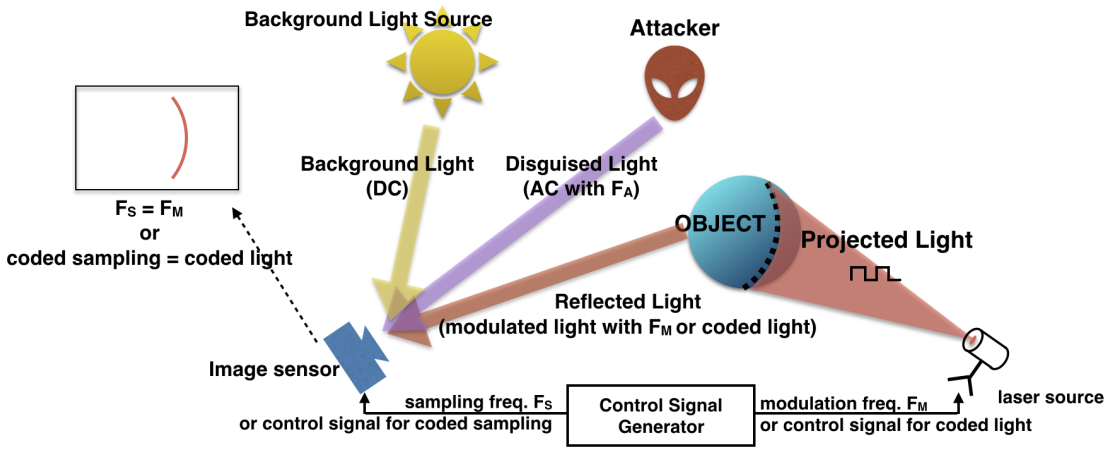

Figure 1.11 Research Goal.

ing environment with the attacker under strong background light. A control signal with the modulation frequency F_M or the coded light is sent to the laser source from the control signal generator in the middle in Fig. 1.11, and a control signal with the sampling frequency F_S or the coded sampling is sent to the image sensor in same way. Then, when the object is irradiated with modulated light modulated with the modulation frequency F_M or light coded with a specific code from the laser source, incident light to the image sensor consists of the reflected light from the object, disguised light modulated with a specific modulation frequency F_A and irradiated from the attacker, and background light from the measurement environment.

$$\text{Incident Light} = \underline{\text{Reflected Light}} + \text{Disguised Light} + \text{Background Light} \tag{1.3}$$

In this incident light, the attack light into the an image sensor can be defined as below:

$$\text{Attack Light} = \text{Disguised Light} + \text{Background Light} \tag{1.4}$$

Where, disguised light is the light modulated by specific frequency F_A. And, background light is constant value in time that is strong illumination. The reflected light is the signal that the image sensor needs to accumulate. So the reflected light is selective-signal on the image sensor. the disguised signal is that the image sensor wants to avoid. So the disguised light is non-selective-signal on the image sensor. The background light is the light from the environment outside of active optical sensing. The intensity of background light has little change with measurement time, so the background light can be treated as DC components. The background light do not include any information. So the background light is non-signal on the image sensor. Therefore, Eq. 1.3 can be re-written as below:

$$\text{Incident Light} = \underline{\text{Reflected Light}} + \text{Disguised Light} + \text{Background Light} \quad (1.5)$$

$$= \underline{\text{Selective-Signal}} + \text{Non-Selective-Signal} + \text{Non-Signal} \quad (1.6)$$

In this situation, the solution against the disguised light from attacker and background light from environment is needed. The disguised light can malfunction or manipulate the sensing system. Strong background light makes the image sensor to be saturated before accumulating the selective-signal. These lights are factors that interfere with the normal operation of the active optical sensing. Therefore, the main goal of this thesis is to propose an image sensor that has capacity of detecting selective-signal from incident light with background light and disguised light from attackers. The two main features are required for overcoming these difficulty.

- Signal Selectivity: The image sensor needs to accept the only reflected light without disguised light and background light. The image sensor with various structured lights

can be further used under disguised light with fixed pattern.

- Background Light Suppression: The image sensor needs to suppress the background light until accumulating the selective-signal sufficiently up to output-able level of signal. In most cases, an optical bandpass filter is used to prevent the background light. The image sensor with background light suppression circuit can be further used even under outdoor conditions.

1.4 Thesis Organizations

In this thesis, Chapter 2 explains the basic theory of active optical sensing and related works, and declares the goals that the proposed image sensors should aim. Chapter 3 introduces the image sensor with selective-signal detection and background light suppression using a demodulation pixel and in-pixel feedback circuit. Chapter 4 introduces an image sensor that has selective-signal detection and background light suppression using a demodulation pixel and a current mirror circuit with compensation of background light. Chapter 5 presents the coded light different from modulated light, describes the operating conditions of the image sensor when using the coded light, and evaluates active optical sensing using the coded light. Chapter 6 summarizes this works and presents the conclusion of this thesis.

Chapter 2

Researches on active optical sensing

2.1 Active optical sensing

The three-dimensional measurement methods are roughly classified as shown in Fig. 2.1. First, when classified by the frequency to be used, it can be divided into a method using ultrasonic wave for sonar system, a method using microwave for radar system, and a method using optical laser. Methods using ultrasound wave and methods using microwaves have advantages. But it is difficult to achieve small size and high resolution. Furthermore, there are passive methods and active methods for methods using optical laser. The passive method is a method that does not use a special light source, and the active method is a method using a special light source. In terms of the instrument security, passive method is easy to be affected by disguised light from outside. Therefore, the focus of this thesis puts on an active optical sensing that is a method using a special light source that can be employed for the more robust operation of an image sensor to enhance instrumental security.

As shown in Fig. 2.2 [9], passive sensings, like stereo vision [32–34] as shown in Fig. 2.2 (a) and depth-from-defocus method [35–37] as shown in Fig. 2.2 (b), do not require a specific wave or light. However active sensing techniques use a micro wave or the structured light.

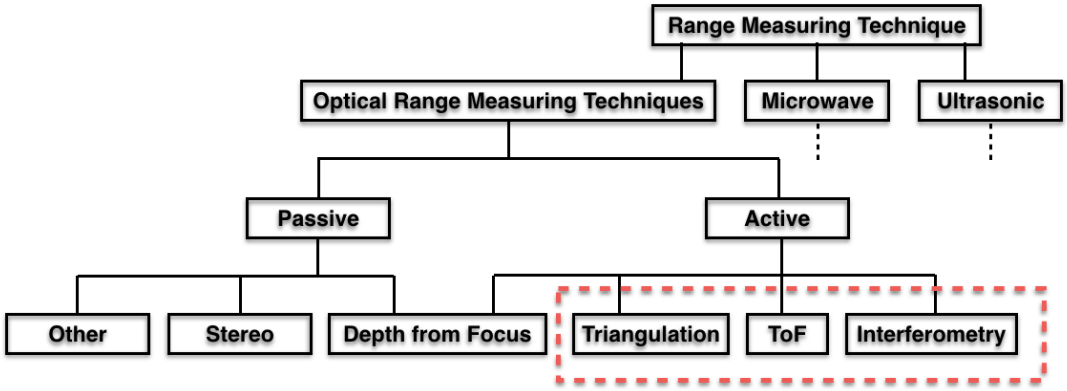

Figure 2.1 3D taxonomy: Overall of the techniques of 3D measurement

Active optical sensing techniques using light-waves can be further classified in three main categories, namely: interferometry [38–45], Time-of-Flight [11, 46–51], and Light-section method [49, 52–58].

Interferometry methods measure depths by using the phase of the optical wave itself as shown in Fig. 2.2 (d). This requires a correlation between the reference wavefront and the wavefront reflected from the object, and coherent mixing. Many variations of the principle of interferometry technique have been developed such as white light interferometry, speckle interferometry, holographic interferometry, and multi-wavelengths interferometry. The high accuracy of the interferometry techniques depend on the coherence length of the light source. Therefore, because interferometry technique is based on the evaluation of very shot optical wavelength, this technique is not sufficient for ranges greater than few centimeters.

In Time-of-Flight (ToF) technique, as shown in Fig. 2.2 (c), two types to acquire an object's geometry are: (i) continuous wave TOF, measuring the phase shift of a modulated optical signal or (ii) pulse TOF, measuring the time of flight. Typical examples of ToF are terrestrial or aerial LIDAR instruments [59, 60]. Due to fast scanning mechanisms, LIDARs can acquire

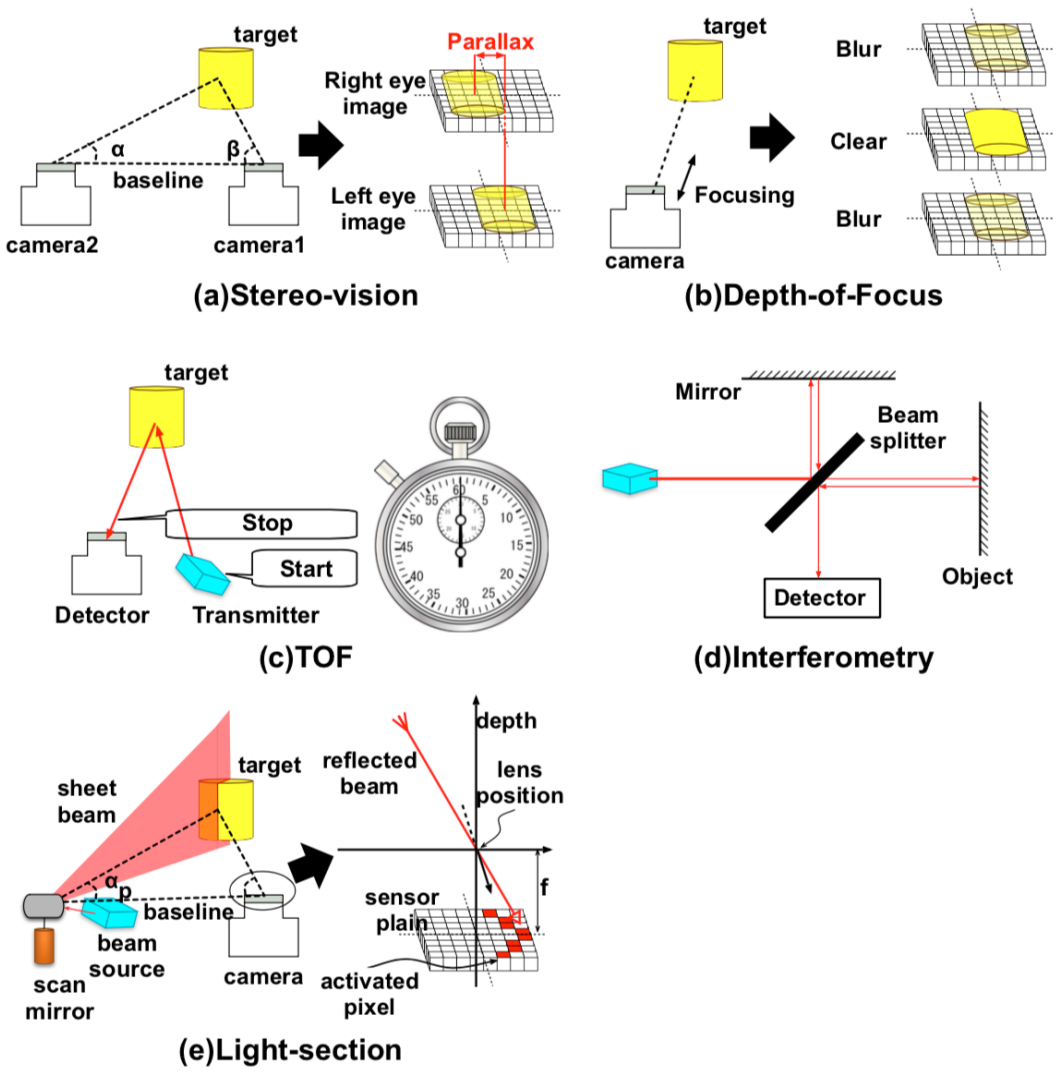

Figure 2.2 Concept of passive and active sensing techniques [9].

above on million of points per second. These instruments has an accuracy ranging from less than on millimeter to some tens of centimeters respectively. However, LIDAR instruments need a high costs and more spaces.

Light-section method techniques is shown in Fig. 2.2 (e). This technique determines a coordinate point of target on a triangle by a known optical base line and the related side angles pointing to the coordinate point of target. Triangulation method is used for calculating

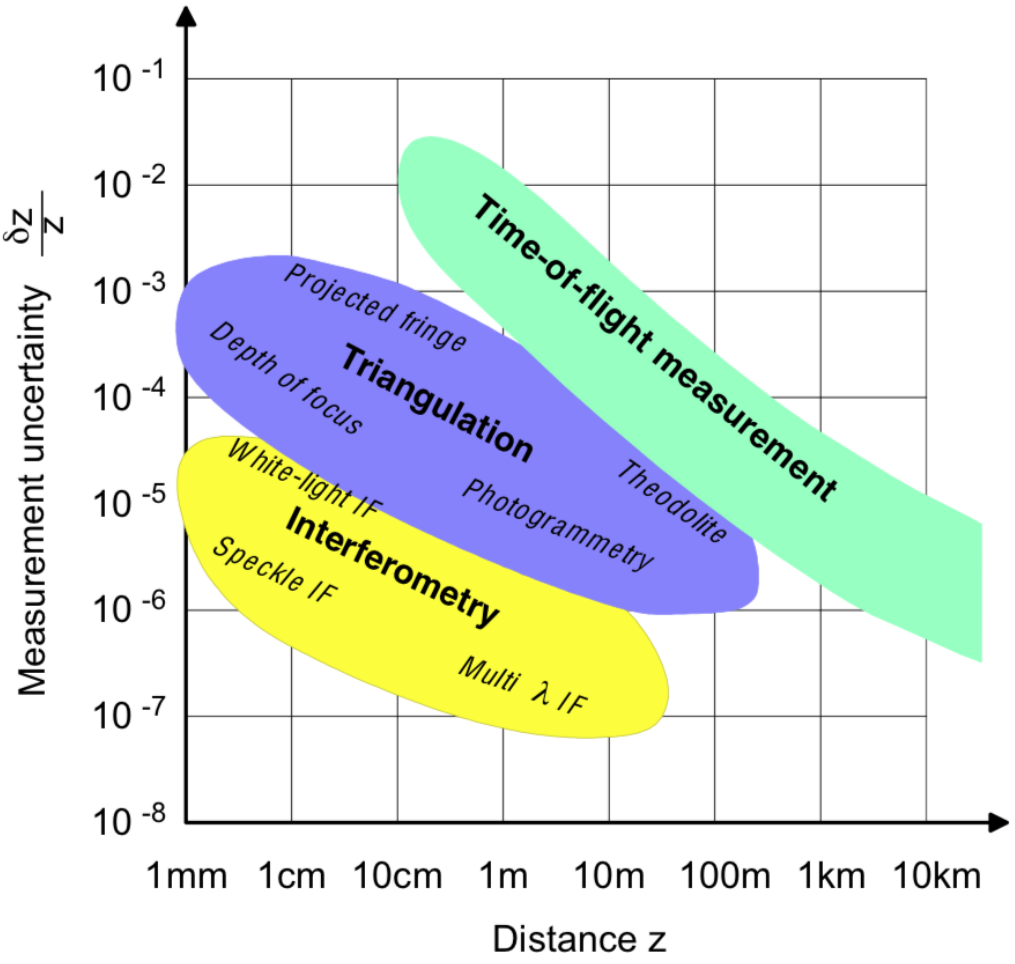

Figure 2.3 Relation between range distance and range accuracy [10].

the unknown point on target in active optical sensing based on structured illumination.

The comparison about relation between distance and resolution is shown in Fig. 2.3. As shown in Fig. 2.3, ToF methods realize wide distance range and interferometry realize high range accuracy. Triangulation technique realizes higher range accuracy and wider distance range at middle range. Each method has different characteristics, so it is better to choose the technique that is more suitable for an application. From their characteristics about distance, it is expected that the requirement for strengthening instrumental security will be increased for triangulation that is widely applied to industrial applications such as product inspection.

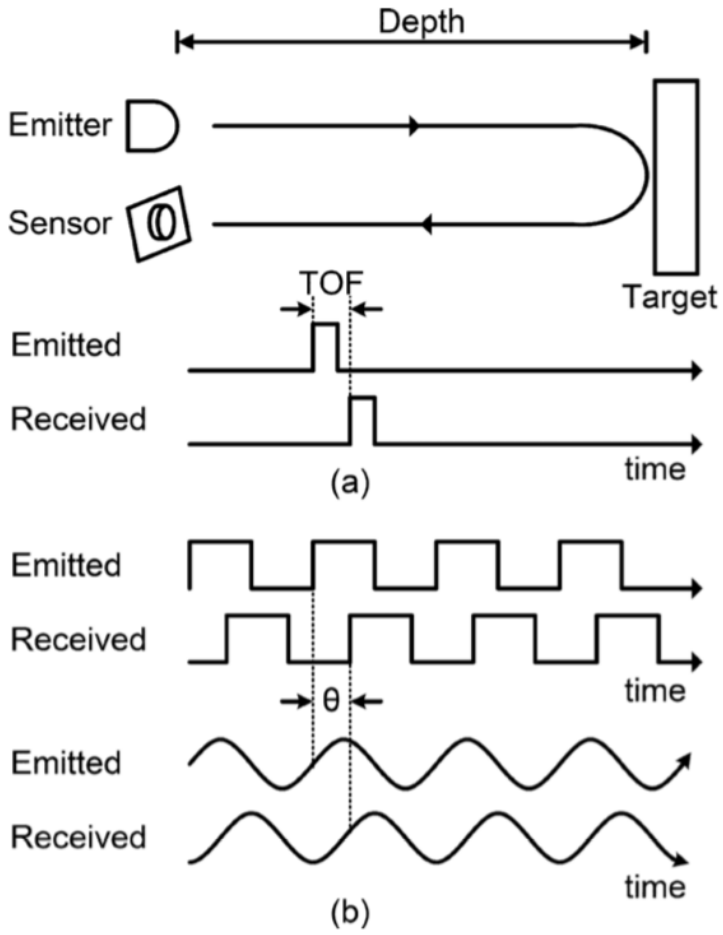

Figure 2.4 Diagram of principle of TOF sensor operations: (a) direct and (b) indirect TOF measurement schemes in [11].

Among these methods, ToF (Time-of-Flight) and triangulation are widely employed in recent applications. So, the principle of ToF (Time-of-Flight) and triangulation will be explained briefly.

2.1.1 ToF(Time-of-Flight)

Fig. 2.4 shows the diagram of principle of TOF (Time-of-Fight) sensor. Light modulated by a specific frequency is irradiated and reflected light is received by a sensor. Since the round trip time of irradiated light varies depending on the distance to the object, the distance

D to the object can be expressed by the following equation.

$$D = \frac{c \cdot TOF}{2} \tag{2.1}$$

Where, c is the speed of the light ($c = 3 \times 10^8 m/s$) and TOF is the round trip time of reflected light. As shown in Fig. 2.4(b), if the synchronous measurements can be repeated to enhance the signal-to-noise ratio (SNR) in indirect TOF measurement scheme. In this case, the lock-in pixels or demodulation pixels are employed to extract the phase shift of the received sine waves. The TOF can be calculated from the measured phase shift:

$$TOF = \frac{\theta \cdot T}{2\pi} \tag{2.2}$$

where T is the period of the emitted wave. f is the frequency of the emitted wave.

2.1.2 Triangulation

Fig. 2.5 shows light-section method using a light sheet. The three-dimensional range finding system based on light-section method consists of an image sensor, a rod lens, a scanning mirror and laser source. A light sheet is made using a rod lens and projected to obtain a contour line. The three-dimensional coordinate on the object can be calculated using the principle of triangulation and the contour line data obtained by an image sensor.

Fig. 2.6 shows the principle of triangulation. In an orthonormal coordinates system of three dimensional space (X, Y, Z), position coordinates of an image sensor is $S(-d/2, 0, 0)$. The coordinates of a light source is $L(d/2, 0, 0)$. For the coordinates $O(X, Y, Z)$ on the target object

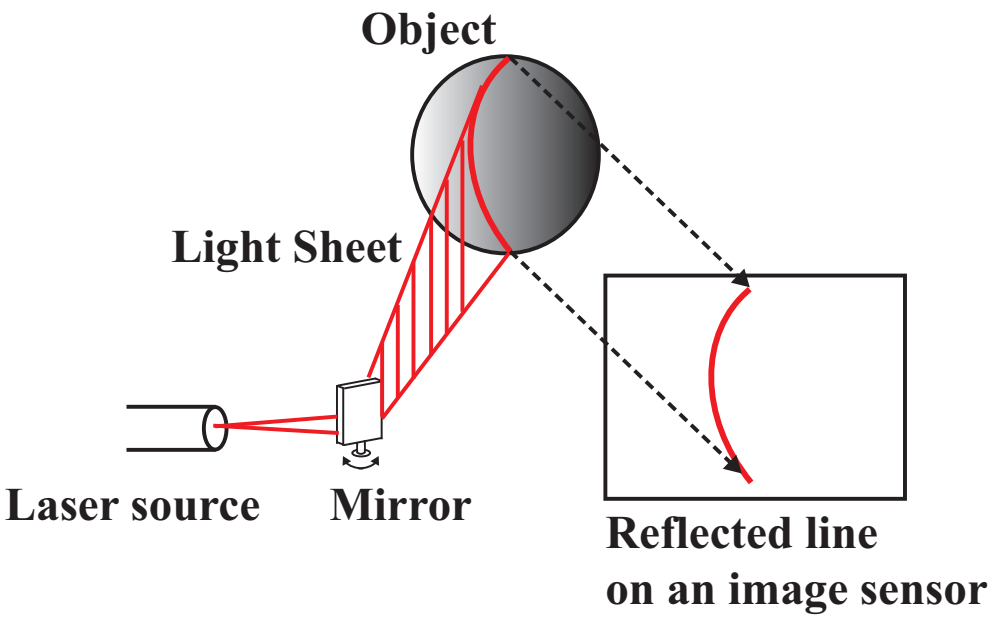

Figure 2.5 Light-section method.

on which sheet light is projected, $\angle OLS = \alpha_1$ and $\angle OSL = \alpha_2$ are formed. Let θ be the angle that plane XZ forms with plane Π that includes the coordinates O, S, L. α_1 and θ are values determined by the setting value of the projection direction of the laser. α_2 is a value directly obtained when the light reflected by the system is imaged on the image sensor surface. In these conditions, three-dimensional coordinates O (X, Y, Z) of a point on the object plane are obtained as follows. A perpendicular is drawn from O (X, Y, Z) on the object plane to the X axis, and for the length k,

$$\tan \alpha_1 = \frac{k}{d/2 - X_O} \tag{2.3}$$

$$\tan \alpha_2 = \frac{k}{d/2 + X_O} \tag{2.4}$$

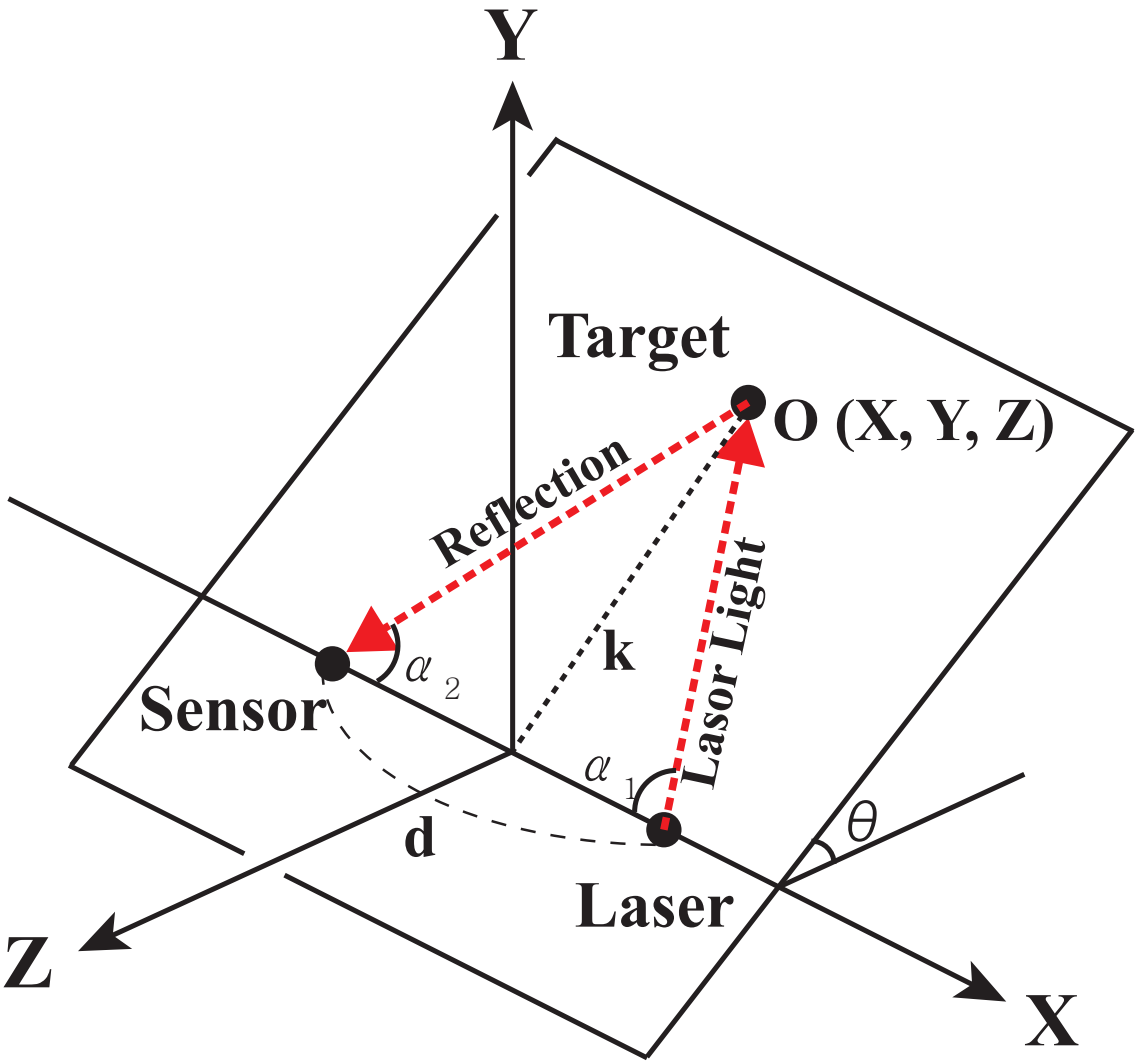

Figure 2.6 Principle of triangulation.

Expanding on X_O and K from Eq. 2.3 and Eq. 2.4,

$$X_O = \frac{d(\tan\alpha_1 - \tan\alpha_2)}{2(\tan\alpha_1 + \tan\alpha_2)} \tag{2.5}$$

$$k = \frac{d(\tan\alpha_1 \cdot \tan\alpha_2)}{\tan\alpha_1 + \tan\alpha_2} \tag{2.6}$$

Where, Y_O and Z_O are explained as follows.

$$Y_O = k \cdot \sin\theta \tag{2.7}$$

$$Z_O = -k \cdot \cos\theta \tag{2.8}$$

So, the coordinates Y_O and Z_O can be re-writed from Eq. 2.7, Eq. 2.8, and Eq. 2.6 as follow.

$$Y_O = \frac{d \cdot \tan\alpha_1 \cdot \tan\alpha_2 \cdot \sin\theta}{\tan\alpha_1 + \tan\alpha_2} \tag{2.9}$$

$$Z_O = \frac{d \cdot \tan\alpha_1 \cdot \tan\alpha_2 \cdot \cos\theta}{\tan\alpha_1 + \tan\alpha_2} \tag{2.10}$$

The coordinates of O(X, Y, Z) on the target object can be calculated by Eq. 2.5, Eq. 2.9, and Eq. 2.10.

2.2 An image sensor with background light suppression

2.2.1 Overall architecture

Fig. 2.7 shows the structure of an image sensor. An image sensor consists of a pixel array, column-parallel correlated double sampling (CDS) circuits and ADCs, a DAC, LATCH/FFs, row address decoders and column address decoders. An image sensing means that the photons in incident light count. The output of an image sensor is digital signals of the incident photons.

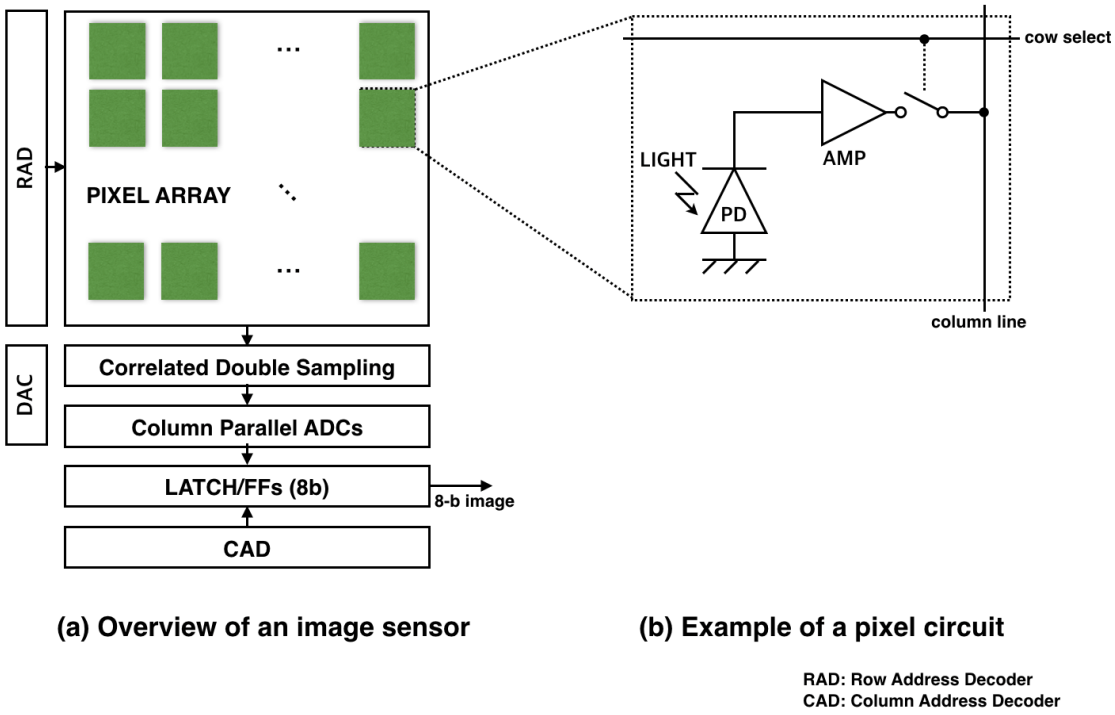

Figure 2.7 Structure of an image sensor: (a) Overview of an image sensor, (b) Example of a pixel circuit.

The operation of an image sensor is as follows: (1) incident photons are converted into electrons, and electrons are accumulated in the photodiode in each pixel during the integration time T_{INT} (2) An amplifier in a pixel circuit converts integrated electrons into voltage. (3) The row address decoder (RAD) selects one row out of pixel arrays. The row of pixel array is read out through the column line. (4) In readout circuits, CDS circuits cancel the fixed pattern noise. (5) Noise-cancelled signals are converted into the digital signals through ADCs. The digital signals are stored in latches or FFs temporarily before the readout. (6) Column address decoders (CAD) select latches or FFs column by column, read out digital signals. (7) The procedure repeats for entire rows (8) After repetition for entire rows, an image of one frame is generated.

Table 2.1 Comparision between types of in-pixel selective-signal detection.

Features	Correlation pixel [12]	Demodulation pixel [61]
Modulated signal	sinusoid signal	ON–OFF signal
Operation mode	multiplying the reflected signal with the reference signal	accumulating and separating the signal using two accumulation regions
Strong point	high accuracy	simpler implementation, high demodulation frequency
Weak point	harder implementation, low illuminant frequency ($\sim 6kHz$)	dynamic range is limited (by the capacity of the accumulation regions)

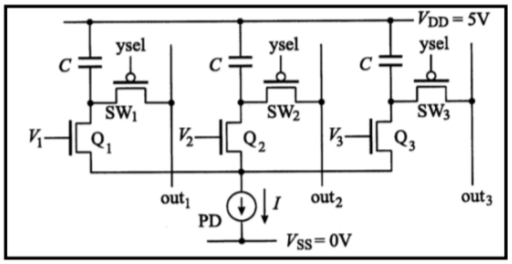

Figure 2.8 Pixel circuit of 3PCIS [12].

2.2.2 In-pixel Selective-signal detection

There are two methods to realize in-pixel selective-signal detection: correlation pixel and demodulation pixel. Table 2.1 shows the summarized table about the previous researches on image sensor with selective-signal detection. The correlation pixel has one photodiode and three multiplier transistors as shown in Fig. 2.8. The correlation pixel uses a sinusoid signal as the modulated light, multiplies the reflected light and the reference signal with the multiplier transistor in the pixel, accumulates and outputs the result. The pixel [12] has high correlation accuracy in low modulation frequecy. However, it is difficult to implement because three-phase reference signal is necessary, the cost of the computing system after measurement is high. And low modulation frequency is also a weak point. Fig. 2.9 shows

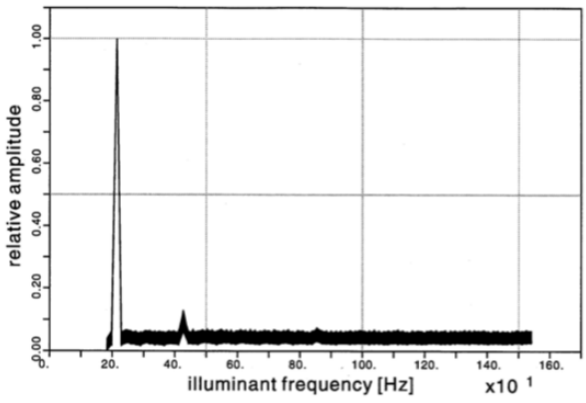

Figure 2.9 Signal selectivity of correlation pixel [12].

the signal selectivity of correlation pixel. Illuminant frequency changes from 200 Hz to 1.6 kHz with reference frequency 200 Hz. The amplitude in Fig. 2.9 is peak when illuminant frequency is equal to the reference frequency 200 Hz. The demodulation pixel [61] has two transfer gates in the pixel, accumulates signals of ON-signal and OFF-signal into the two accumulation regions in pixel separately, and outputs the results. The demodulation pixel uses an ON-OFF signal as the modulated light. The demodulation pixel is comparatively easy to be implemented. However, limited dynamic range is a weak point by the capacity of the accumulation regions.

Fig. 2.10 shows the structure and operation of the demodulation pixel that is employed in the image sensor used in Chapter 3, Chapter 4, and Chapter 5. A demodulation pixel has one photodiode, two transfer gate transistors TX_1, TX_2, and two accumulation regions C_1, C_2 in a pixel as shown in Fig. 2.10 (a). Fig. 2.10 (b) shows the operation of demodulation pixel with modulated light. The received light into image sensor consists of shrunk irradiated light and background light. When the reflected light is incident, the transfer gate transistor TX_1 turns on when the ON-signal light comes in. And the transfer gate transistor TX_2 turns on when

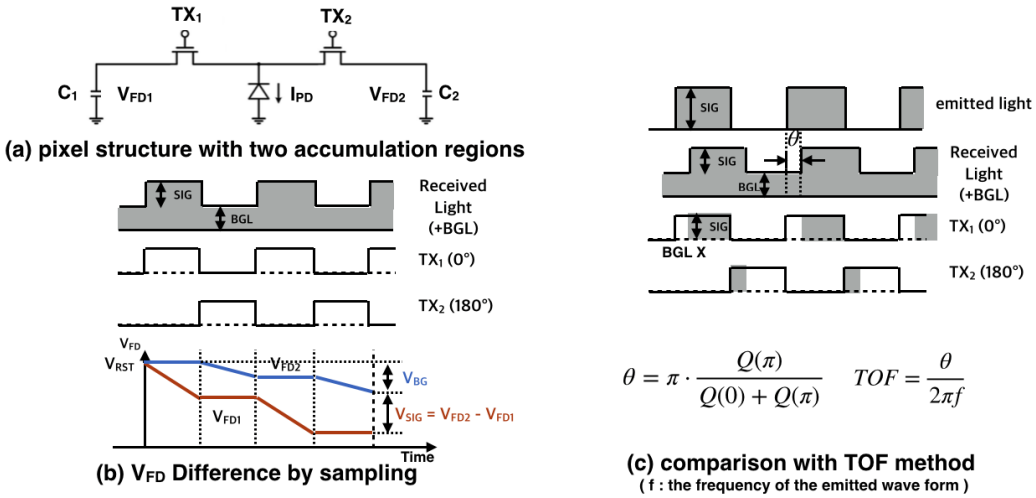

Figure 2.10 Selective-signal detection using demodulation pixel: (a) pixel structure with two accumulation regions (b) V_{FD} difference by sampling (c) comparison with TOF method.

the OFF-signal light comes in. The demodulation pixel separates the ON- and OFF-signal from incident light, and accumulates them in two accumulation regions C_1, C_2 respectively. The voltage V_{FD1} of accumulation regions C_1 means the sum of ON-signal induced charge and background light induced charge. The voltage V_{FD2} of accumulation regions C_2 means the sum of OFF-signal induced charge and background light induced charge, is equal to background light-induced charge. The difference between the charges in two accumulation regions means the signal light as below.

$$V_{SIG} = V_{FD2} - V_{FD1} \tag{2.11}$$

When the modulation frequency of incident light is equal to the sampling frequency of the transfer gate transistor, V_{SIG} becomes maximum value. If the modulation pixel does not saturate during the accumulation time, the signal light component is calculated except the background light component by subtracting V_{FD1} from V_{FD2} as shown in Eq. 2.11. In the TOF

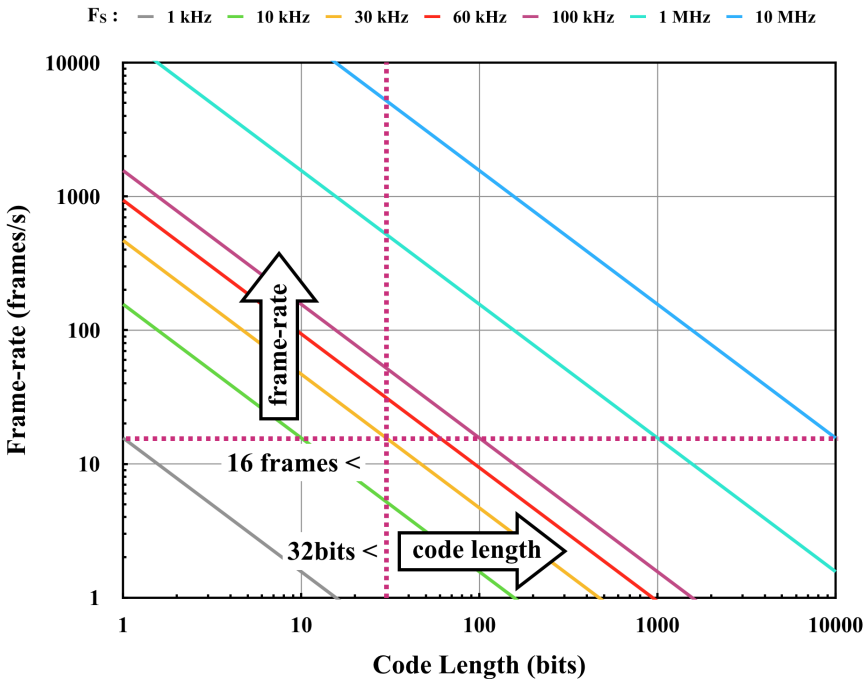

Figure 2.11 Relation between code length and frame-rate on 64 × 64 pixels array

method using the demodulation pixel, a common-mode voltage control circuit is used for eliminating only the background light component from both accumulation areas, because the background light can not be easily subtracted by the principle of TOF as shown in Fig. 2.10 (c). After all, as the demodulation pixel in the TOF method, the background light component removing circuit is necessary so as not to saturate before extracting the signal light component for the modulation pixel to detect selective-signal.

Fig. 2.11 shows the relation between code length and frame-rate on 64 × 64 pixels array. Considering the practical level about code length and frame rate [62], the sampling frequency over 30 kHz is required.

2.2.3 BGL suppression schemes

Strong background light has the following two effects on the image sensor of active sensing scheme such as the three-dimensional measurement system and causes the measurement error.

- Noise increase
- Saturation

There is the countermeasures against strong background light as follow.

1. Increase the intensity of light source [2]
2. Using the light source with the wavelength on weak background light
3. Using an optical filter that can eliminate the background light [63]
4. Using Pulse light source and high speed shutter
5. Background light suppression

Items 1 to 3 are limited to specific situation during the measurement, and the effect is restricted.

For items 4 and 5, previous works have been studied on image sensor side [11,48,64–74] as summarized in Table. 2.2. These schemes can be categorized in four types: 1) voltage-mode subtraction [64, 65]; 2) minimum-charge transfer (MCT) [66, 73]; 3) charge-domain subtraction [48, 67, 68, 74]; 4) current-mode subtraction [69]. Overall, the dynamic range has been achieved from 70 dB to nearly 120 dB as shown in Fig. 2.12. The voltage-mode subtraction

Table 2.2 Summary of BGL suppression methods with demodulation pixel for TOF.

Category	Column-level monitoring/feedback	In-pixel integration capacitor
Voltage-mode subtraction	unity-gain buffer [64]	CDS [65]
Minimum-charge transfer (MCT)	N/A	Minimum-charge transfer (MCT) [66]
Charge-domain subtraction	active circuits [67]	anti-parallel capacitors [48], integration capacitors [68]
Current-mode subtraction	current-mode subtraction [69]	N/A

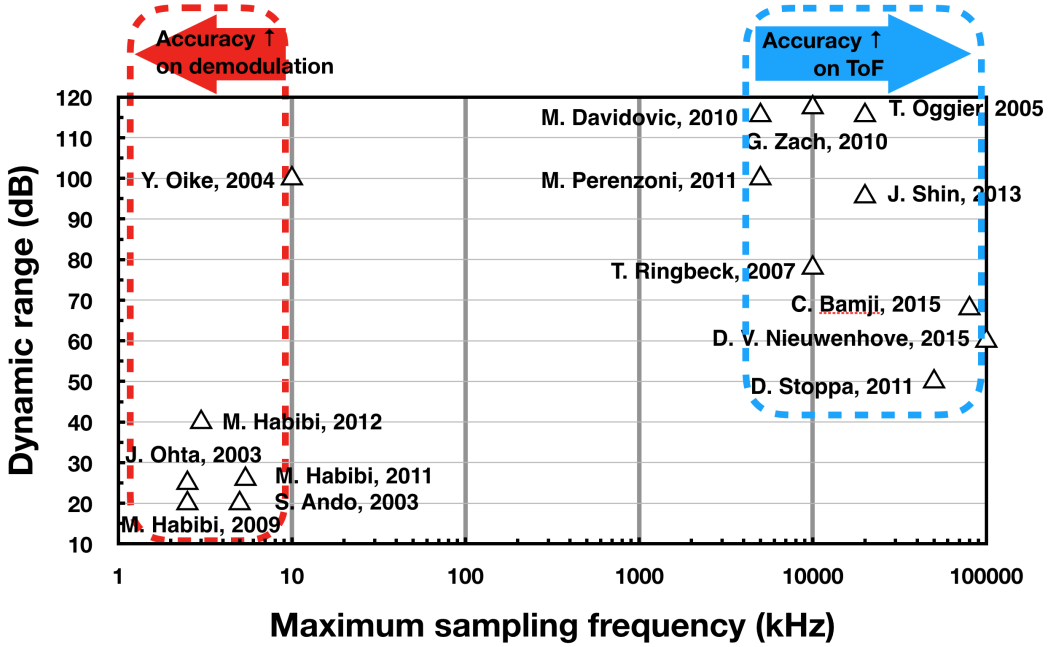

Figure 2.12 Trend on BGL suppression with demodulation pixel for in-pixel selective-signal detection and ToF

scheme suppressed the BGL using a unity-gain buffer [64] or correlated-double-sampling (CDS) [65] in the pixel. A large intermediate storage is employed in the minimum-charge schemes (MCT) to store both BGL and signal charges. However, the MCT scheme cannot remove the BGL charges that exceed the well-capacity of the intermediate node. Active circuits [67], anti-parallel capacitors [48], flipping the integration capacitors [68], or injecting

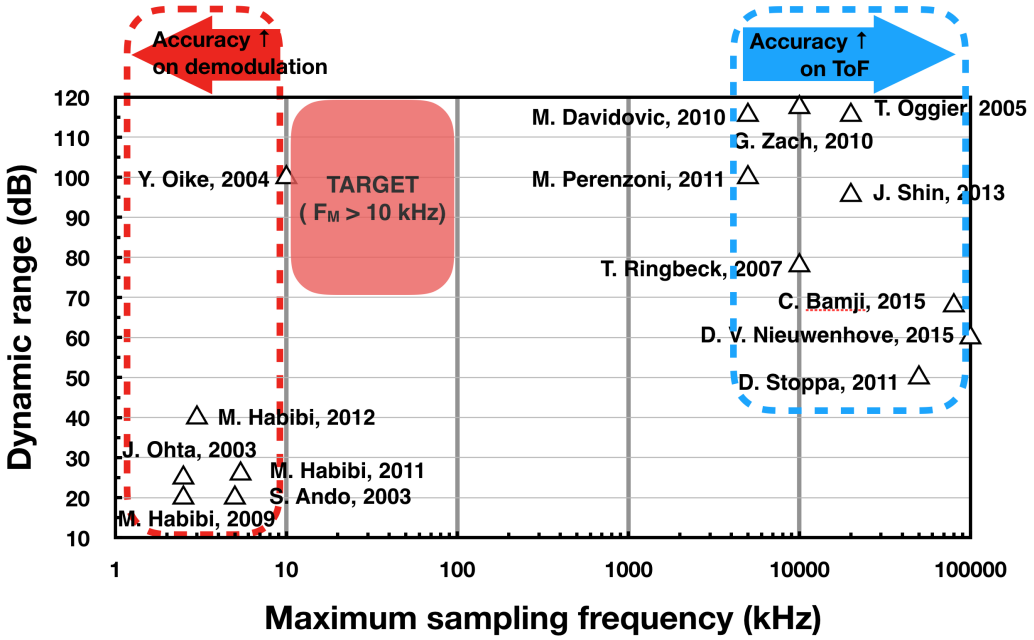

Figure 2.13 Target of proposed image sensors with in-pixel selective-signal detection

hole packets [74] are employed for common-mode charge elimination in the charge-domain subtraction scheme. A current source in each pixel is employed to compensate for the photocurrent by BGL in the current-mode scheme [69]. There are weak points that the suppression capability was restricted to the storage capacitor in the pixel, or the entire operation is slow due to the column-by-column monitoring and feedback. Therefore, we approach background light suppression circuit that can monitor and feedback in the pixel without in-pixel capacity for integration.

Fig. 2.13 shows the trend of the image sensors [12, 14, 61, 75–77] with selective-signal detection in terms of the maximum modulation frequency and dynamic range. In terms of the maximum modulation frequency, 10 kHz is the maximum modulation frequency. The dynamic range has been achieved from 20 dB to nearly 100 dB as shown in Fig. 2.13. There is a requirement for an image sensor that can operate up to the high modulation frequency

over 10 kHz. Therefore, the target of proposed image sensor with selective-signal detection is the image sensor that has wide dynamic range ($\geq$ 70 dB) and high modulation frequency of 10 kHz or more as red area shown in Fig. 2.13.

2.3 Summary

In this chapter, the basic knowledge of active optical sensing has been described. The overall architecture of an image sensor for active optical sensing is described. The method using demodulation pixel is selected for implementation methods for selective-signal detection in image sensors. Countermeasures and trends of previous works on image sensors against strong background light are reported. The target of image sensor with selective-signal detection and background light suppression is that the modulation frequency is over 10 kHz with wide dynamic range.

Chapter 3

An image sensor with selective-signal detection and background suppression

3.1 Introduction

Applications based on active optical sensing are widely used in various applications and fields. Some applications of 3-D measurement, particularly such as mobile devices and automobiles, require both measurement stability and reliability. In real environment, the ambient light is often much stronger than the projected light and reflected light. Therefore, the solutions against the strong background light are required for the image sensors [2] under real environment such like sunlight. The position sensors and conventional image sensors can obtain the position of the projection light position of active optical sensing system from the position of the peak intensity of the sensor array plane. Therefore, Strong light projection is required for these sensors in real environment, such as outdoor environment with strong sunlight. A high-sensitivity image sensor with background light suppression is required in this case.

In addition to strong background light, as explained in Chapter 1, an attack with a signal modulated by modulation frequency F_A could come from an attacker in outside. The measurement system tries to detect an attack and take an action to avoid the attack with changing

the range of modulation frequency of modulated light that is used in the measurement. If the image sensor can not operate outside the range of the modulation frequency of disguised light used in the attack, it is hard for the measurement system to avoid. In addition, on the system-based countermeasures described in Chapter 1, in order to allow at least one sensor to operate correctly in multiple sensors with different modulation frequencies, the wider the range of modulation frequency that can be selected, the more likely it is that the correct operating sensor will remain.

Selective-signal detection sensors can be one of the solutions to the problems. Many kinds of techniques have been used to design selective-signal sensors in the standard CMOS technology. Correlation pixels in [12, 78] have also been constructed by using differential MOSFET pair mixers and integration capacitors. Some of others smart image sensors have been reported for detecting modulated light [79]. Switched capacitor circuits [14, 80] are used to perform the charge transfers and demodulation functions. However, previous works [12, 14, 78–80] operate at low frequencies ($\leq 10\ kHz$) relatively.

This chapter proposes novel optical sensing system which is based on light-section method with the modulated light and the image sensor and presents an image sensor that have selective-light detection with the background light suppression. For the selective-signal detection from incident lights, a demodulation pixel [46, 61] is employed. And in-pixel charge injection mode suppression circuit, that is called Adaptive Charge Unit (ACU), is employed to prevent the saturation problem by the background light. Demodulation pixel realizes selective-signal detection in high modulation frequency. And Adaptive Charge Unit (ACU) for background light realizes wide dynamic range. The image sensor has been designed,

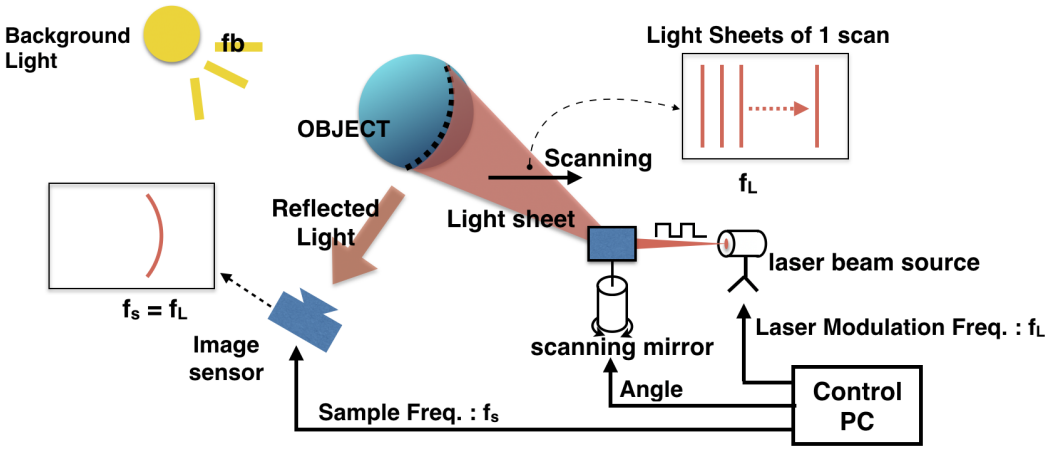

Figure 3.1 Proposed active optical sensing system [13].

fabricated, and successfully measured.

This paper is organized as follows: Chapter 3.2 introduces a proposed optical sensing architecture based on modulation light and triangulation. Chapter 3.3 explains the demodulation pixel and the Active Charge Unit (ACU). Chapter 3.4 describes the specification of our designed and fabricated image sensor and its array structure. Chapter 3.5 discusses the measurement results of our image sensor. Finally, conclusions are mentioned in Chapter 3.6.

3.2 Proposed active optical sensing system

The architecture of the proposed active optical sensing system [13] is described in this section. Proposed active optical sensing system, the image sensor that is employed for selective-signal detection with background suppression, and the operation of the pixel circuit are explained.

3.2.1 System Architecture

Fig. 3.1 shows a proposed active optical sensing system [13] based on a light-section method using modulated light and an image sensor. In this system, the laser light source is modulated by a pulse generator. The modulated light sheet is projected onto the object. And the reflected light from the object go into the image sensor with the background light. The capability to detect the projected light is required in the image sensor of the proposed active optical sensing scheme. The image sensor is controlled by a sampling frequency that is synchronized with the modulation frequency of the laser beam source. The sensor can sense only the reflected light from incident lights.

3.2.2 Seletive-Signal Detection

As mentioned in Eq. 1.3, we assumed that the incident light consists of reflected light, disguised light, and background light. The disguised light and background light in the incident light are not needed for the system because the disguised light disturbs the normal operation and the background light saturates the image sensor. The image sensor needs to receive the only reflected light from incident light. Therefore, the selective-signal detection is required to the image sensor in the proposed system.

3.2.3 Background Light Suppression

The background is always mixed in the incident light as shown in Eq. 1.3. Although the image sensor has the capability of light selectivity, it can be problem for the image sensor to be saturated by background light before sufficient accumulation for signal light in exposure

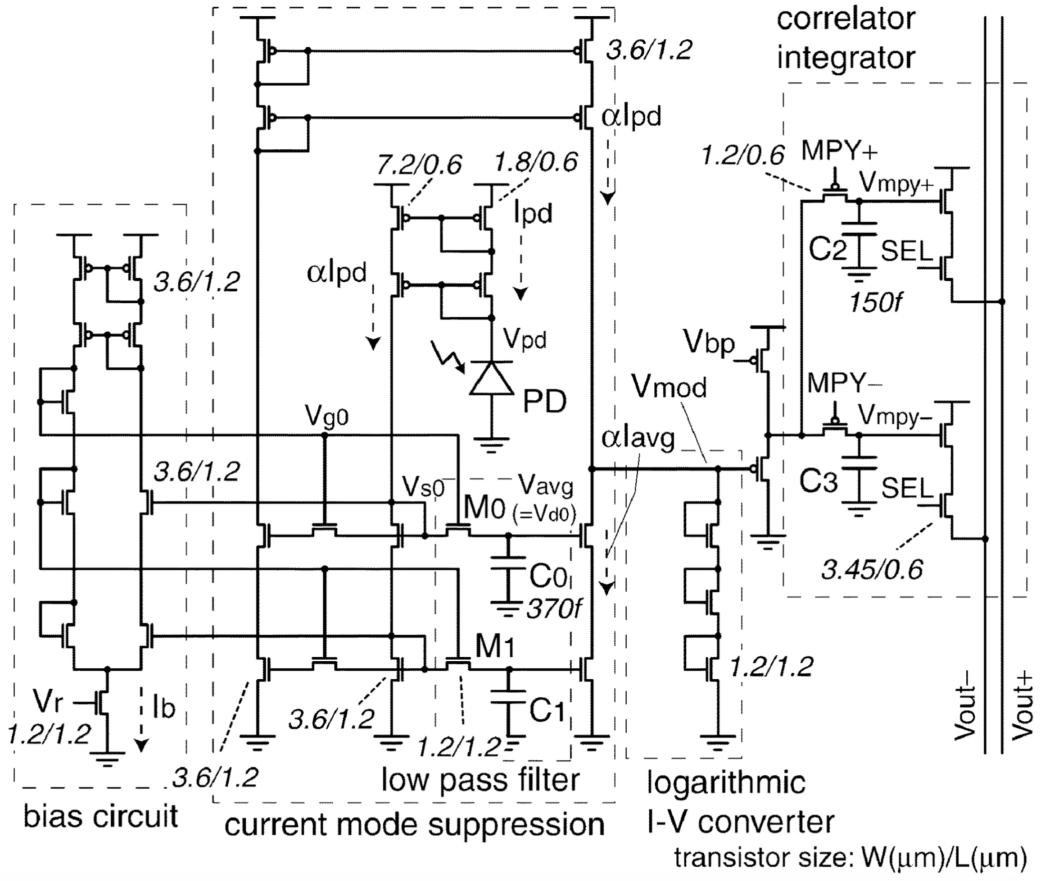

Figure 3.2 circuit of traditional method [14].

time. The background light, as non-signal light, needs to be eliminated for exposure time. Therefore, the image sensor needs to have a circuit for preventing saturation problem in the proposed system.

3.3 Pixel Circuit Realization

As illustrated in Fig. 3.2, traditional method [14] using logarithmic pixel and LPF is insufficient by the reason that is limited sampling frequency range (F_S: 10kHz). This pixel [14] consists of logarithmic pixel, current mode suppression with low-pass filter, and correlator integrator on the signal pass. The current mode suppression is subtraction from V_{mod} to V_{avg}.

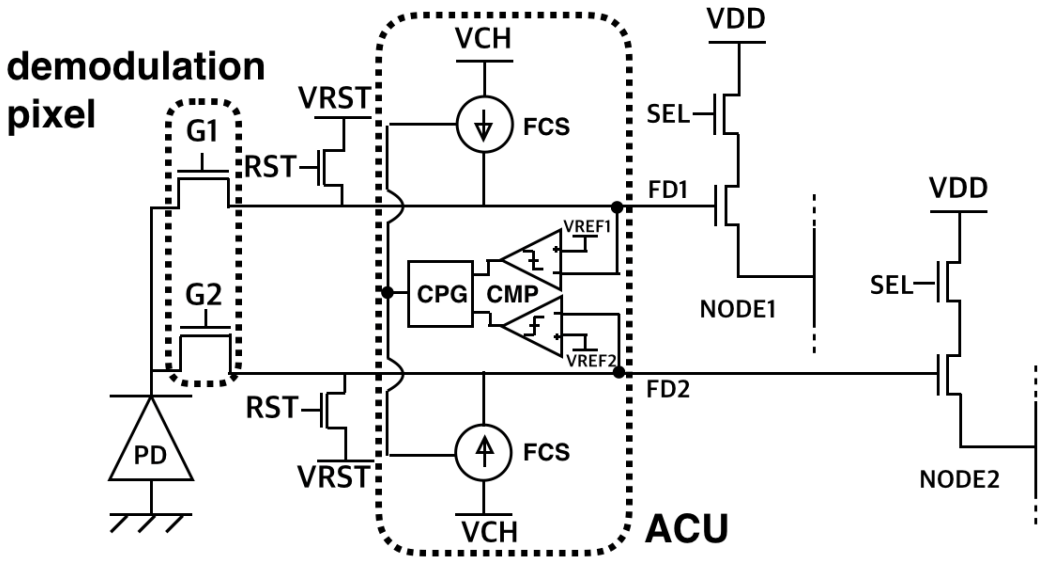

Figure 3.3 Proposed pixel circuit [13].

The time for calculating V_{avg} with low-pass filter is needed. So, sampling frequency is limited by the time constant. But, proposed circuit is more suitable for higher sampling frequency because the circuits on the signal pass are separated to circuit for demodulation and suppression. Fig. 3.3 shows a schematic of the pixel circuit to satisfy the requirement from the proposed optical sensing system. The pixel circuit mainly consists of demodulation pixel and in-pixel charge injection mode suppression circuit that is named the Adaptive Charge Unit (ACU). Demodulation pixel are employed for selective-signal detection. During integration time, ACU in each pixel is employed to suppress the saturation problem. In this pixel circuit, the difference of voltages between NODE1 and NODE2, $V_{NODE2} - V_{NODE1}$, means the value of the light selectivity among incident lights. The higher value of $V_{NODE2} - V_{NODE1}$ means the more synchronous between the sampling frequency and the modulation frequency of the incident light. After integration time, a row is selected. the signals accumulated in FD1

and FD2 are put on the column lines NODE1 and NODE2. the signals are sent to the readout circuit as shown in Fig. 3.12, and the difference voltage between NODE1 and NODE2, $V_{NODE2} - V_{NODE1}$, are calculated in the readout circuit as below.

$$V_{SIG} = V_{NODE2} - V_{NODE1} \tag{3.1}$$

$$V_{NOUT} = A \cdot V_{SIG} \tag{3.2}$$

The differential amplifier NAMP removes the background light component from the two NODEs, amplifies only the signal component. Single-slope ADC converts V_{NOUT} to a digital value. The digital value are stored in flip-flops before the output to the outside of the chip.

3.3.1 Demodulation pixel

The pixel has two gate transistor G1, G2 shown in Fig. 3.3. Fig. 3.4 (a) shows a timing diagram of the sensing scheme. First, when the modulated light is OFF, the reset operation is operated by turning RST on. It is noted that the two reset transistors are connected each other, thus FD1 and FD2 are reset by this operation simultaneously. When the modulated light is turn on, gate transistor G1 is turned on to transfer accumulated charges to the floating diffusion FD1. Then the modulated light is turned off, and gate transistor G1 is turned off and gate transistor G2 is turned on to transfer accumulated charges to the floating diffusion FD2. In ON-state of the modulated light, both modulated and background light components are stored in the floating diffusion FD1. Next, in the OFF-state of the modulated light, only the

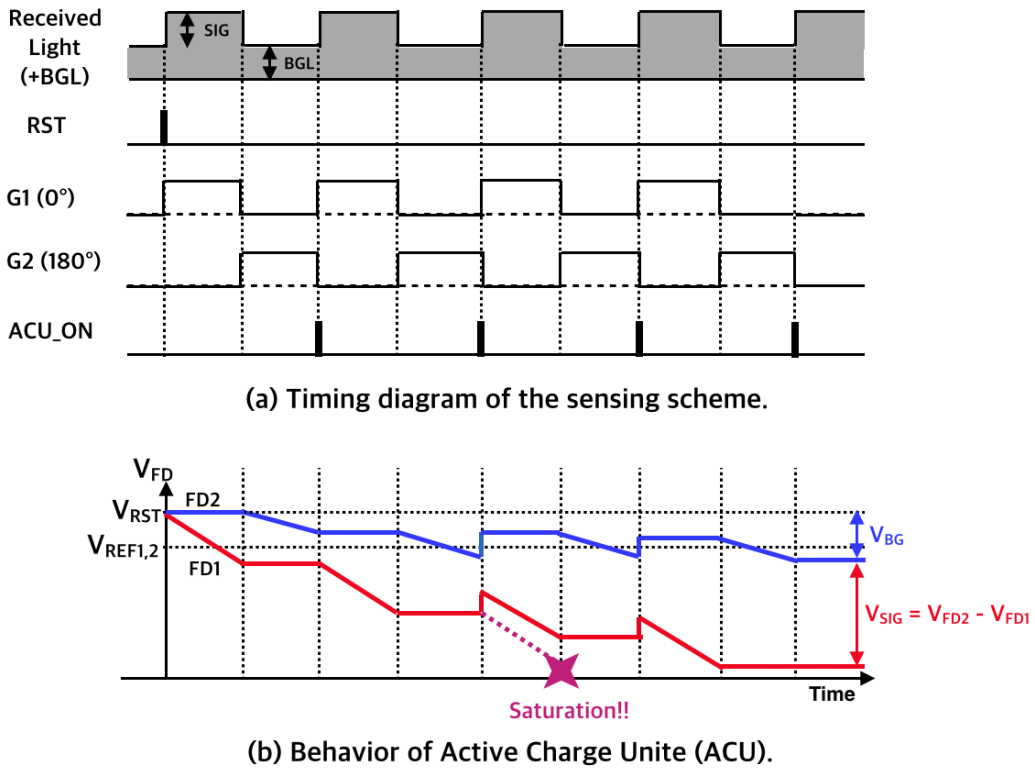

Figure 3.4 Timing diagram of the sensing scheme and Behavior of Active Charge Unit (ACU).

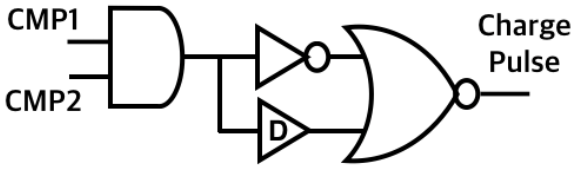

Figure 3.5 Charge Pulse Generator (CPG).

static light component is stored in the floating diffusion FD2. By repeating this process, the charges in the ON- and OFF-states are accumulated in the floating diffusion FD1 and FD2, respectively.

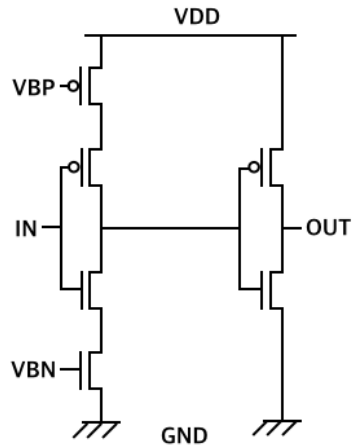

Figure 3.6 Delay unit.

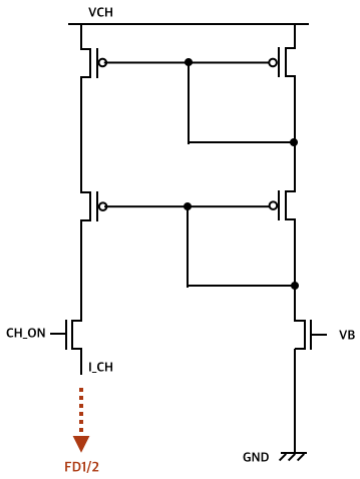

Figure 3.7 FD Charge Source.

3.3.2 Active Charge Unit (ACU)

Active Charge Unit (ACU) prevents the saturation problem by strong background light as illustrated in Fig. 3.4 (b). During integration time, ACU is monitoring the voltage levels of two floating diffusions FD1 and FD2 and performs the charge injection into the two nodes FD1, FD2 when its voltage levels of two nodes are in the specific condition that The voltage of FD1 and FD2 are lower than V_{REF1}, V_{REF2} respectively. ACU consists of two comparators,

Charge Pulse Generator (CPG), FD Charge Source (FCS).

- FD Charge Source (FCS): FD Charge Source (FCS) consists of cascade current mirror, switch and a bias transistor. Fig. 3.7 shows a schematic of the FD Charge Source (FCS). There are two FCSs in the pixel circuit. The FCSs are connected to two floating diffusions FD1, FD2 respectively. The charge amount can be controlled by charge pulse width and the voltage VCH of FCS.

-

- Charge Pulse Generator (CPG): Fig. 3.5 shows a schematic of Charge Pulse Generator (CPG). CPG makes the charge pulse from the output of the comparators. Charge Pulse width can be controlled by Delay Unit described in Fig. 3.6.

- FD Level Detecting using comparators: During exposure time, the two comparators in pixel are monitoring by comparing the voltages of Two node FD1, FD2 with VREF1, VREF2 respectively. When the both the voltages of FD1 and FD2 are lower than the voltages of VREF1 and VREF2 respectively, the outputs of comparators turn on.

During integration time, the ACU operates charge-injection to the two floating diffusion FD1 and FD2 as below,

$$\Delta V_{FD1,2} = \frac{I_{Charge}}{C_{FD1,2}} \times T_{ChargePulseWidth} \tag{3.3}$$

Where, I_{Charge} is the current from FCS (FD Charge Source) to two floating diffusions FD1 and FD2. $C_{FD1,2}$ are constant value from pixel circuit. Then, $\Delta V_{FD1,2}$ can be controlled by only $T_{ChargePulseWidth}$.

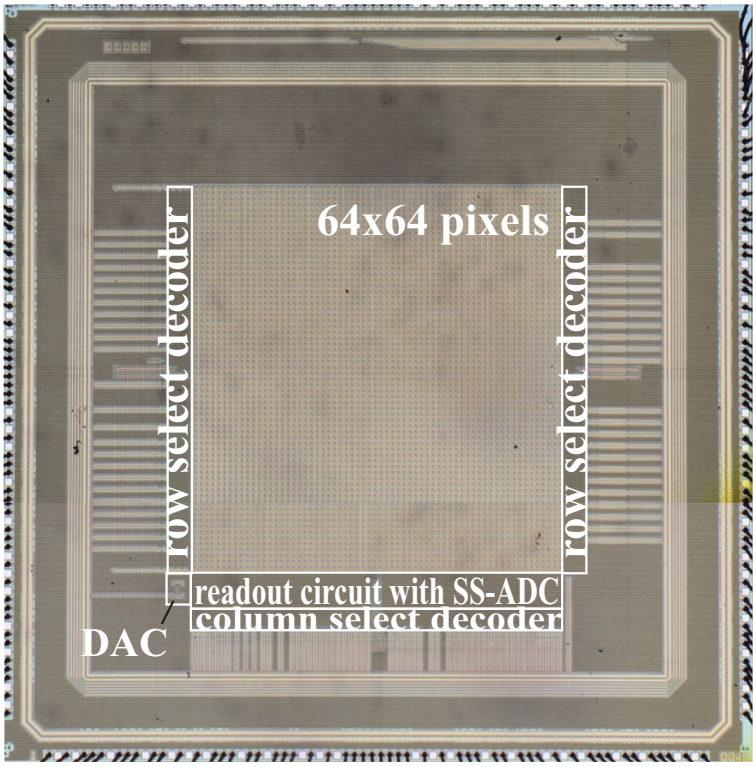

Figure 3.8 Microphotograph of the fabricated chip.

Table 3.1 Specification of fabricated image sensor.

Process	0.18um Standard
Chip Size	$5mm \times 5mm$
Resolution	64×64
Pixel Size	$40 \times 40um^2$
Fill Factor	12.7%
Power Voltage	$3.3V$

3.4 Chip Implementation

The proposed image sensor has been designed and fabricated in 0.18-μm CMOS process. Fig. 3.8 And Fig. 3.9 show a microphotograph of the fabricated image sensor and a layout of the pixel circuit based on 3-T pixel with p-n photodiode respectively. The pixel circuit occupies 40um×40um with 12.7% fill factor. Fig. 3.11 show a structure of the image sensor. It has a 64x64 pixel array with column-parallel 8-bits single slope ADC(SS-ADC) in readout

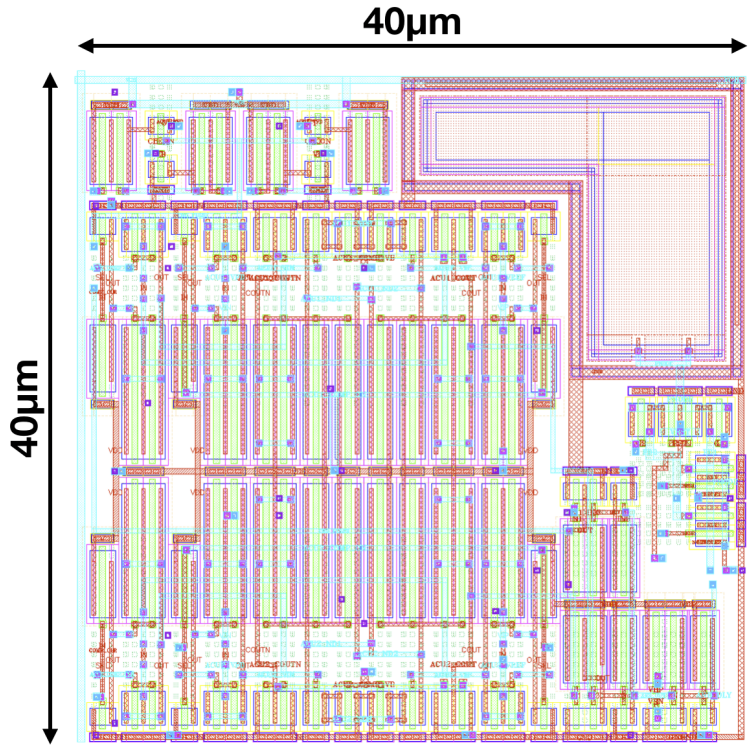

Figure 3.9 Pixel layout.

circuits, row-select address decoder, column-select address decoder, and a DAC. The chip size is 5.18mm×5.18mm. The specification of fabricated image sensor is summarized in Table. 3.1.

3.4.1 3-T Pixel with p-n photodiode

In this impletation, we have employed the 3-T pixel with p-n photodiode because of using the common CMOS process. Fig. 3.10 shows a schematic, cross section, and operation diagram of 3-T pixel with p-n photodiode respectively. As shown in Fig. 3.10 (a), 3-T pixel consists of p-n photodiode and three transistors. The transistors are employed for reset, source-follower AMP, and row select. In most common CMOS process, the method to make a p-n photodiode is to implant an n-layer on top of the p-type substrate as shown in Fig. 3.10

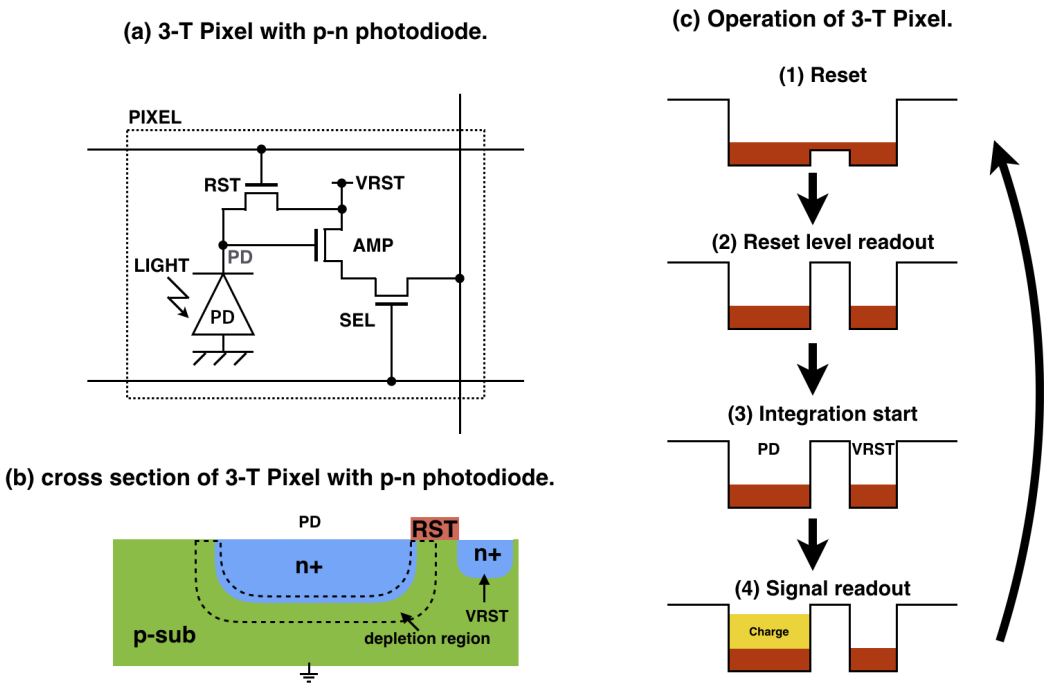

Figure 3.10 3-T pixel with p-n photodiode: (a) Schematic of 3-T pixel, (b) Cross section of p-n photodiode, (c) Operation diagram

(b). The operation procedure of 3-T Pixel has four steps as follows:

1. Reset: The PD node is reset to V_{DD}.

2. Reset level readout: For the correlated double sampling, which cancels the fixed-pattern-noise (FPN) in pixel circuit, V_{PD} is read out.

3. Integration: V_{PD} is decreased by the integration of photocurrents generated in p-n photodiode.

4. Signal readout: V_{PD} is read out through source follower after integration time T_{INT}.

Each pixel have different FPN that is mainly generated from the V_T variation in reset transistor and source follower transistor. V_T variation in reset transistor is removed by subtracting the reset level from the signal level. After the operation procedure of 3-T pixel, V_{OUT} is read out

from 3-T pixel as below:

$$V_{OUT} = V_{RST} - V_{SIG} \tag{3.4}$$

$$= \frac{Q}{C_{PD}} \tag{3.5}$$

Where, Q is the charges generated in a p-n photodiode, and C_{PD} is the capacitance of a p-n photodiode (PD).

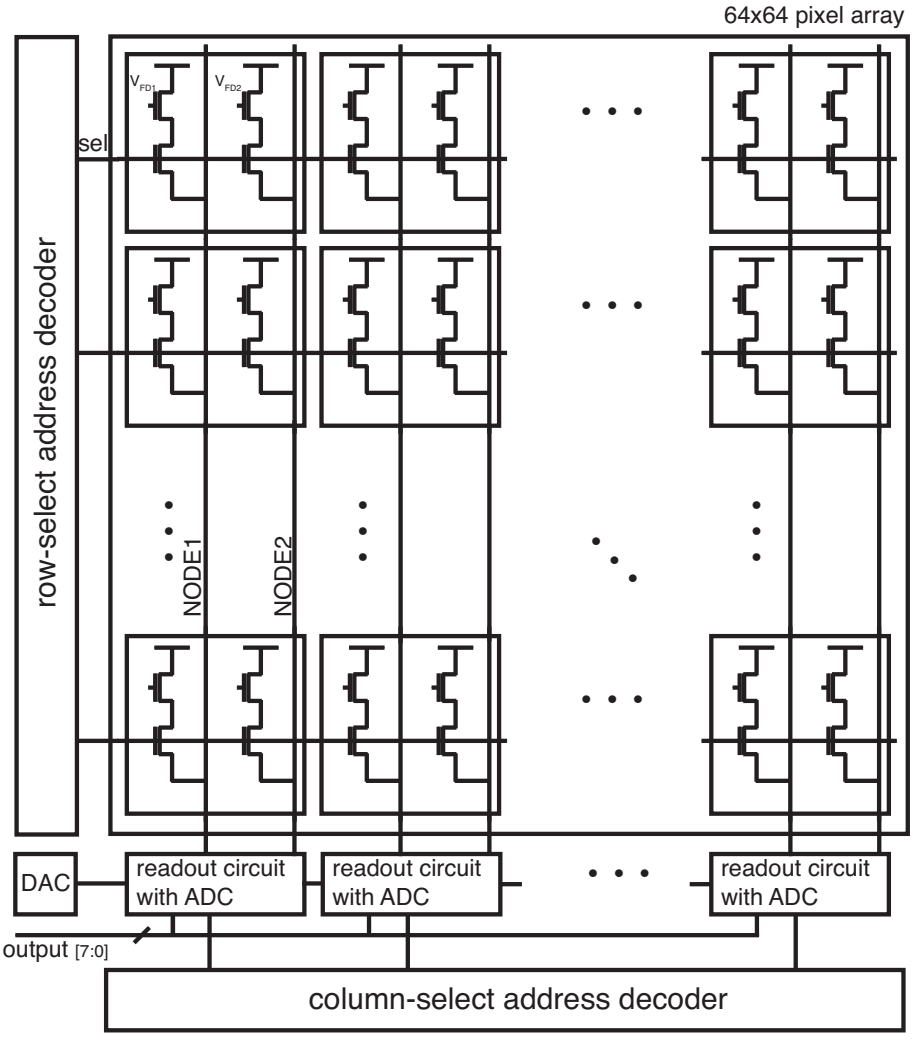

Figure 3.11 Array structure of the image sensor.

3.4.2 Pixel Array Structure

Fig. 3.11 is an array structure of the image sensor. The image sensor consists of an 64×64 pixel array of the present pixel circuit, a row-select address decoder, a column-parallel readout circuit with SS-ADC, a column-select address decoder, and a DAC. A specific pixel can be scanned and selected by the row-select and column-select address decoder. After analog-to-digital conversion using column-parallel SS-ADC, its digitized values can be acquired from outside of chip.

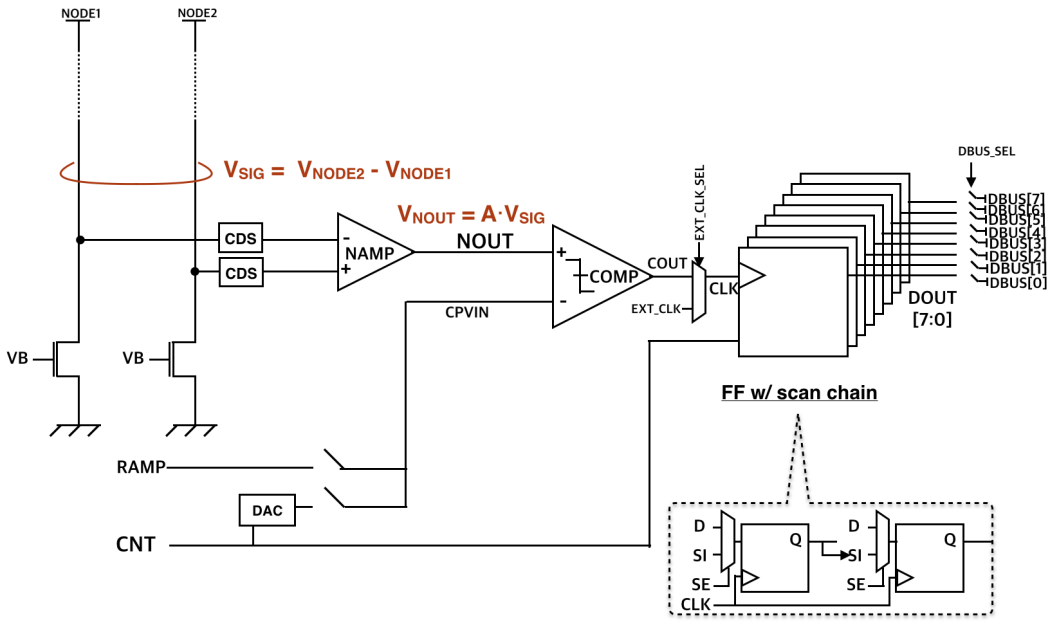

Figure 3.12 Schematic of the readout circuit.

3.4.3 Readout circuit

Fig. 3.12 shows a schematic of the readout circuit. Readout circuit consists of column-parallel single-slope ADC, 8-bit FFs, a differential amplifier and switches for readout to outside of the chip. The difference voltage between NODE1 and NODE2 is amplified at

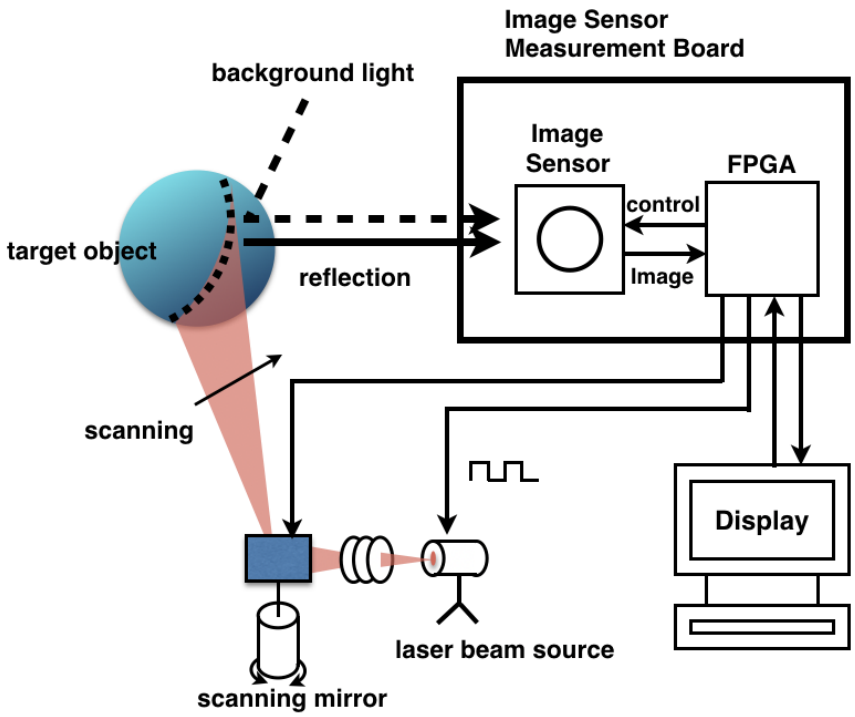

Figure 3.13 Measurement system structure.

the differential amplifier. The output of the differential amplifier is compared with the ramp signal from the DAC or outside of the chip. When the output of amplifier overwhelms the ramp signal, the output of comparator turns '1' to '0' and the 8-bits FFs latch the counter value at that time and keeps the values. After ADC process, the digitized data in each column readout circuits are addressed to digital data bus outside of the chip in sequence.

3.5 Measurement Results

3.5.1 Measurement Setup

As shown in Fig. 3.13, the measurement system of the fabricated sensor has been constructed. It consists of a laser source (wavelength 670 nm), the fabricated sensor with a lens mounted on a test board with FPGA as shown in Fig. 3.14, a pulse generator, a light projector

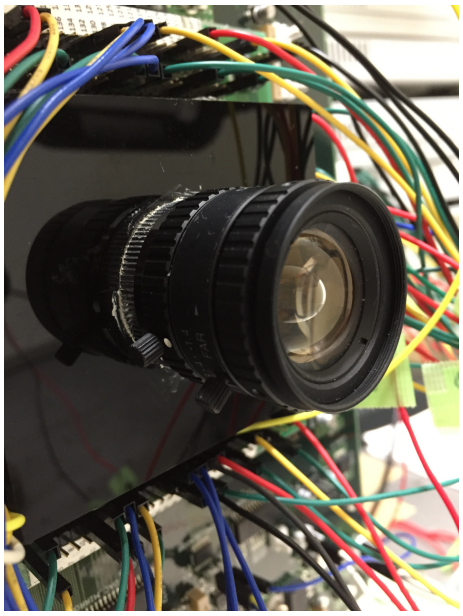

Figure 3.14 Photograph of the sensor with lens on a test board

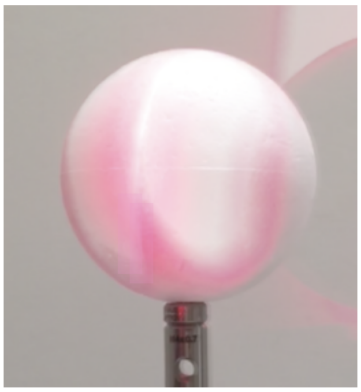

Figure 3.15 target of measurement: a white ball.

for ambient illumination, and a lux meter. The sensitivity, the dynamic range, and the selectivity of the fabricated sensor are evaluated with the measurement system. The target of the measurement is a white ball shown in Fig. 3.15. Fig. 3.17 shows the timing diagram of the control signals in this measurement. The integration time is 100*um*. The light source uses modulated light with modulation frequency from 1 kHz to 60 kHz. For gate control, the sampling frequency is fixed to 10 kHz, the gate G1 is set to the sampling frequency with phase

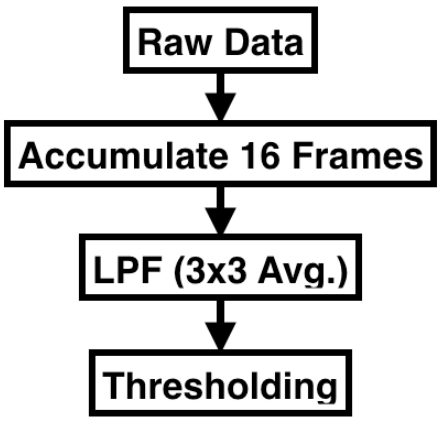

Figure 3.16 Procedure of Post-processing.

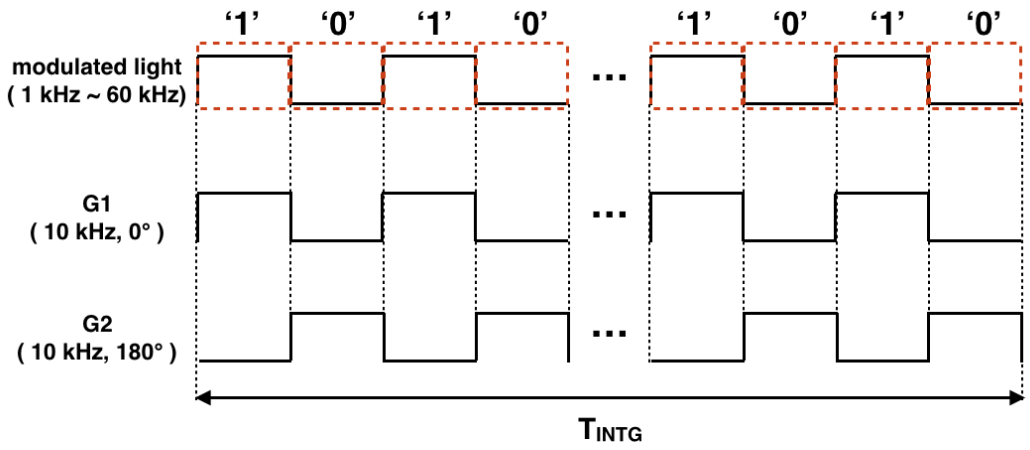

Figure 3.17 Timing diagram of sinusoid gating with sinusoid light.

0°, and the gate G2 is set to the sampling frequency with phase 180°. Fig. 3.16 shows the procedure of post-processing for measurement. After accumulating and averaging 16 frames for temporal low pass filtering, 3x3 average spatial filter is performed for spatial low pass filter. The peak values are obtained by thresholding as shown in Fig. 3.18.

3.5.2 Selective Light Detection

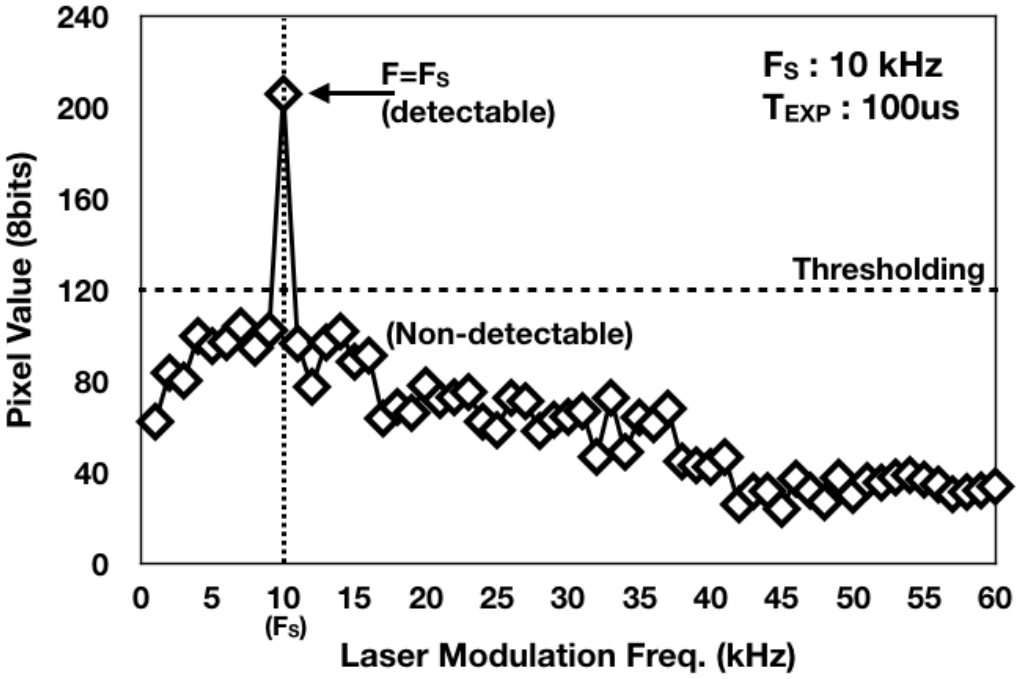

Figure 3.18 Selective-Signal Detection.

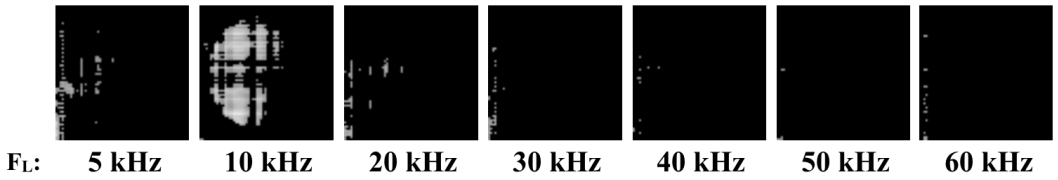

Figure 3.19 Output images when sampling frequency F_S is 10 kHz with various laser frequency F_L.

The ADC output from readout circuit at various incident light frequencies is shown in Fig. 3.18. In this measurement, the sampling frequency F_S is 10kHz and the exposure time T_{EXP} is 100us. Only when the sampling frequency F_S is equal to the frequency of the modulated light, the ADC output becomes a peak and the incident light with the other frequencies is suppressed as shown by Fig. 3.18. By employing a set of laser frequencies such as 10, 20, and 40 kHz, the proposed sensing scheme has high sensitivity for a multiple light projection

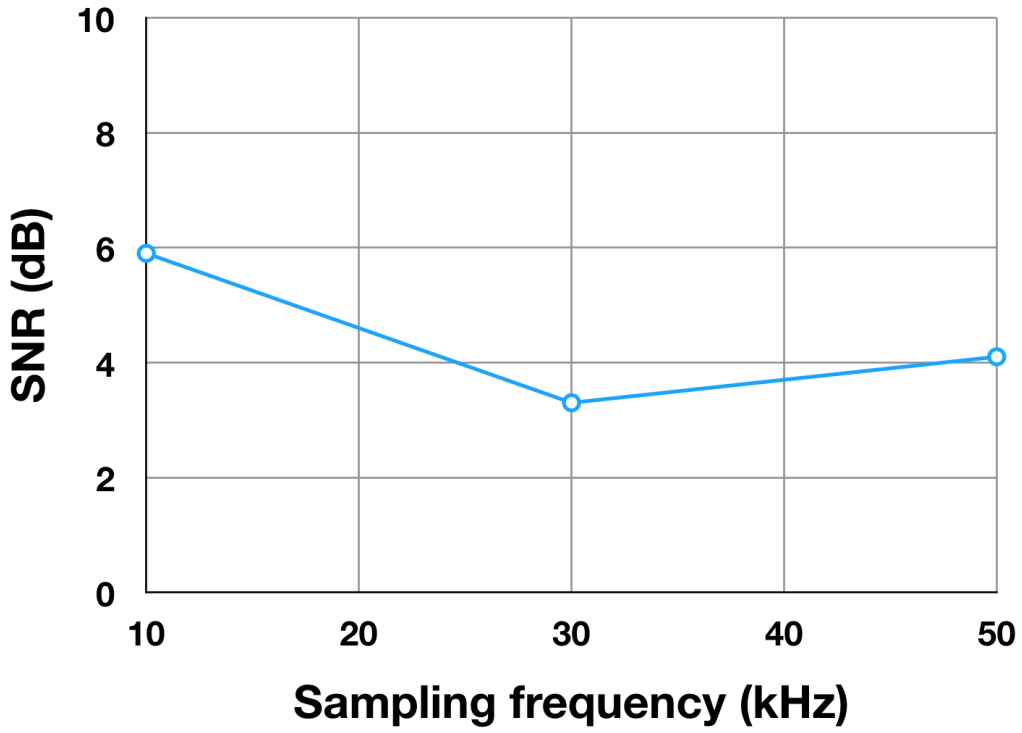

Figure 3.20 Maximum sampling frequency and SNR of selective-signal detection

system. When sampling frequency F_S is 10 kHz with various laser frequency F_L such as 5, 10, 20, 30, 40, 50, 60 kHz, the output images are shown in Fig. 3.19. Fig. 3.20 shows the relationship between sampling frequency and SNR. In the experiment, the maximum sampling frequency is 50 kHz. And the maximum SNR is 5.9 dB at sampling frequency 10 kHz.

3.5.3 Signal Background Ratio and Dynamic Range

Fig. 3.21 shows the relationship between the intensity of background light and the minimum projected light intensity that can be detected. In the measurement of the signal-to-background ratio and dynamic range, the integration time is $100us$. Both the modulation frequency F_L and the sampling frequency F_S are $10kHz$. For evaluation of the sensitivity of the image sensor, the intensities of the projected light and the background light are measured

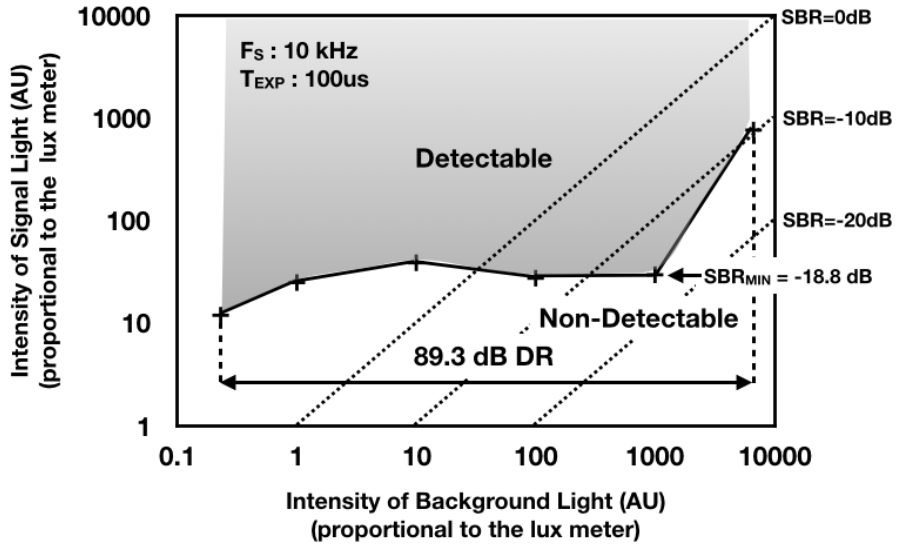

Figure 3.21 Signal Background Ratio (SBR) and Dynamic Range.

by lux meter. The minimum signal-to-background ratio (SBR) means the sensitivity of the image sensor. The Signal-to-background ratio (SBR) [81] is defined as below.

$$SBR = 20log\frac{I_{SIG_{MIN}}}{I_{BG}} \tag{3.6}$$

Fig. 3.21 shows that the present image sensor can detect the projected light that can be weaker than the background light. It means that the present image sensor can suppress the background light. The minimum signal-to-background ratio (SBR) is -18.8 dB. The dynamic range is 89.3 dB.

3.5.4 Comparison and Discussion

Because of different parameters which are relevant depending on the application, an overall comparison with the previous researchs [14, 61] is very difficult. The measurement results

Table 3.2 Measurement Results and Comparison.

Parameters	[14]	[61]	This Work
BGL* Suppression Technique	Current mode + correlation	Separation of AA⋆ & FD	Charge Injection
SBR (dB)	-22.8	NA	-18.8
BGL DR (dB)	100	25	89.3
Maximum sampling frequency (kHz)	10	2.5	50

BGL* : Background light

AA⋆ : accumulation area

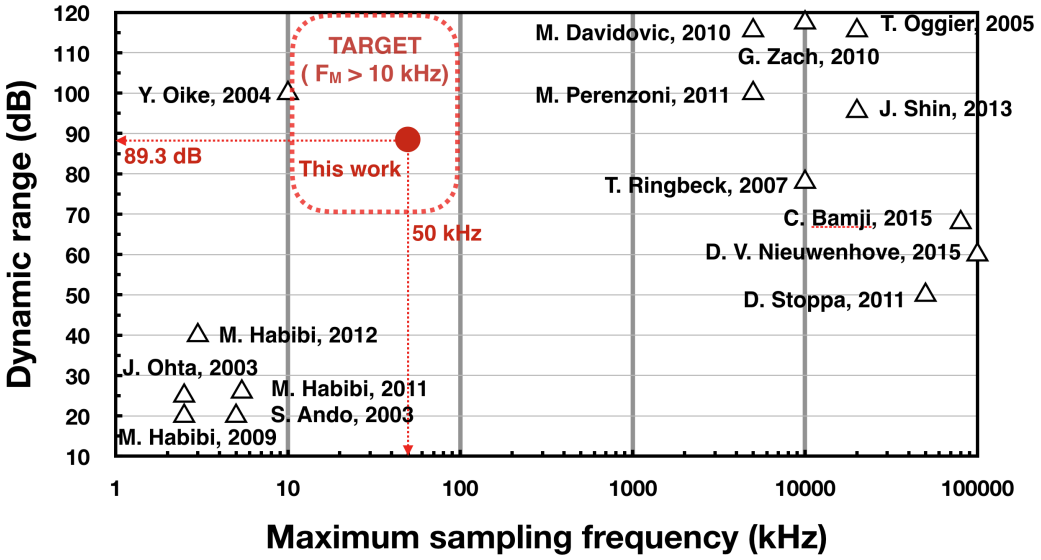

Figure 3.22 Comparison with previous works on image sensors with in-pixel selective-signal detection.

are summarized and compared in Table 3.2.As shown in comparison table with [14, 61], this work has the maximum modulation frequency that is higher than [14, 61]. However, the present image sensor has less SBR than -22.8 dB SBR reported in [14], less dynamic range then [14]. Fig. 3.22 shows the position of this work in comparison with previous works on image sensors with in-pixel selective-signal detection. The position of this work is

located in the higher range in terms of modulation frequency than in previous studies, and it is located near 100 dB in terms of dynamic range. In terms of the modulation frequency, this image sensor has more potential to be applied for secure sensing and high-speed applications such as visible light communication system such as Vehicle-to-Everything communication system [82–85], beacon system [86].

3.6 Summary

A optical sensing system, which is based on light-section method with the modulated light and the image sensor that can detect the selective-signal light modulated by specific frequency, has been proposed. For selective-signal detection, the demodulation pixel are employed in pixel circuit. To avoid saturation for wide dynamic range, Adaptive charge unit (ACU) in each pixel is introduced. And the image sensor has been designed, fabricated and successfully measured. The signal selectivity of the image sensor is confirmed from the measurement. The minimum SBR, the dynamic range, and the maximum modulation frequency of the image sensor are -18.8 dB, 89.3 dB, 50 kHz respectively in measurement. The image sensor achieved wider modulation frequency range than previous works.

Chapter 4

An image sensor with compensation of background light using current mirror

4.1 Introduction

Many applications using active optical sensing have been broadly used for living support (Ambient Assisted Living), industrial inspection, robot vision, security, automatic driving, mobile equipment, games etc. in recent years. Especially in automotive industry, active optical sensing method was widely employed for AEB (Auto Emergency Braking), automatic driving etc in outdoor environment. In real environment, the ambient light is often much stronger than the projected light and reflected light. In the case of the sun on a sunny day, the light intensity is from 100 klx to 200 klx, that is 10^2 to 10^5 times bigger than projected light source in active optical sensing system [2]. Under this situation, both reliability and stability against strong background light are required.

Even on sunny days, The acquisition of three dimensional data in some applications of active optical sensing such as three dimensional range-finding system is disturbed [2]. For example, Kinect [19, 20], which is a game console, sometimes does not operate properly under strong sunlight. Strong background light has the following two effects on the image sensor of active sensing scheme such as the three-dimensional measurement system and causes the

measurement error: (1) noise increase and (2) saturation. Considering measurements in real environments except planned and restricted places such as laboratories and indoor studio, strong background light is a big problem to the image sensor.

A method of background light suppresstion using an optical method [63] has also been proposed, but it is insufficient. Strong background light has two major effects on the image sensors in active optical sensing systems, which are measurement noise increase and saturation of the image sensor, which cause distance error. In order to satisfy to the demands for high operational reliability in the outdoor as mentioned above, particularly to strong background light, some pixel circuits [14, 87] in the field of sensor devices are introduced. But these image sensor have complicated structures, and their pixel sizes and poor SBR (Signal-to-Background light Ratio) are problematic for high-resolution application in strong background light. Therefore, in this chapter, An image sensor to detect selective-signal is required with more compact pixel circuit and better SBR.

In this chapter, we propose active optical sensing system using modulated light. The modulated light and the demodulation pixel used in the system are explained in Chapter 4.2. In Chapter 4.3, the basic pixel is introduced. And the structure and the behavior of the pixel are explained. In Chapter 4.4, the cause of current duplication error in current mirror of the basic pixel circuit is analyzed and the two types of current duplication error improved pixel circuits are introduced. In Chapter 4.6, chip implementation is mentioned. The evaluation results on simulation are showed in Chapter 4.7. Finally we discuss the conclusion and future works.

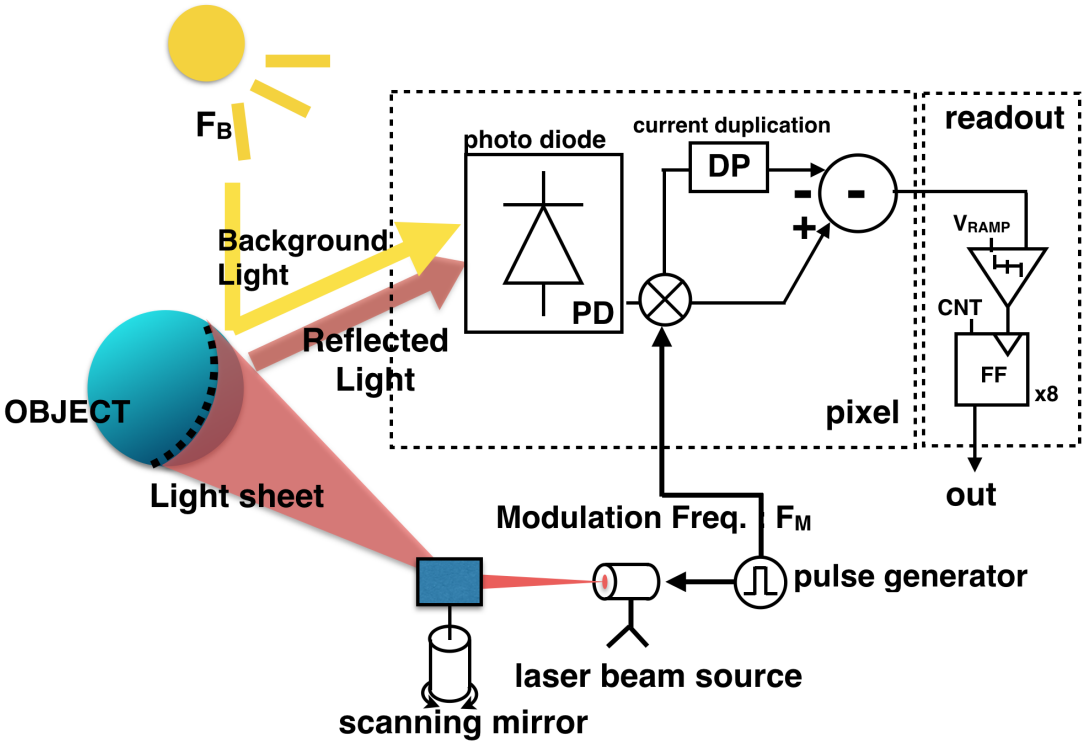

Figure 4.1 Proposed active optical sensing system.

4.2 Proposed active optical sensing system

4.2.1 Structure of the proposed system

Fig. 4.1 shows the active optical sensing scheme proposed for high sensitivity and wide dynamic range. The proposed system consists of laser beam source, scanning mirror, an image sensor, and control PC/FPGA to control laser beam source. In the active optical sensing scheme, a sheet laser light source modulated by a pulse generator is projected on a target object. Scanning the sheet laser light on the object is operated by rotation of scanning mirror. The image sensor receive both the background light and the reflected light of the projected light from laser source.

4.2.2 Selective-Signal Detection

As mentioned in Eq. 1.3, the incident light consists of reflected light, disguised light, and background light. From incident light, the image sensor needs to accumulate the only reflected light among the incident light. Therefore, in the proposed scheme, the capability of detecting a selective-signal is required to the image sensor.

4.2.3 Background Light Suppression

As shown in Eq. 1.3, the dc-level background also is always mixed in the incident light. Though the image sensor has the function of selective-signal detection, it can be problem for the image sensor that has been saturated by background light before accumulating selective-signal sufficiently in integration time. The background light, as non-signal light, needs to be eliminated for integration time. Therefore, the image sensor needs to have a countermeasure for preventing saturation problem in the proposed system.

4.3 Pixel Circuit Realization

4.3.1 Proposed Basic Pixel Circuit

Fig. 4.2 shows the basic pixel circuit. The pixel circuit consists of a reset gate transistor, a demodulation pixel, a current mirror circuit with sample and hold circuit, source follower amplifier and switch transistor for row selection. The circuit has two transfer gate transistors, BGS and INTG that are employed for selective-signal detection. The current mirror circuit has sample and hold circuit and charge absorber transistor BGS_N The current mirror circuit is employed to prevents saturation of the pixel circuit by flowing duplicated I_{BG} through

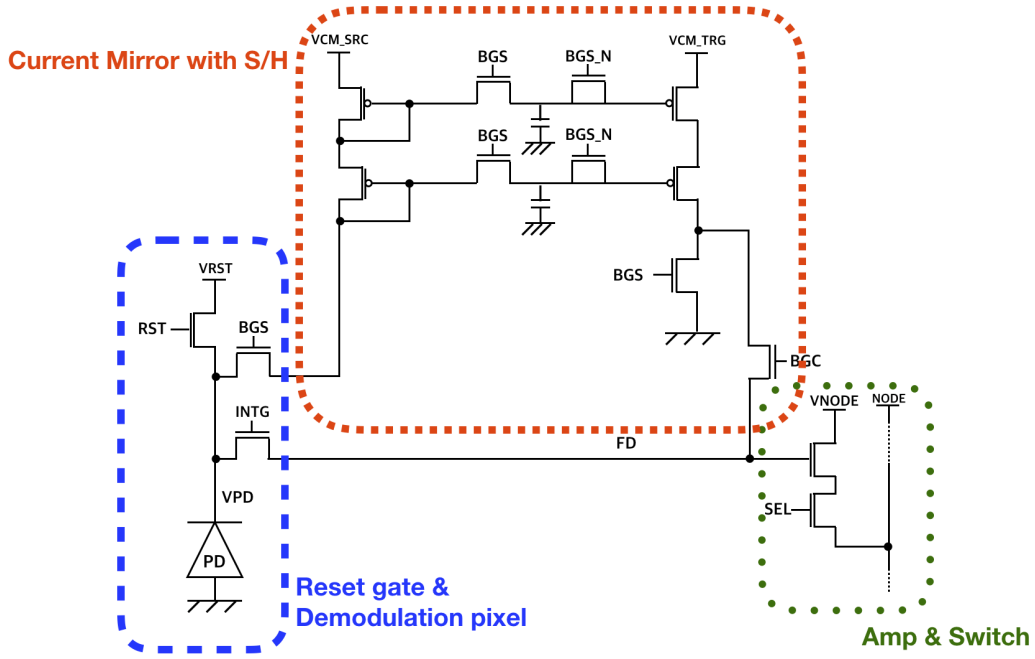

Figure 4.2 Schematic of the pixel circuit.

the gate transistor BGC into node FD during integration time under strong background light. Additionally, by employing the current mirror circuit, it was possible to suppress the background light without in-pixel monitoring and calculate only the signal light component within the pixel simultaneously, thereby reducing the number of transistors in the pixel.

4.3.2 Operation Mode

Fig. 4.4 illustrates the control timing diagram of the proposed pixel circuit. The control mode has two modes: (1) The first mode is the sampling mode that samples and duplicates I_{BG}, the photocurrent by background light; (2) The second mode is an INTG mode that is the integration mode that accumulates I_{SIG} while the current mirror circuit compensates duplicated I_{BG} to node FD. The duplicated I_{BG} is duplicated at the sampling mode. After two

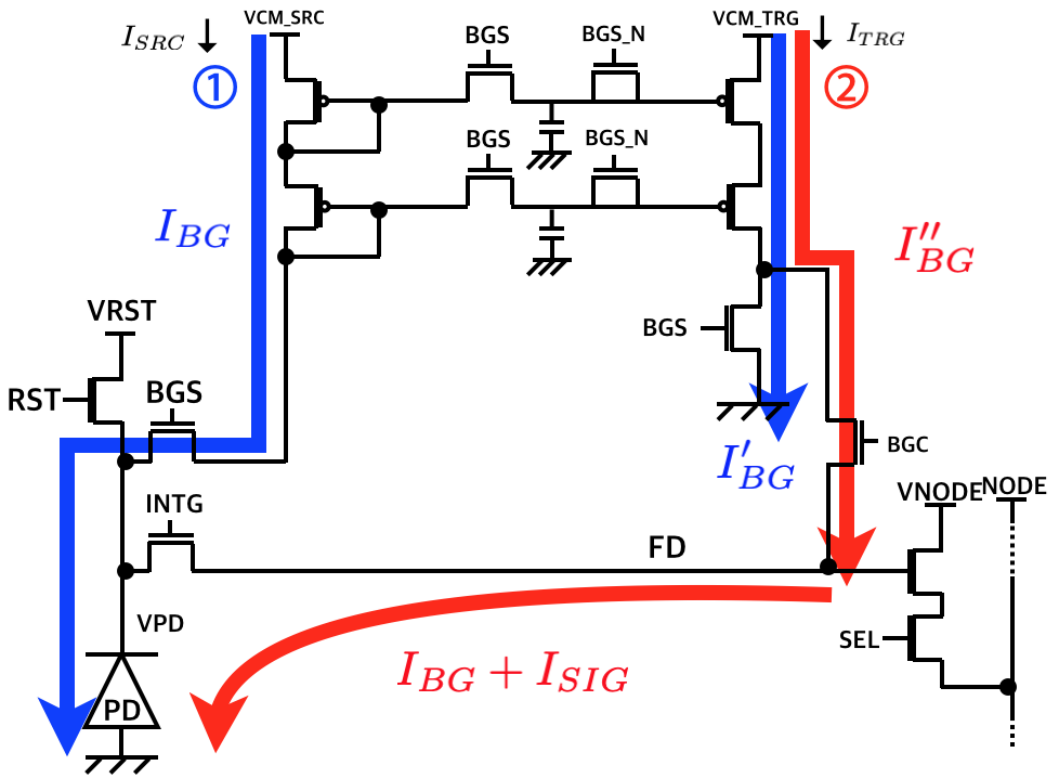

Figure 4.3 Diagram of operation mode: ① Sampling background light, ② Integrating signal with compensation of background light.

modes are done, the voltage variation of node FD is expressed as follows:

$$\Delta V_{FD} = \frac{I_{TRG} - (I_{BG} + I_{SIG})}{C_{FD}} = \frac{I''_{BG} - (I_{BG} + I_{SIG})}{C_{FD}} \tag{4.1}$$

Where I'_{BG} is the duplicated I_{BG} at the sampling mode and is equal to I_{BG} ideally. And C_{FD} is a capacitance of node FD. When I_{BG} and I''_{BG} are same value, ΔV_{FD} are caused by only I_{SIG}. In Eq. 4.1, if the condition as below is assumed:

$$\text{IF } I_{BG} = I'_{BG} = I''_{BG} \tag{4.2}$$

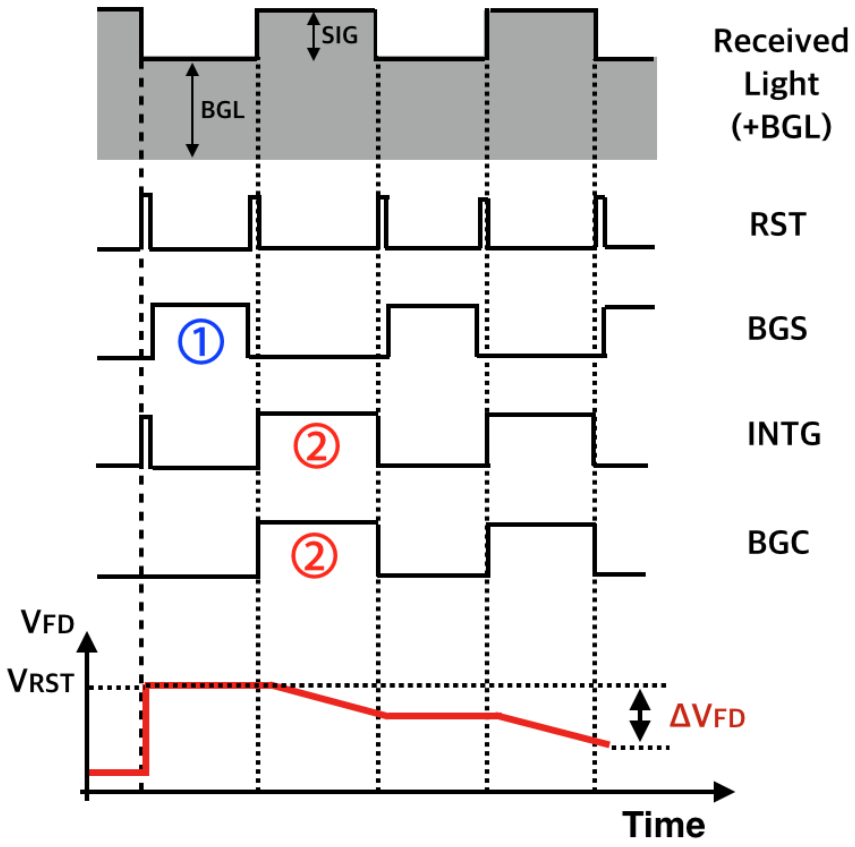

Figure 4.4 Timing Diagram: ① Sampling background light, ② Integrating signal with compensation of background light.

I_{BG}, I'_{BG}, and I''_{BG} flows through the three paths shown in Fig. 4.3. These all are equal to the background light induced photocurrent. If I_{BG}, I'_{BG}, and I''_{BG} are equal, the background light component is cleanly removed. Therefore, Eq. 4.1 is re-written as below:

$$\Delta V_{FD} = \frac{I''_{BG} - (I_{BG} + I_{SIG})}{C_{FD}} = \frac{I_{BG} - I_{BG} - I_{SIG}}{C_{FD}} = -\frac{I_{SIG}}{C_{FD}} \tag{4.3}$$

Eq. 4.3 means that the photo current by background light is canceled, and the photo current by only signal light is integrated in floating diffusion FD. This operation is repeated N times. The value of FD is read out to readout circuit.

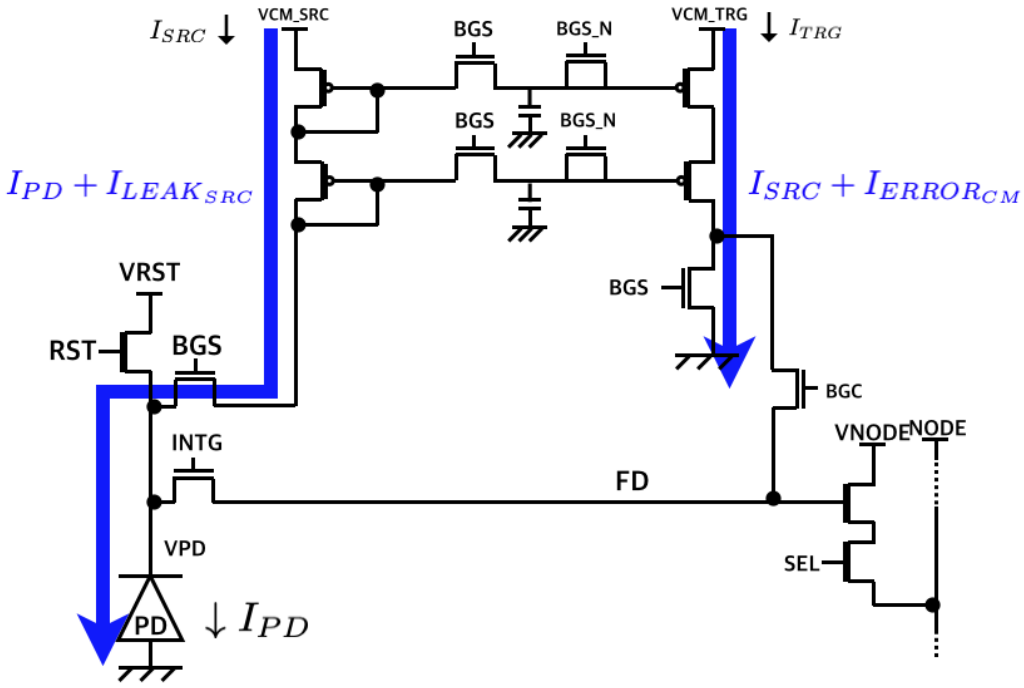

Figure 4.5 Current I_{SRC} and I_{TRG} in sampling mode.

4.4 Analysis of duplication error

4.4.1 Current error in current mirror circuit

Fig. 4.2 shows that the current mirror circuit in the proposed pixel circuit has sampling gate transistors and charge absorber transistors that are different from normal current mirror. These sampling gate transistors and charge absorber transistors cause the current duplication error in current mirror. In these additional circuits, some leakage currents are generated at its transistors.

Fig. 4.6 shows the relationship between the total current error in current mirror and the photocurrent by background light, I_{BG}. The solid line in Fig. 4.6 is the error of duplicated current between I_{BG} and I'_{BG} in the proposed pixel circuit illustrated in Fig. 4.2. The error is over 30 pA on all cases of I_{BG}. It means that the leakage current in current mirror circuit

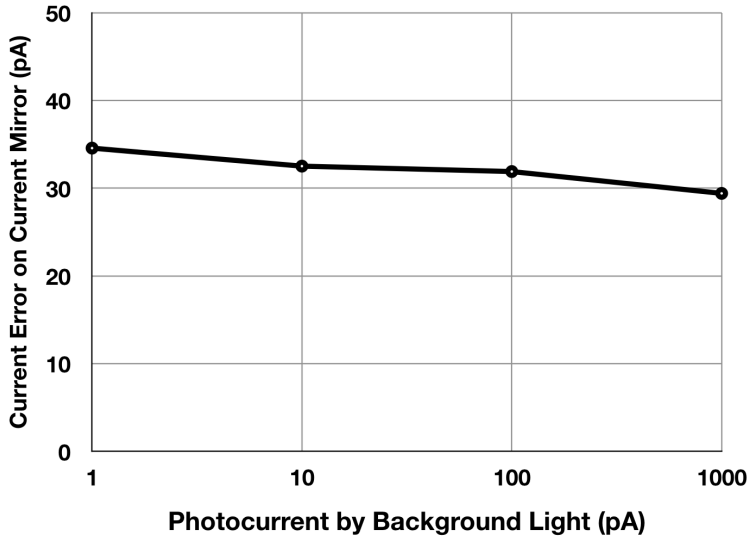

Figure 4.6 Current Error in Current Mirror Circuits.

is over 30 pA. Considering the amount of photocurrent I_{PD}, the leakage current cannot be ignored . This error of current mirror lowers the performance of the pixel circuit. When the photocurrent is lower than the error current of the current mirror, the photocurrent is not integrated normally in the proposed pixel circuit.

For the analysis of the error current, the current I_{SRC} on source node and I_TRG on target node in current mirror circuit can be definde as below:

$$I_{SRC} = I_{PD} + I_{LEAK_{SRC}} \tag{4.4}$$

$$I_{TRG} = I_{SRC} + I_{ERROR_{CM}} \tag{4.5}$$

Where, I_{PD} is the current through the photo diode. $I_{LEAK_{SRC}}$ is the total leakage current on source node in current mirror circuit. $I_{ERROR_{CM}}$ is the duplication error between source node and target node. Based on Eq. 4.5, The total current mis-matched error on current mirror

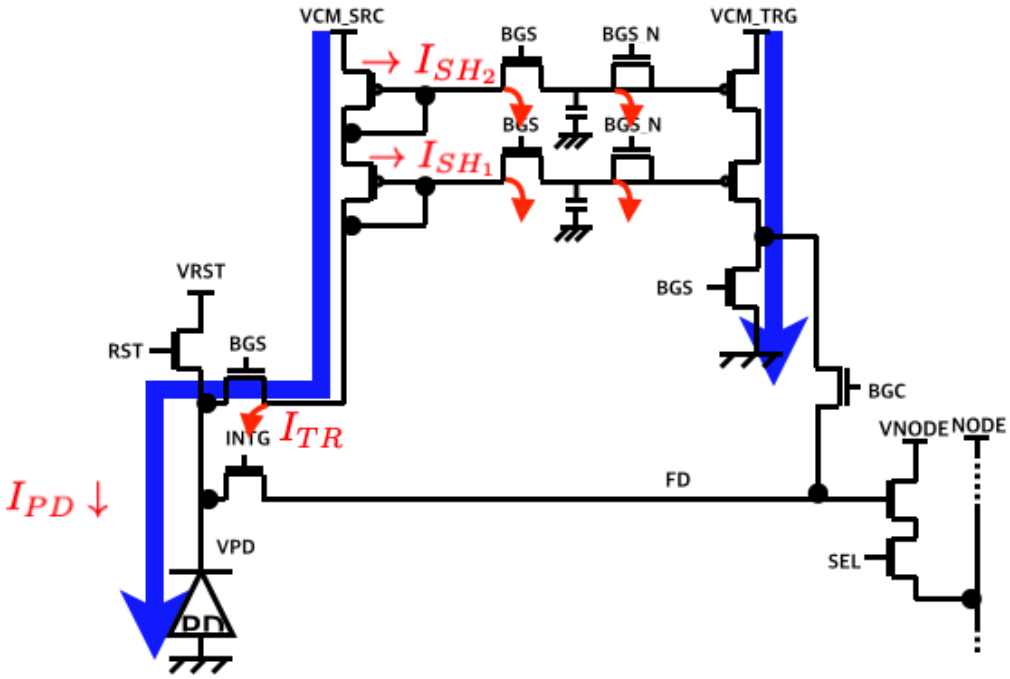

Figure 4.7 Leakage currents at transistors on source node.

circuit can be written as below:

$$I_{ERROR_{TOTAL}} = |I_{TRG} - I_{PD}| \tag{4.6}$$

$$= |I_{LEAK_{SRC}} + I_{ERROR_{CM}}| \tag{4.7}$$

Eq. 4.7 shows that the total error current consist of $I_{LEAK_{SRC}}$ and $I_{ERROR_{CM}}$. Therefore, it is necessary for enhancing the basic pixel circuit to reduce $I_{LEAK_{SRC}}$ and $I_{ERROR_{CM}}$.

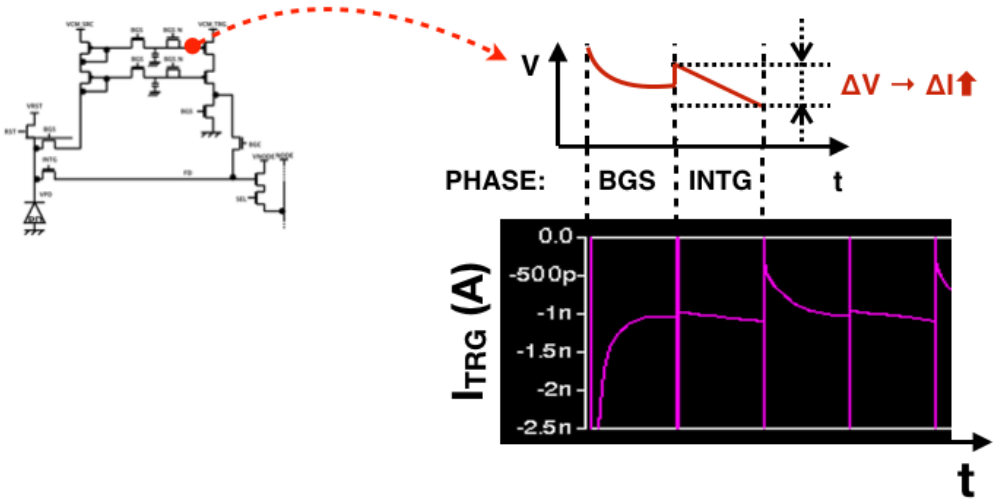

Figure 4.8 S/H level decreased by leakage currents (I_{BG}: 1nA, F_S: 10 kHz).

4.4.2 Cause and effect of leakage currents

The leakage currents through the transistors on source node in the current mirror are shown in Fig. 4.7. The current on source node, I_{SRC}, is consisted of as below:

$$I_{SRC} = I_{PD} + I_{TR} + I_{SH_1} + I_{SH_2} \tag{4.8}$$

Where, I_{PD} is the photo current through the photo diode. And I_{TR}, I_{SH_1}, and I_{SH_2} is the leakage current through the transfer gate transistor, sample and hold path 1, and sample and hold path 2 respectively. On the sample and hold path, the leakage currents are also generated at transistor for sampling and transistor for charge absorber. The target current, I_{TRG}, duplicates the current on source node including these leakage current. Therefore, the more current flows on the target node than the photo current generated at photo diode. Moveover, the leakage currents on source node decrease the voltage level of the sample and hold path in current

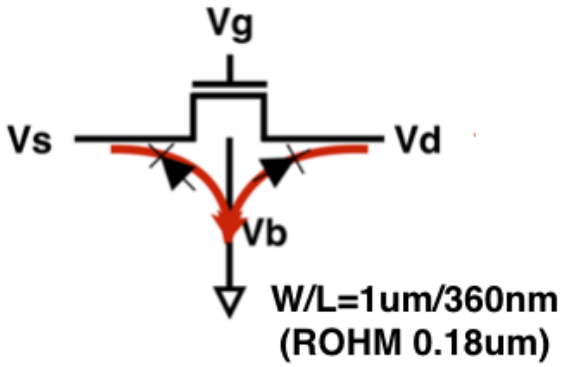

Figure 4.9 Leakage current on MOSFET (in simulation).

mirror as shown in Fig. 4.8. By the leakage currents, I_{SH_1}, I_{SH_2}, the voltage level sampled and hold in BGS phase lowers in INTG phase. Then, the gate voltage of the PMOS transistor in current mirror lowers as well. As a result, the current on target node of current mirror, I_{TRG}, increases slightly in INTG phase. Considering the leakage current and the duplication error, Eq. 4.2, Eq. 4.3 could be re-written respectively as below:

$$I_{BG} + I_{ERROR_{TOTAL}} = I_{BG} + I_{LEAK_{SRC}} + I_{ERROR_{CM}} = I''_{BG} \tag{4.9}$$

$$\Delta V'_{FD} = -\frac{I_{SIG} - I_{ERROR_{TOTAL}}}{C_{FD}} \tag{4.10}$$

In real condition, $I_{ERROR_{TOTAL}}$ is lager than 0. Eq. 4.10 means that $\Delta V'_{FD}$ is less than ΔV_{FD} in ideal condition.

The cause of the leakage current on transistors is a current by reverse bias PN junction as shown in Fig. 4.9. The parasitic current is generated as leakage current at sample and hold path in current mirror. In HSPICE simulation, when the bias voltage V_B of the MOSFETis 0

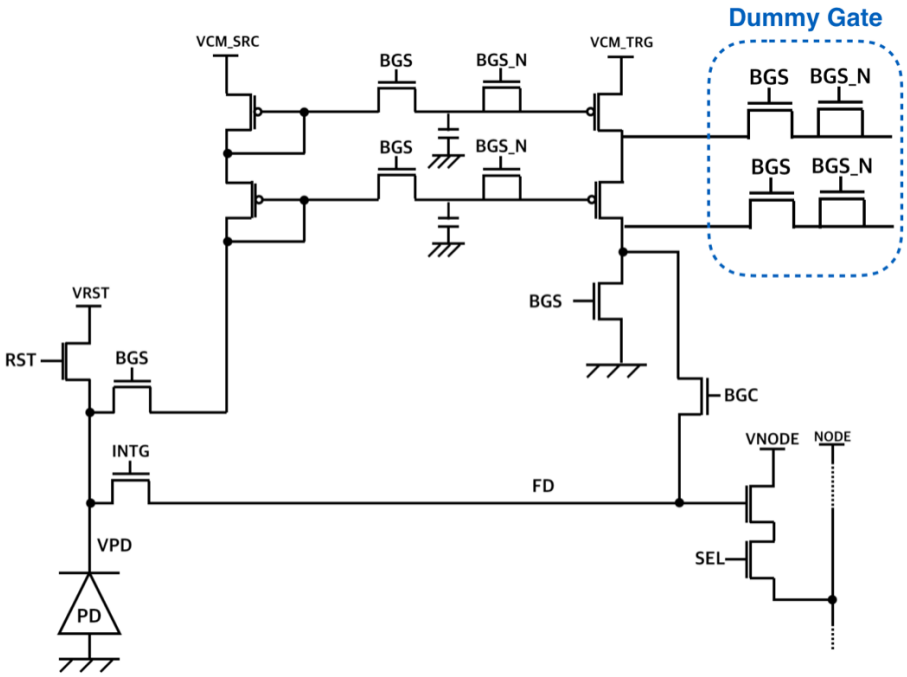

Figure 4.10 Current Mirror with Dummy Gates (Type A)

V and the drain voltage V_D is between 1.5 and 2.5 V, the leakage current is generated between 3 and $8pA$.

4.5 SBR-Enhanced Pixel Circuit

We further propose two types of pixel circuit which corrects the error of the current mirror mentioned in Chapter 4.4. The first type is pixel circuit with dummy gates (Type A) to reduce the influence to floating diffusion voltage V_{FD} from the error of current mirror. The Second type is pixel circuit with separated bias voltage V_B to minimize the leakage current at the transistors in the pixel circuit.

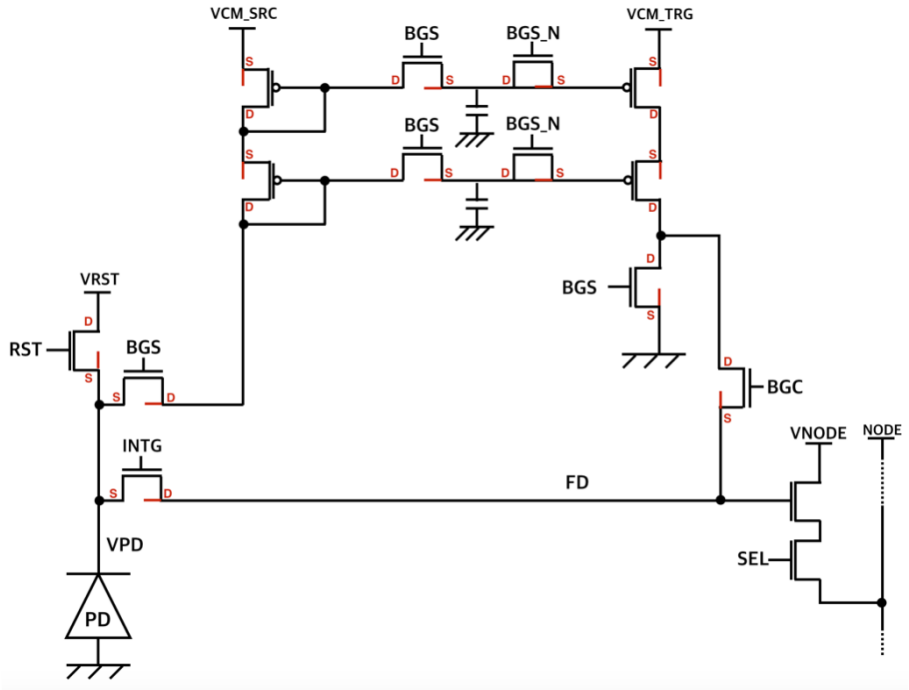

Figure 4.11 Current Mirror with Separated V_B (Type B)

4.5.1 Current Mirror with Dummy Gates (Type A)

As illustrated in Fig. 4.2, the sample and hold circuit, which is the cause of the leakage current, is employed only to the source node of the current mirror. Some dummy gates could be added to make a symmetry between the source node and the target node of the current mirror as shown in Fig. 4.10. The dummy gates are same size as the transistors of the sample and hold circuit between the source node and the target node. The dummy gates generate the same amount of leakage current that is generated in the sample and hold circuit on source node. Therefore, the error current into node FD is decreased by removing the leakage current from target node.

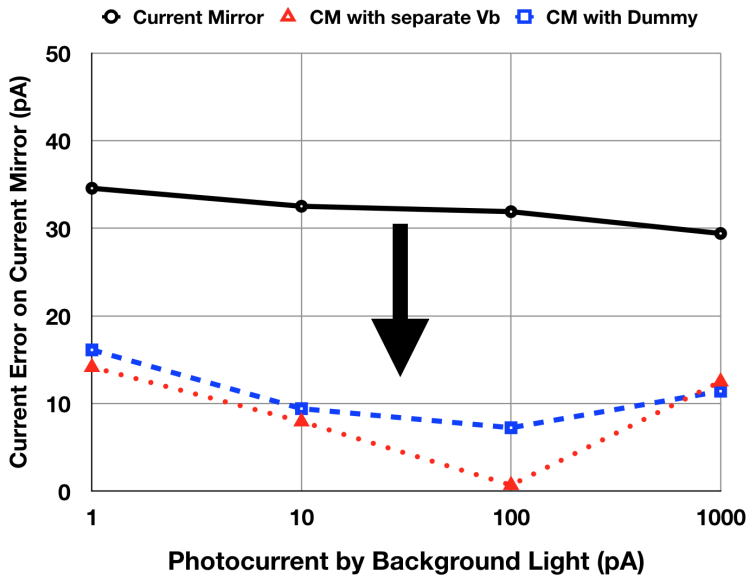

Figure 4.12 Current Duplication Error in Type A and Type B.

4.5.2 Current Mirror with Separated VB (Type B)

The leakage current by reverse biased PN junction in sample and hold circuit is the cause of the error current between the source node and the destination node in current mirror. As illustrated in Fig. 4.11, we have tried to minimize the leak currents of sample and hold circuit and the other transistors by connecting the substrate of each transistor with the source or the drain.

4.5.3 Current Duplication Error of Type A and Type B

Fig. 4.12 shows the relationship between photocurrent by background light, I_BG, and the current duplication error on current mirror. And the current duplication error of type A and B are compared with it of basic circuit. Fig. 4.12 shows that the errors of the current mirrors of type A and type B are decreased by 20 pA or more than the current mirror of basic pixel circuit (solid line). Compared to the basic type of proposed circuit, it can be confirmed that

Figure 4.13 Chip layout

the current duplication error decreases by 53% or more in the type A and 57.5% or more in the type B.

4.6 Chip Implementation

The proposed image sensor has been designed and being fabricated in LAPIS $0.18-\mu m$ CIS process. Fig. 4.13 and Fig. 4.14 show a layout and a microphotograph of the image sensor. It has a 128x128 pixel array with column-parallel ADC. The pixel circuit occupies $30\mu m \times 25\mu m$. The chip size is $5mm \times 5mm$. The specification of fabricated image sensor is

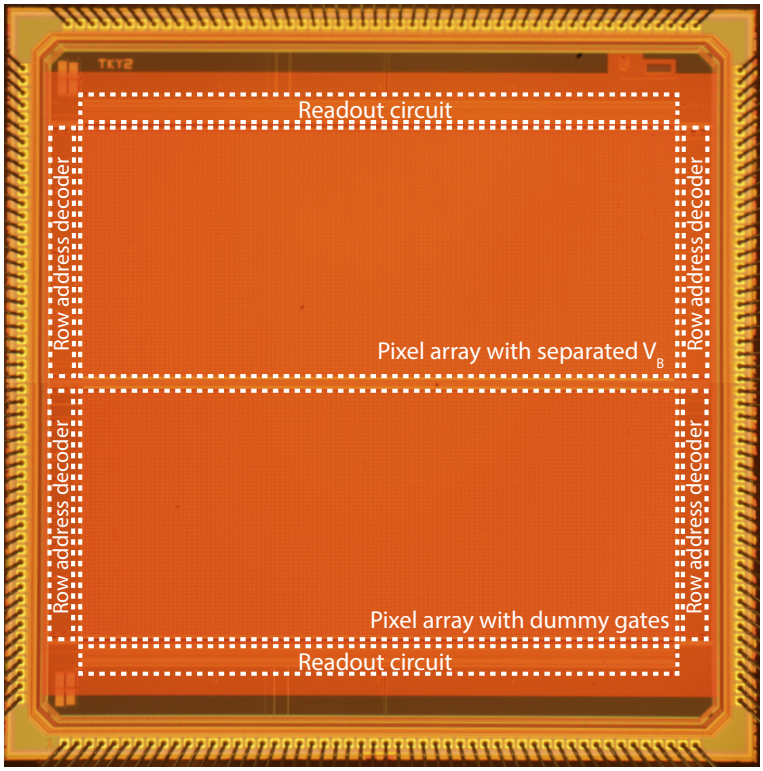

Figure 4.14 Microphotograph of the fabricated chip.

Table 4.1 Specification of proposed image sensor.

Process	0.18*um* CIS
Chip Size	$5mm \times 5mm$
Resolution	128×128
Pixel Size	$30um \times 25um$
Fill Factor	2.4%
Power Voltage	3.3*V*

summarized in Table. 4.1.

4.6.1 4-T Pixel with pinned photodiode

In this impletation, we have employed the 4-T pixel with pinned photodiode because of using the CIS (CMOS Image Sensor) process. Fig. 4.15 shows the 4-T pixel with pinned photodiode. As shown in Fig. 4.15, the detection node which is called floating diffusion

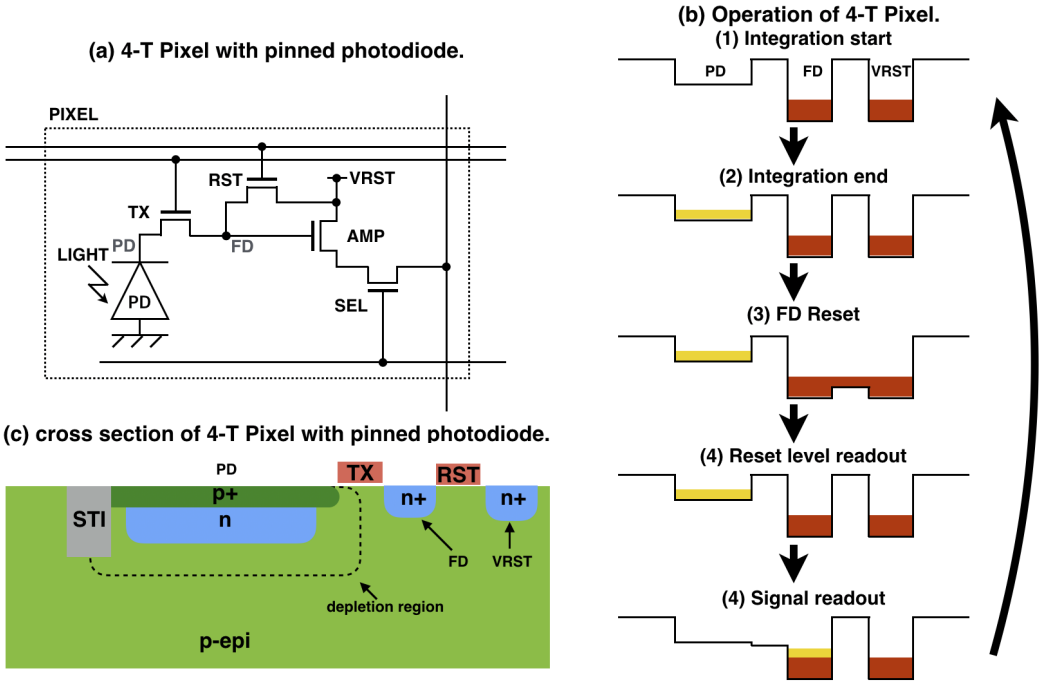

Figure 4.15 4-T pixel with p-n photodiode: (a) Schematic of 4-T pixel, (b) Cross section of pinned photodiode, (c) Operation diagram

(FD) is separated from photodiode. As shown in Fig. 4.15 (a), 4-T pixel circuit consists of pinned photodiode and four transistors. The transistors are employed for transfer, reset, source-follower AMP, and row select. The operation procedure of 4-T Pixel with pinned has five steps as follows:

1. Integration: V_{PD} is decreased by the integration of photocurrents generated in pinned photodiode.

2. Reset: The FD node is reset to V_{DD}.

3. Reset level readout: For the correlated double sampling, which cancels the fixed-pattern-noise (FPN) in pixel circuit, V_{FD} is read out.

4. Charge transfer: When the transfer transistor turns on, the charges in pinned photo-

diode is transferred into the floating diffusion. At this transfer, the charges are fully transferred because the potential of pinned photodiode is higher than floating diffusion node.

5. Signal readout: V_{FD} is read out through source follower.

The CDS operation in 4-T pixel cancels both the FPN and the kTC noise. A SNR of 4-T pixel is better than SNR of 3-T pixel because kTC noise of 4-T pixel is cancelled in above the operation procedure. And the conversion gain of 4-T pixel(Eq. 4.12) is higher than 3-T pixel(Eq. 3.5). After the operation procedure of 4-T pixel, V_{OUT} is read out from 4-T pixel as below:

$$V_{OUT} = V_{RST} - V_{SIG} \tag{4.11}$$

$$= \frac{Q}{C_{FD}} \tag{4.12}$$

Where, Q is the charges generated in pinned photodiode, and C_{FD} is the capacitance of floating diffusion (FD). The capacitance of FD (C_{FD}) consists of the junction capacitances of two transistors, TX and RST, the gate capacitance of one transistor, source follower AMP.

4.6.2 Pixel Array Structure

Fig. 4.27 is an array structure of the image sensor. The array structure has two types of prototype image sensors: the upper half is the type of CM with separated V_B, the lower half is the type of CM with dummy gates. The each half image sensor consists of an array of a pixel array of the each type, a column-parallel readout circuit with SS-ADC, a row-select address

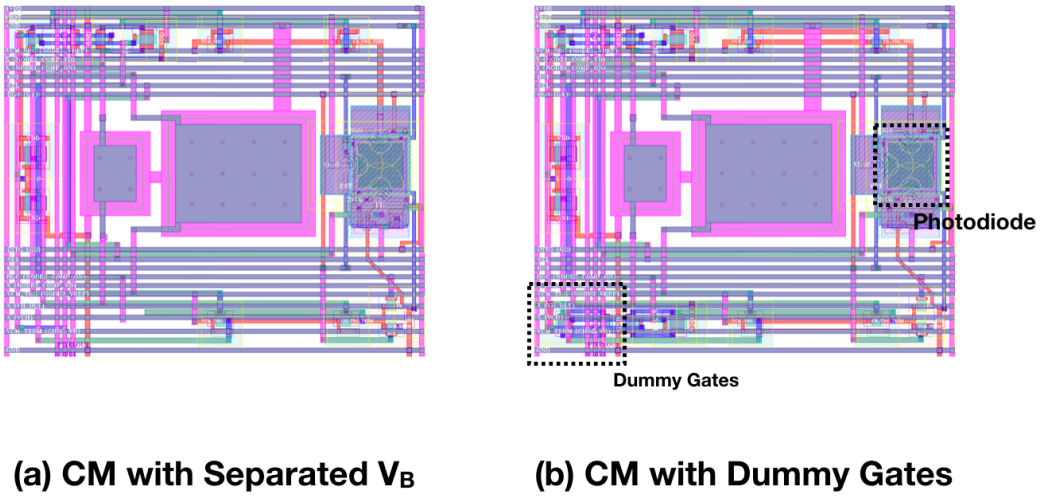

Figure 4.16 Pixel layout: (a) Current Mirror with Separated V_B, (b) Current Mirror with Dummy Gates.

decoder, a column-select address decoder, and a DAC. A specific pixel can be selected by the row-select and column-select address decoder. After ADC on column-parallel SS-ADC, its digitized value can be read from outside of the chip. Fig. 4.16 shows pixel layouts of two types of pixel circuits. Fig. 4.16 (a) is a pixel circuit using current mirror circuit with separated V_B. Fig. 4.16 (b) is a pixel circuit using current mirror circuit with dummy gates. As shown in Fig. 4.16 (a), huge distance between transistors is needed for satisfying DRC because of transistors with separated V_B. For reuse the column parallel readout circuit, the layout size of pixel circuit with dummy gates is big as it of pixel circuit with separated V_B. The layout size of pixel circuit with dummy gates can be optimized and shrunk.

4.6.3 Readout circuit

A schematic of the readout circuit is shown in Fig. 4.17. The readout circuit consists of a differential amplifier, comparator, DAC, 8-bit FFs and switches for readout to outside of the chip. For chip test, The readout circuit has additional circuits: six source followers, RAMP

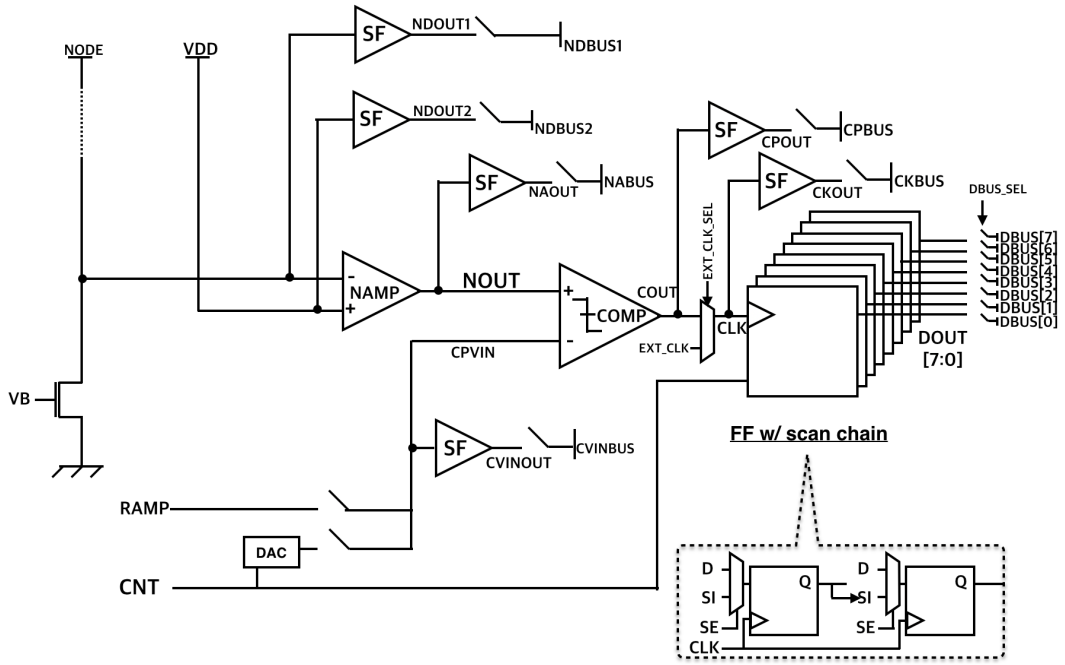

Figure 4.17 Schematic of readout circuit.

input from outside chip, scan chain for FFs. The difference voltage between NODE1 and NODE2 is amplified at the differential amplifier. The output of the differential amplifier is compared with the ramp signal from the DAC. When the output of amplifier overwhelms the ramp signal, the output of comparator turns ‘1’ to ‘0’ and the 8-bits FFs restore the counter value at that time and keep the value. The counter value (CNT in Fig. 4.17 is put in from FPGA in Chip measurement system. After ADC, the data in FFs are accessed to digital data bus outside of the chip in sequence.

Figure 4.18 Photograph of the sensor with lens on a test board

4.7 Measurement Results

4.7.1 Measurement Setup

The measurement system of the fabricated sensor consists of a laser source (wavelength 670 nm), the fabricated sensor with a lens mounted on a test board with FPGA as shown in Fig. 4.18, a pulse generator, a light projector for ambient illumination, and a lux meter. The sensitivity, the dynamic range, and the selectivity of the fabricated sensor are evaluated with the measurement system. The target of the measurement is a white ball shown in Fig. 4.19. Modulated light modulated by modulation frequency from 1 kHz to 60 kHz are used. The sampling frequency of a gate INTG is fixed to 10 kHz. After accumulating and averaging 16 frames for temporal low pass filtering, 3x3 average spatial filter is performed for spatial low

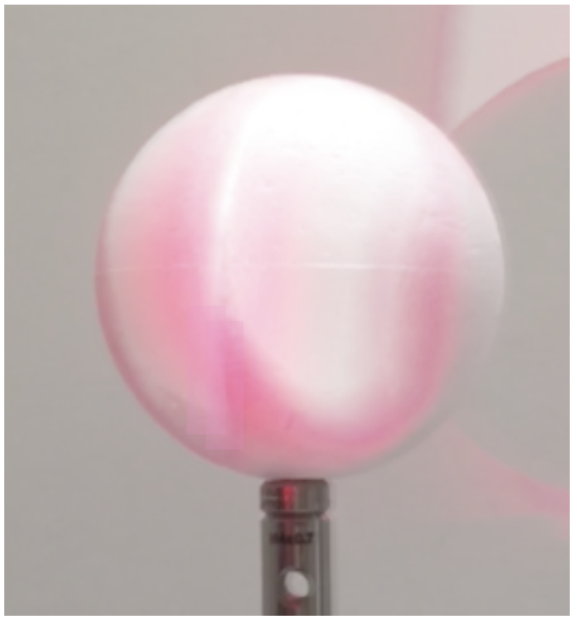

Figure 4.19 Target object.

pass filter.The peak values are obtained by thresholding.

Signal-to-Background Ratio (SBR) [81] is employed for the sensitivity and is defined as below.

$$SBR = 20log\frac{I_{SIG_{MIN}}}{I_{BG}} \tag{4.13}$$

Where, $I_{SIG_{MIN}}$ is the minimum light intensity that can be detected. I_{BG} is the background-induced photocurrent. It is proportional to the photo current. The lower the value of SBR, it means that the better the performance. If the SBR is negative, it means that $I_{SIG_{MIN}}$ is lower than I_{BG}. Therefore, if the SBR of the image sensor is negative, it means that the image sensor can detect the reflected light weaker than the background light.

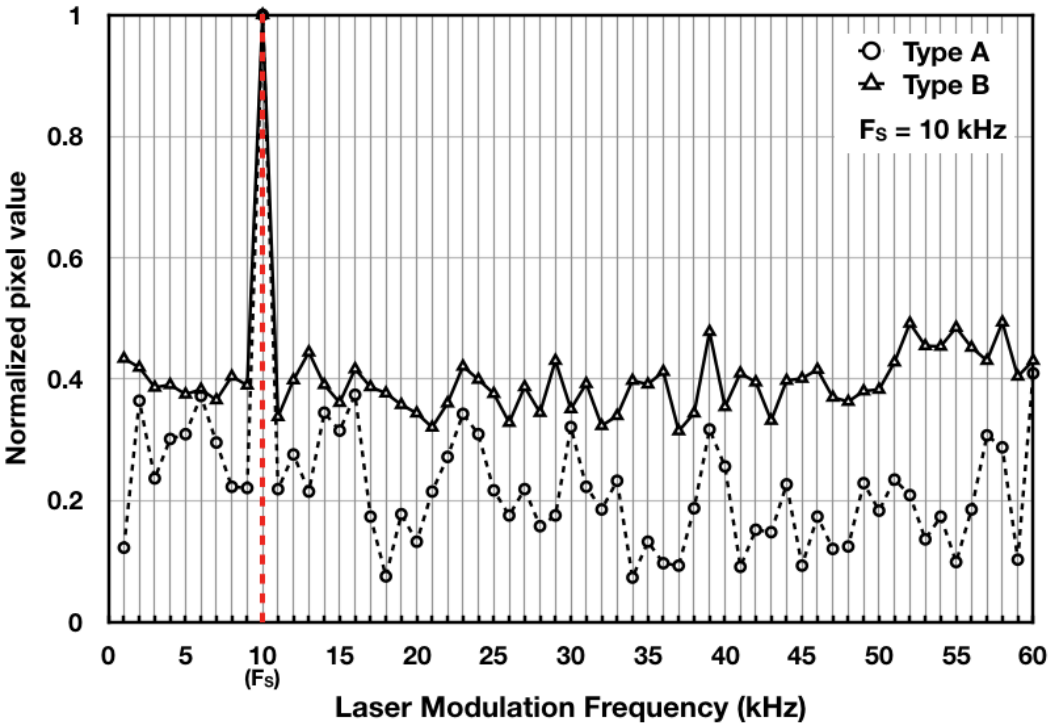

Figure 4.20 Selective-Signal Detection.

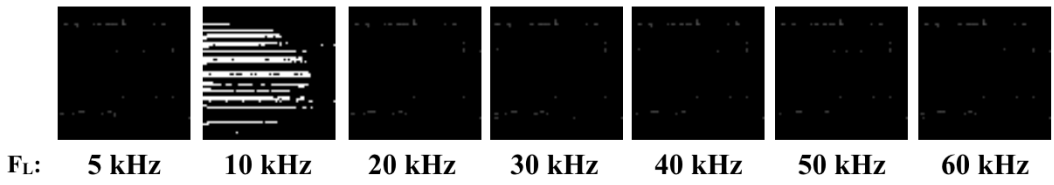

Figure 4.21 Output images of type A when sampling frequency F_S is $10kHz$ with various laser frequency F_L.

4.7.2 Selective Signal Detection

Fig. 4.20 shows the relationship between various incident light frequencies and the normalized pixel value from readout circuit. The sampling frequency F_S is $10kHz$, the exposure time T_{EXP} is $400us$. As shown by Fig. 4.20, only when the sampling frequency F_S is equal to the frequency of the modulated light, the pixel value becomes a peak. The SNR of type A and type B is 7.8 dB and 6.1 dB respectively. The incident light modulated by the other fre-

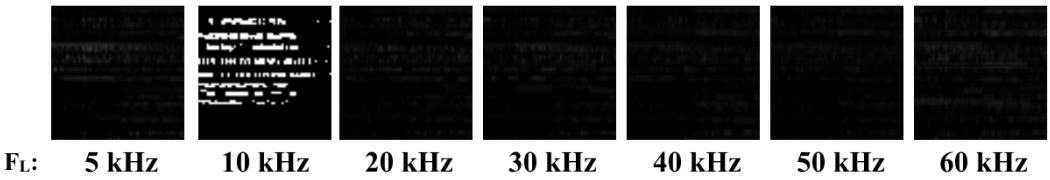

Figure 4.22 Output images of type B when sampling frequency F_S is $10kHz$ with various laser frequency F_L.

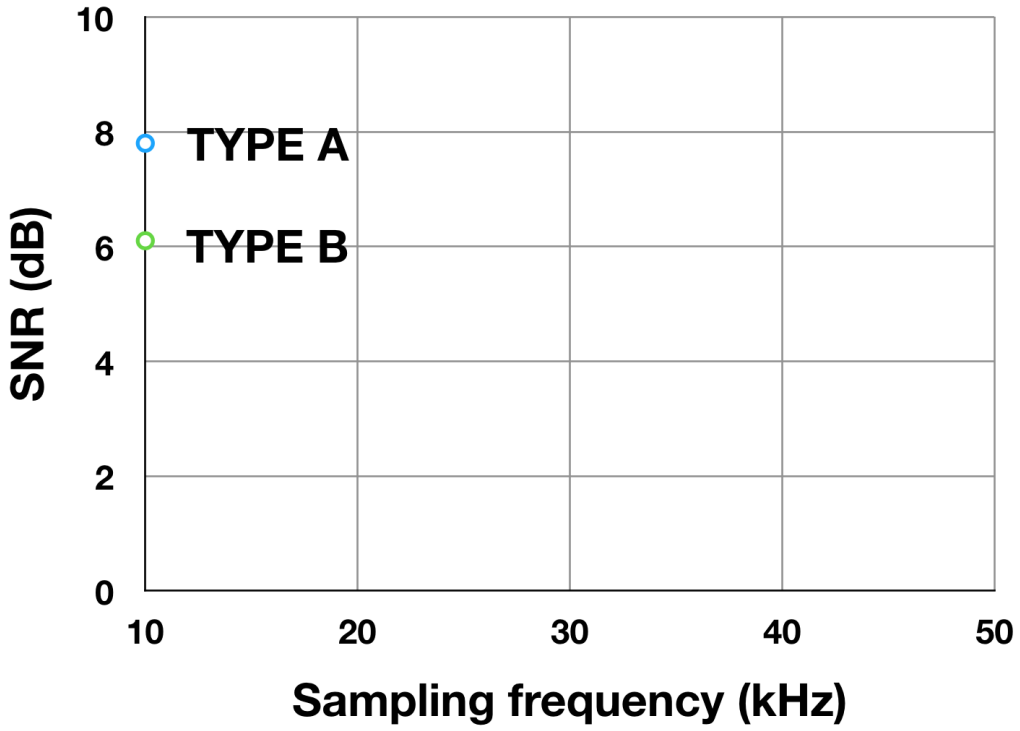

Figure 4.23 Maximum sampling frequency and SNR of selective-signal detection

quencies is suppressed. The proposed sensing scheme has high sensitivity for a multiple light projection system by using a set of laser frequencies such as 10, 20, and 40 kHz. Fig. 4.21 and Fig. 4.22 show the output images of type A and type B when sampling frequency F_S is 10 kHz with various laser frequency F_L such as 5, 10, 20, 30, 40, 50, 60 kHz. Fig. 4.23 shows the relationship between sampling frequency and SNR. In this experiment, the only one sampling frequency can be operated at 10 kHz. So, the maximum sampling frequency is

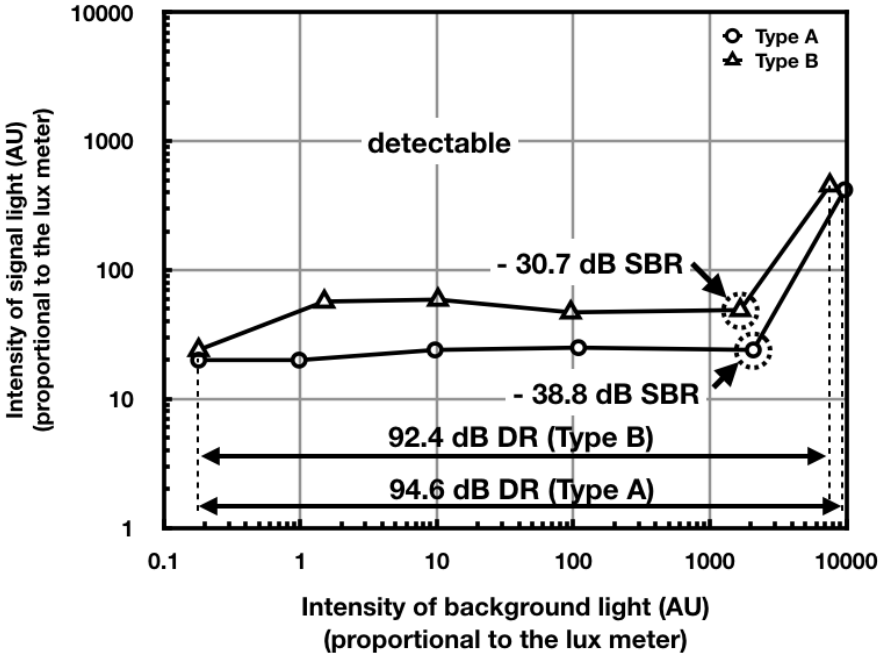

Figure 4.24 Dynamic range and signal background ratio (SBR).

10 kHz. And the maximum SNRs are 7.8 dB and 6.1 dB respectively at sampling frequency 10 kHz.

4.7.3 Background Light Suppression Performance

Fig. 4.24 shows the relationship between the intensity of background light and the minimum projected light intensity that can be detected. In the measurement, Both the modulation frequency F_L and the sampling frequency F_S are $10kHz$. The minimum signal-to-background ratio (SBR) means the sensitivity of the image sensor. The Signal-to-background ratio (SBR) [81] is defined as below.

$$SBR = 20log\frac{I_{SIG_{MIN}}}{I_{BG}} \tag{4.14}$$

Table 4.2 Evaluation Results and Comparison.

Parameters	[14]	[87]	This works	
			Type A	Type B
BGL* Suppression Technique	Current mode + correlation	Charge Injection	Current mode + compensation	
Maximum sampling frequency (kHz)	10	50	10	
SBR (dB)	-22.8	-18.8	-38.8	-30.7
BGL DR (dB)	100	89.3	94.6	92.4
# of trans./pixel	43 (inc. 4 MOS cap)	64	19 (inc. 2 MIM cap)	15

BGL* : Background light

Fig. 4.24 shows that the image sensors of two types can detect the projected light that can be weaker than the background light. It means that the image sensors can suppress the background light. The minimum signal-to-background ratio (SBR) of type A and type B are -38.8 dB and -30.7 dB respectively. The dynamic range of type A and type B are 94.6 dB and 92.4 dB respectively.

4.7.4 Comparison and Discussion

The summarization and comparison with previous works is shown in Table. 4.2. Table. 4.2 shows that this work has better SBR than previous works [14,87]. And this work achieved less the number of transistors in a pixel than previous works. The summarization and comparison with our previous work is shown in Table. 4.2. This work has better SBR than our previous work [87], and achieved less the number of transistors in a pixel than our previous works in Chapter 3. And, in terms of dynamic range, this work also has better dynamic range

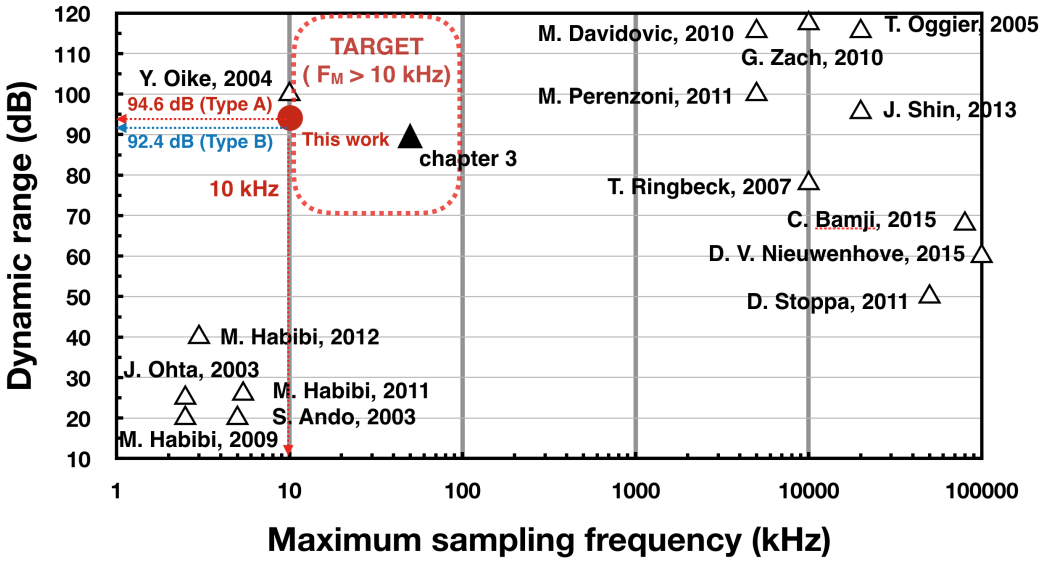

Figure 4.25 Comparison with previous works on image sensors with in-pixel selective-signal detection.

of background light than our previous work in Chapter 3. Fig. 4.25 shows the position of this work in comparison with previous works on image sensors with in-pixel selective-signal detection. The performance position of this work is located in the same range in terms of modulation frequency with in [87], and it has better dynamic range of background light than our previous work in Chapter 3. we thought that these results came from better background light suppression with the duplication capability of current mirror in a pixel circuit. This duplication capability relies on the length of the period on which only background light is incoming. Fig. 4.26 shows the limitation of sampling frequency of the proposed image sensor. The limitation of sampling frequency is come from the current mirror in the pixel on BGS phase. The current mirror circuit needs the enough length of the period of background light sampling phase, BGS phase. The maximum of settling time on 10 kHz is about 31.3us. It means that the maximum of sampling frequency could not be higher than about 16.0 kHz. Therefore, on lower sampling frequency domain, around 10 kHz, this image sensor works

better than our previous work in Chapter 3. In this situation, if the operation is needed in higher sampling frequency domain, the image sensor in Chapter 3 could be possible solution. And the image sensor proposed in this chapter works better in terms of the min SBR and wide dynamic range with lower sampling frequency.

4.8 Summary

In this chapter, active optical sensing system using the image sensor with selective-signal detection and background light suppression is proposed. Basic pixel circuit using current mirror with background light compensation is proposed toward high-resolution applications under strong background light. Two types of current-duplication-error-reduced pixel circuit are proposed further. The signal to background light ratio (SBR) of dummy-added type and V_B-separated type are -38.8 dB and -30.7 dB respectively with dynamic range 94.6 dB and 92.4 dB in the simulation. The number of transistors in a pixel of dummy-added type and V_B-separated type are 19 and 15 respectively. All type of pixel circuits achieved better SBR and DR with less the number of transistors in a pixel circuit than previous works.

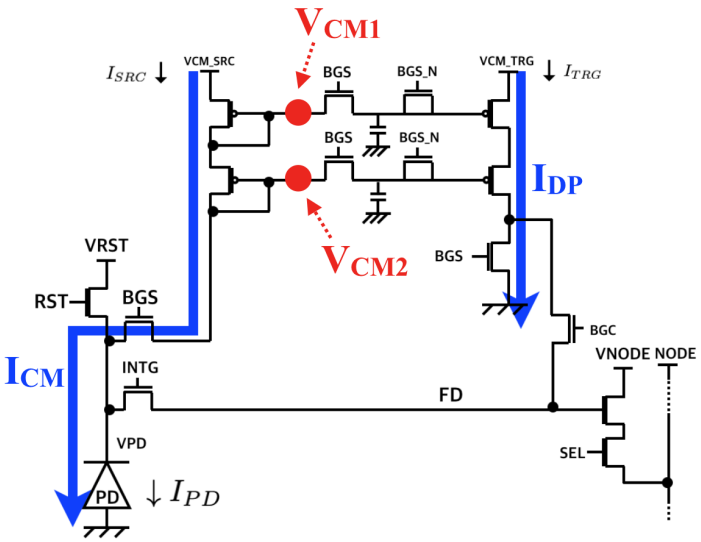

(a) Operation of BGS Phase

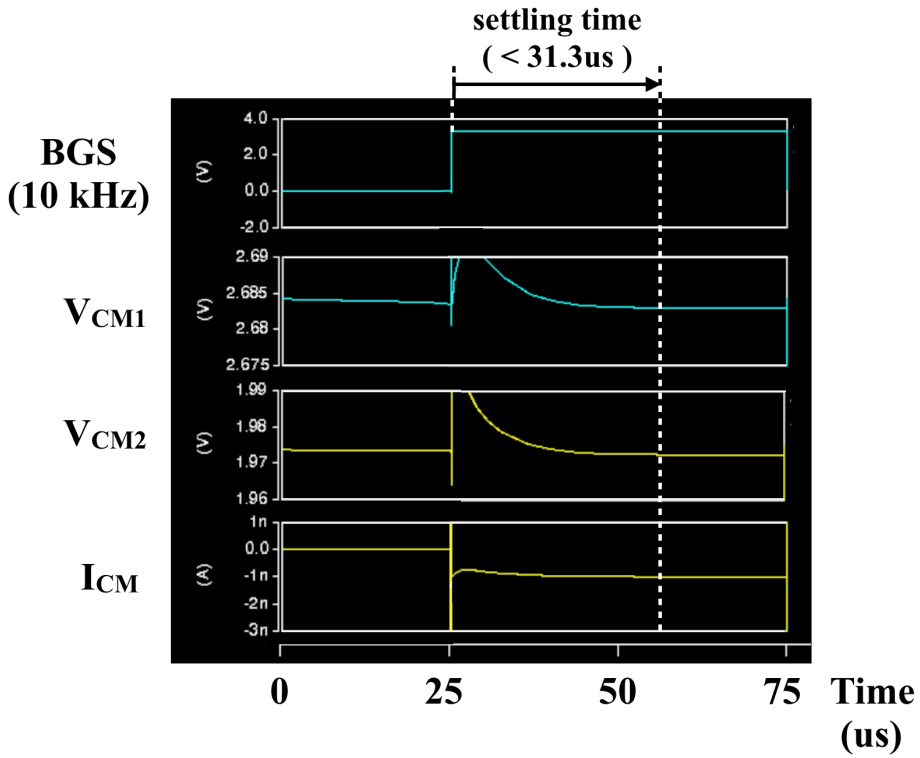

(b) Settling time of sampling voltages in current mirror on BGS phase

Figure 4.26 Limitation of sampling frequency by current mirror: (a) Operation of BGS Phase (b) Settling time of sampling voltages in current mirror on BGS phase

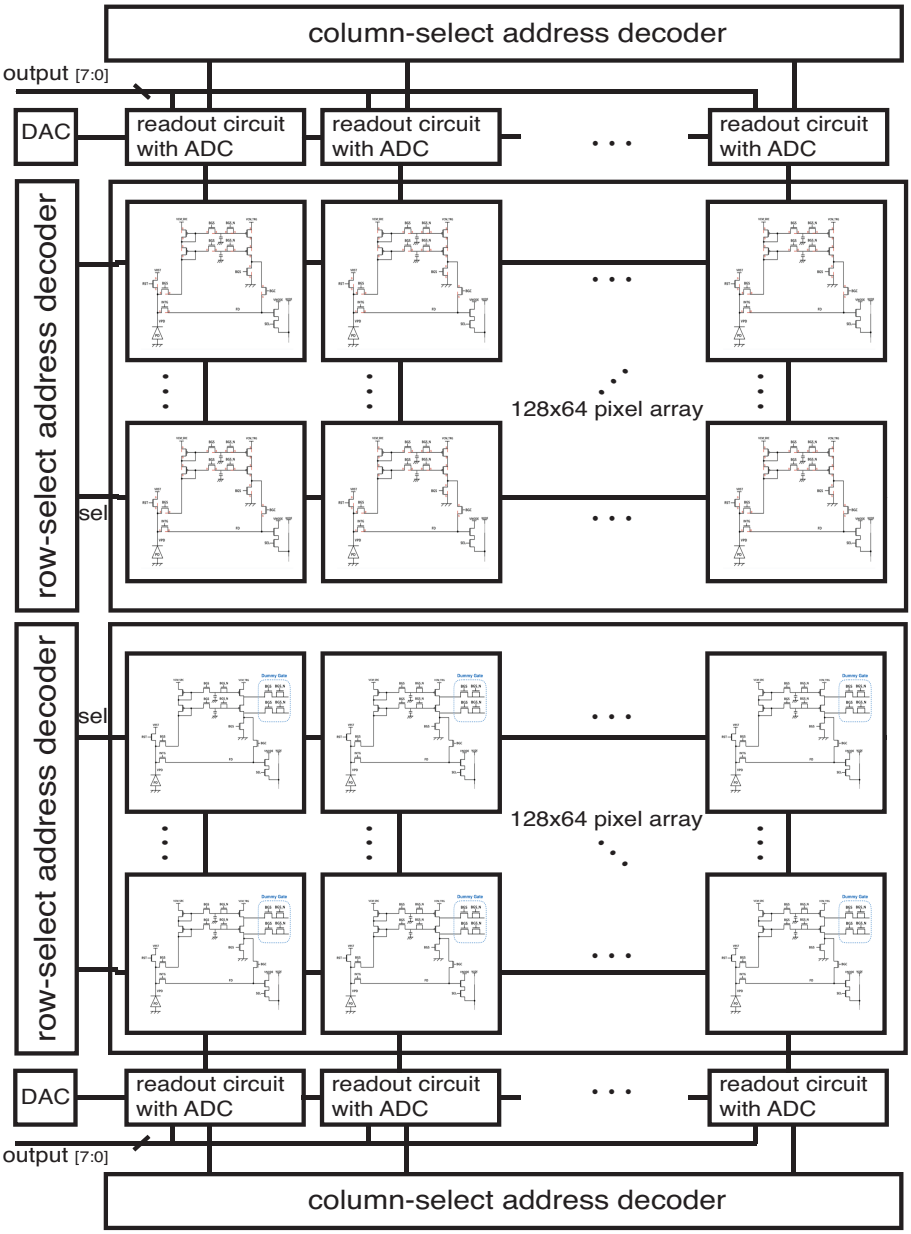

Figure 4.27 Array structure of the image sensor: Upper half is the type of CM with separated V_B, lower half is the type of CM with dummy gates.

Chapter 5

A study of active optical sensing with coded light

5.1 Introduction

Active optical sensing are widely employed in various applications and fields in recent years [88, 89]. These applications have common assumption that the measurement data from the measurement system based on its active optical sensing are correct. A direct attack on the inside of the system even if it can not be done, there is a concern that the system can be attacked by spoofing the measurement result. The security and reliability of the measurement are needed and required depending on the applications. Under this situation, previous works are performed to improve information security such as data communication, storage, analysis. However, the researches or works for instrumental security at the stage of collecting information is still insufficient. Above all, enhancing the security on the stage of collecting information using an image sensor is required in the instrumental system based on active optical sensing.

Range-finding that measures the distance between objects is one of the most fundamental operations in the applications of measuring information in the real world. The range-finding as shown in Fig. 5.1 , the distance to the object is acquired as an image called range-map.

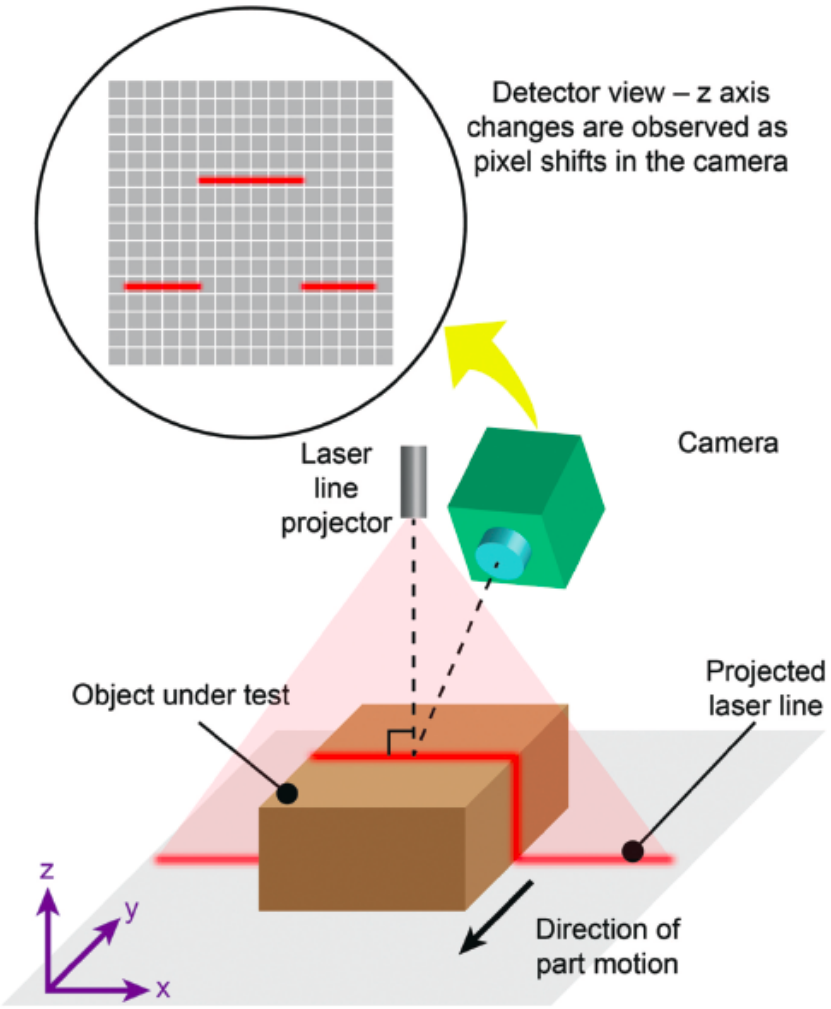

Figure 5.1 Example of 3-D applications: 3D machine vision using laser triangulation [15].

It is expected to be used for applications such as obstacle detection and product inspection. There are several range-map acquisition methods such as stereo matching [90–92], time-of-flight [11, 46–51], and light-section method [49, 52–58]. Light-section method based on triangulation is widely used in industrial applications [88, 89]. In this chapter, active optical sensing with coded light is proposed and evaluated.

The structure of the instrumental system and the weak-point of this system are explained in Chapter 5.2.1. The new coding scheme for optical sensing is introduced and explained the

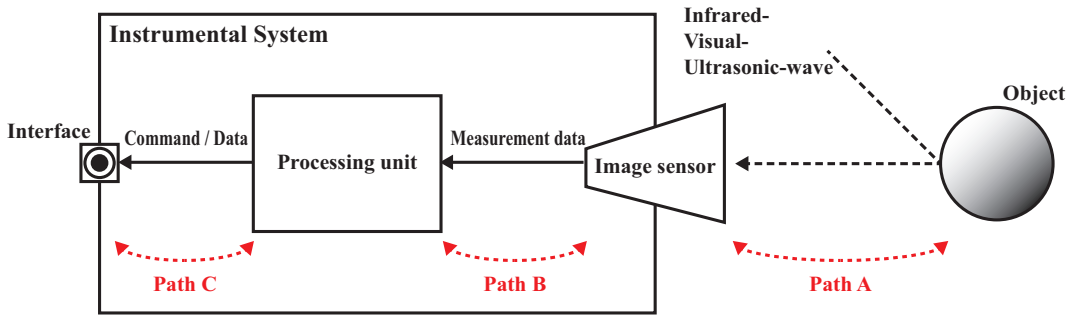

Figure 5.2 Structure of instrumental system.

conversion to coded light in Chapter 5.2. The measurement results with proposed coded light are showed in Chapter 5.3. Finally we discuss the conclusion and future tasks.

5.2 Proposed active optical sensing

5.2.1 Weak point in instrumental security

The instrumental security means the security of the system that consist of instrumental device such as image sensor. The structure of the instrumental system is illustrated abstractly in Fig. 5.2. The instrumental system measures the data of the object using an instrumental device, an image sensor, on the path A. Next, the measurement data are sent to the processing unit on the path B. Finally, the command or data are sent to outside of the system on the path C and an interface. Considering the security threat to the instrumental system, tapping or tampering can be performed on the path B or C. Conventionally, it is known that such attacks can be protected by encrypting messages and adding message authentication codes (MAC) [5]. However, a definitive protection technology against attack in this path A has not been established. At this work, the new active sensing scheme using the image sensor and the coded light is proposed. The measurement results using the new scheme are also introduced.

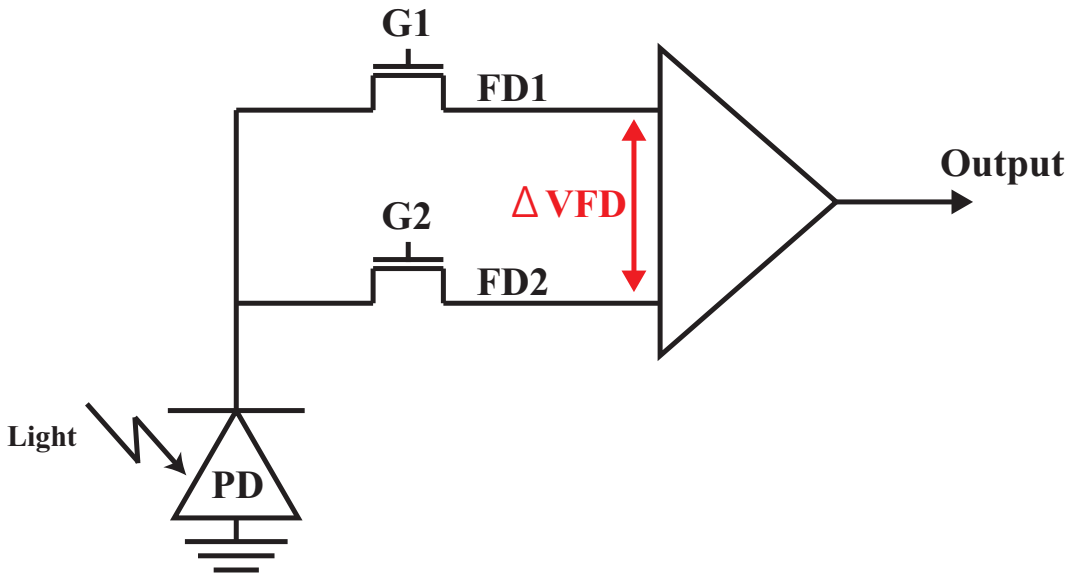

Figure 5.3 Diagram of demodulation pixel in pixel circuit.

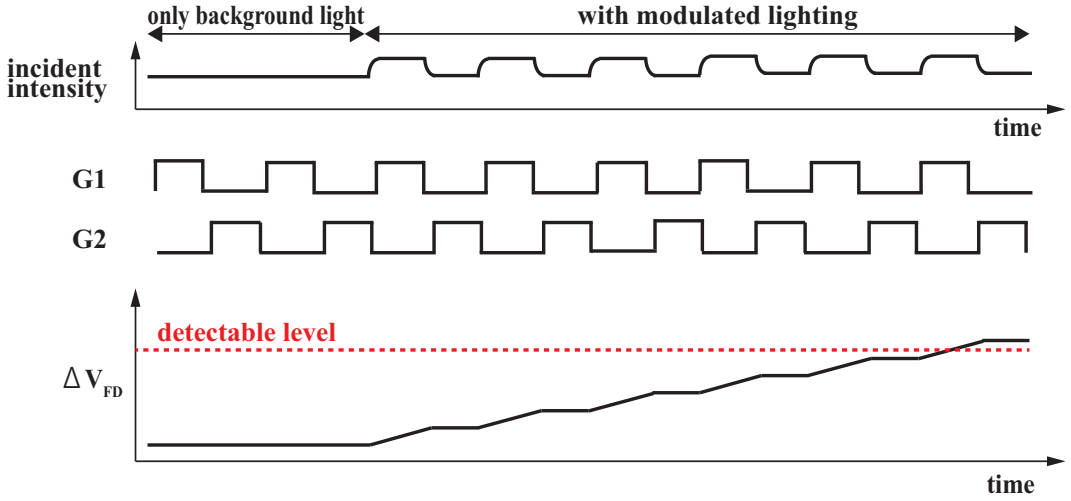

Figure 5.4 Normal operation with modulated light.

5.2.2 Problem of previous modulation scheme

The proposed new coding scheme is based on the image sensor with the demodulation pixel illustrated in Fig. 5.3. The pixel circuit consist of one photodiode, two transistors for transfer gate, and additional circuits such as source follower amplifier, row-select transistor and so on.

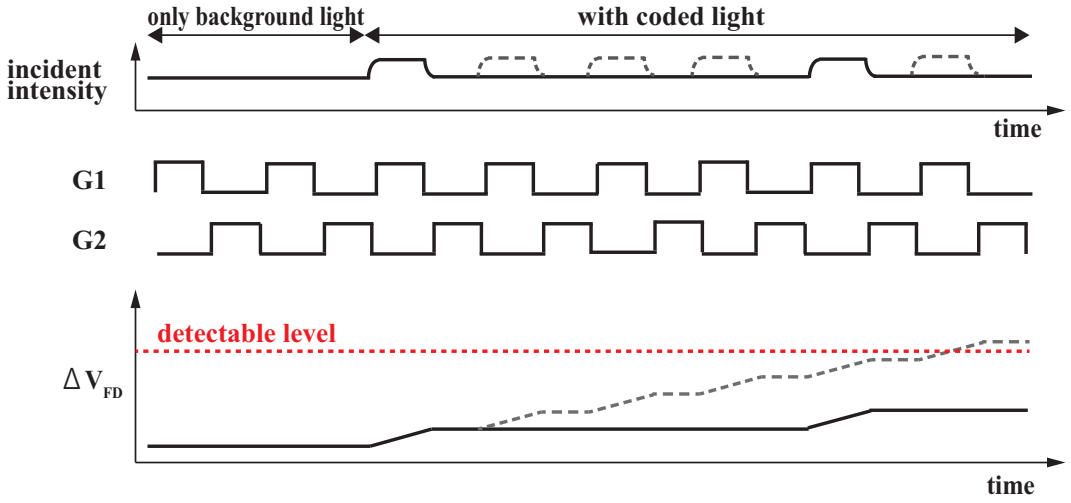

Figure 5.5 Problem of integration time change with coded light.

Fig. 5.4 shows the relationship between the integration time and the differential voltage ΔV_{FD}, and describes the normal operation with modulation light with the image sensor [13]. ΔV_{FD} is the the differential voltage between floating diffusions. The signal light as ON–OFF signal is modulated with specific frequency. Therefore, the signal light always turns ON to OFF and OFF to ON. Using this light, the image sensor integrates photons from the reflected light, and increases the differential voltage between floating diffusions, ΔV_{FD}, monotonously. Fig. 5.5 shows the relationship between the integration time and the differential voltage ΔV_{FD} with the image sensor [13], and also describes problematic operation with coded light like as simple bit stream. As shown in Fig. 5.5, the problematic situation is that the coded light has the more OFF-signal than ON-signal. It makes the image sensor integrate less photons than the normal operation with modulation light in Fig. 5.4 because the OFF–signal can not make the differential voltage, ΔV_{FD}, bigger. So the integration time can be longer. In the opposite case, if the coded light has the more ON–signal, the integration time can be shorter. Therefore, the integration time can vary depending on which the coded light is used. The

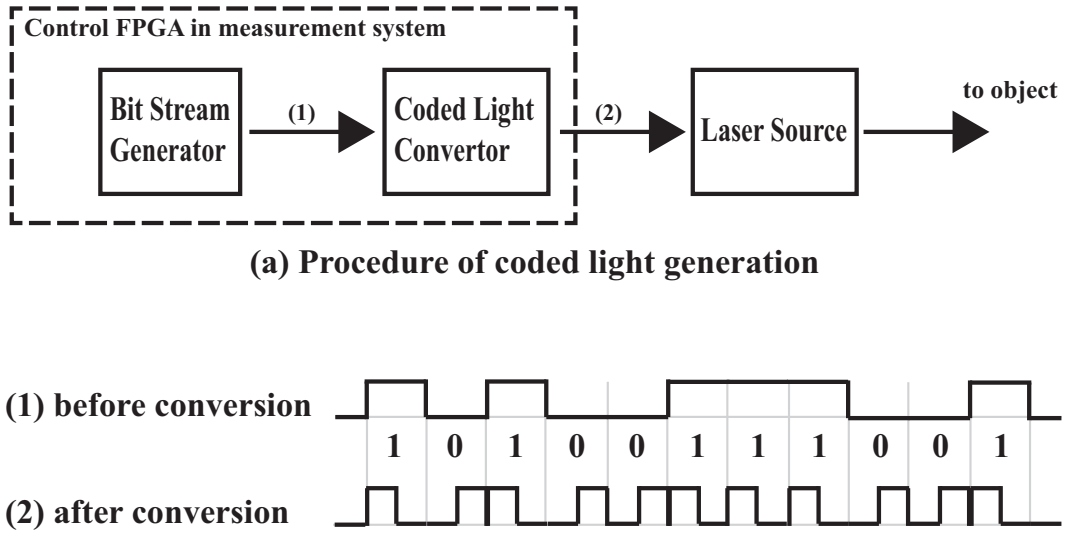

Figure 5.6 Conversion scheme for new optical coded-signal: (a) Procedure of coded light generation, (b) Conversion in coded light convertor

variation of the integration time effects the performance of the active sensing scheme such as frame-rate.

5.2.3 Conversion scheme for coded light generation

Considering the problematic operation described in Chapter 5.2.2, the requirements is requested for new optical coded-signal as below:

- Constant integration time
- Unpredictability

For keeping constant integration time, the number of bit `'1'` must be equal to the number of bit `'0'`. And, for making unpredictable bitstream, the bitstream must be as random as possible. Fig. 5.6 shows the conversion scheme for new optical coded-signal satisfied the above requirements. Fig. 5.6 (a) shows a procedure of coded light generation that consist of

a bit stream generator and a coded light convertor in a control FPGA in measurement system, and a laser source. In this work, a clock generator is employed for the bit stream generator in a control FPGA in measurement system. Random bit generator such as linear feedback shift register (LFSR) and encryption key generator could be a candidate for the bit stream generator in future work. Similar to Manchester encoding [93], The bit `'1'` is converted to HIGH–to–LOW and the bit `'0'` is converted to LOW–to–HIGH. However, dissimilar to Manchester encoding [93], the HIGH levels in HIGH–to–LOW and LOW–to–HIGH are important for constant integration time, not the edges of HIGH–to–LOW and LOW–to–HIGH.

5.3 Measurement results

5.3.1 Measurement Setup

The measurement system introduced in Chapter 3.5.1 is employed for the measurement using coded light. The target of the measurement is a white ball shown in Fig. 3.15. Fig. 5.7 shows the timing diagram of the control signals with coded light in the measurement. Fig. 5.7 (a) and (b) are illustrated two cases of coded sampling with coded light and the other case of coded sampling with sinusoid light respectively. The integration time is 100*um*. The modulated light is modulated by the modulation frequency from 1 kHz to 60 kHz. The coded light is converted on the modulated light by the modulation frequency 10 kHz. Fig. 5.7 (a) means the case that the image sensor wants to accumulate the only reflected light in Fig. 1.11. Fig. 5.7 (b) means the case that the image sensor wants to avoid the disguised light from a certain attacker in Fig. 1.11. Before the measurement, the analysis of the coded light is performed by the light detector as shown in Fig. 5.8. Fig. 5.8 (a) shows the structure for

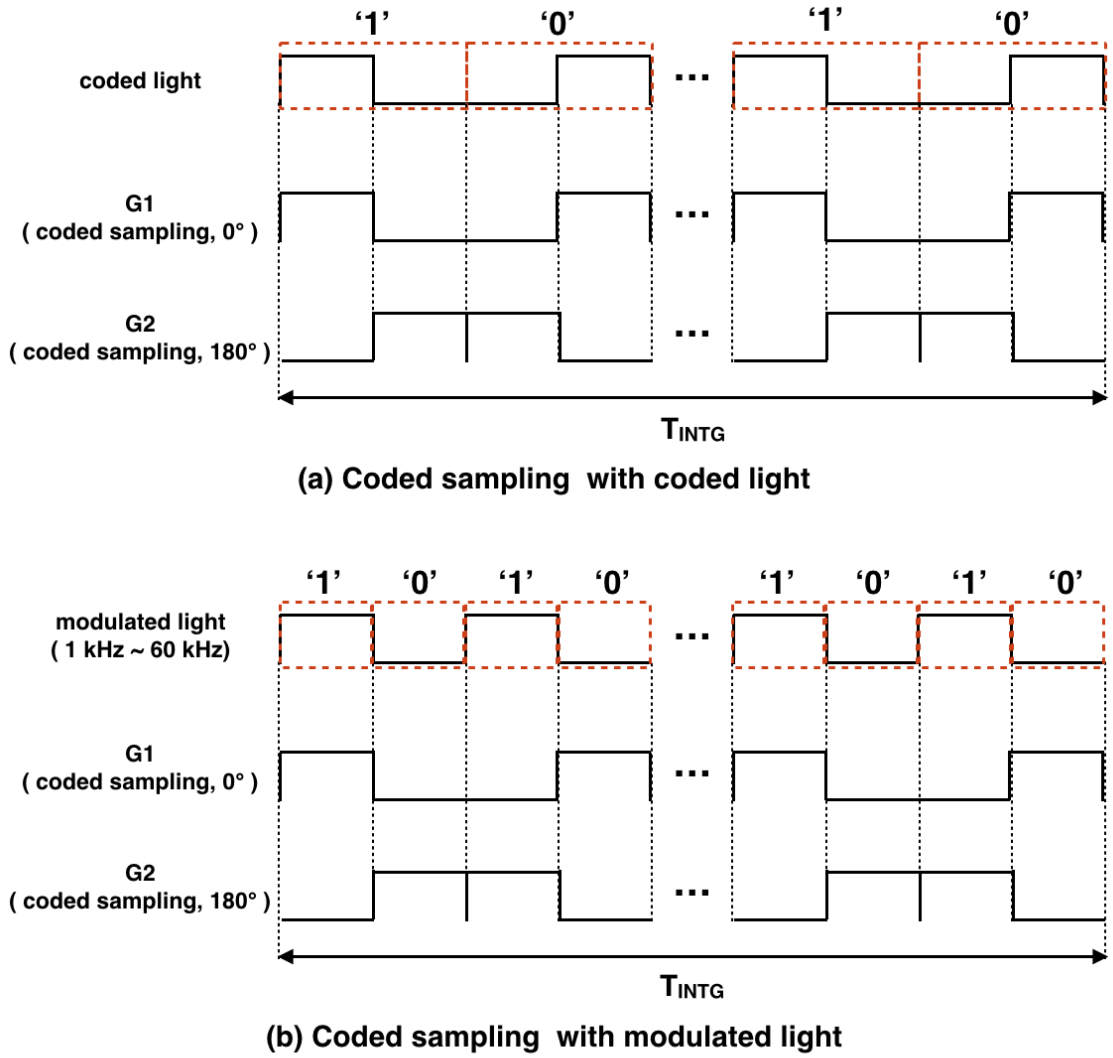

Figure 5.7 Timing diagram of coded sampling with coded light: (a) coded sampling with coded light, (b) coded sampling with sinusoid light.

the analysis of delay and coded of the laser source. Fig. 5.8 (b) shows the schematic of the laser detector that consist of a photo-diode, two-stage inverting operational amplifier, and two inverters. This analysis is for two things:the delay of the light source and the code of the light source. The gate control signals in image sensor, G1 and G2 illustrated in Fig. 5.3, are controlled by the delay value T_{d1} shown in Fig. 5.8 (a).

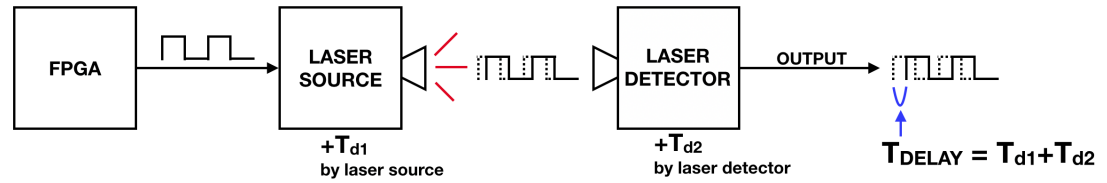

(a) Analysis of delay and code of the laser source

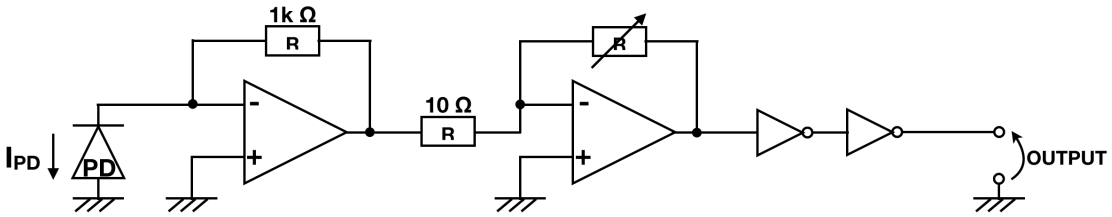

(b) Schematic of light detector

Figure 5.8 Analysis of the coded light : (a) Analysis of delay and code of the laser source, (b) Schematic of the laser detector.

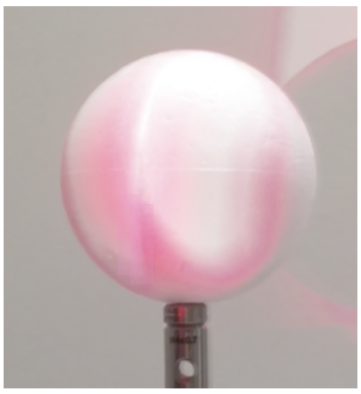

Figure 5.9 target of measurement: a white ball.

5.3.2 Selective light Detection with coded light

Fig. 5.10 shows signal selectivity that is pixel values on the coded sampling with the coded light and the modulated lights modulated by various frequencies (1 kHz ~ 60 kHz). As shown by Fig. 5.10, only when the case is coded sampling with coded light, the pixel value becomes a peak and the cases of coded sampling with modulated light are suppressed. And the signal

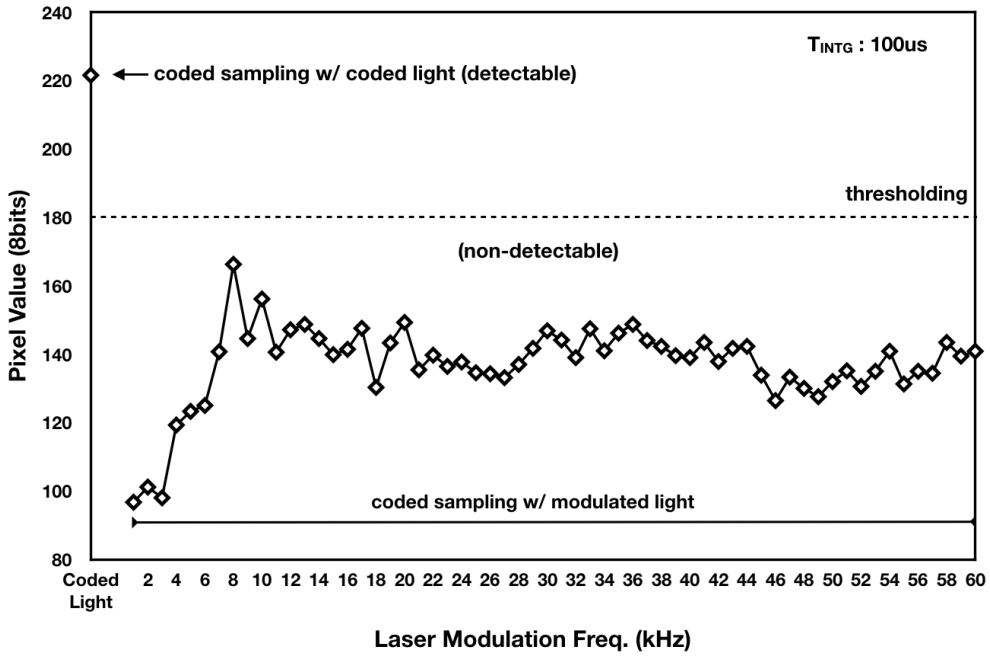

Figure 5.10 Signal selectivity on coded sampling with coded light and modulated light (1 kHz ~ 60 kHz).

Figure 5.11 Output images: (a) coded gating with coded light, (b)~(g) coded gating with various laser frequency F_L = 5,10,20,30,40,50 kHz.

selectivity with coded light is confirmed in same integration time at the case with modulation light. Fig. 5.11 shows the output images on coded sampling with the coded light and the modulated light (F_L = 5,10,20,30,40,50 kHz). Fig. 5.11 (a) shows that the coded light is detected by the coded sampling. Fig. 5.11 (b)~(g) show that the modulated lights are ignored by the coded sampling.

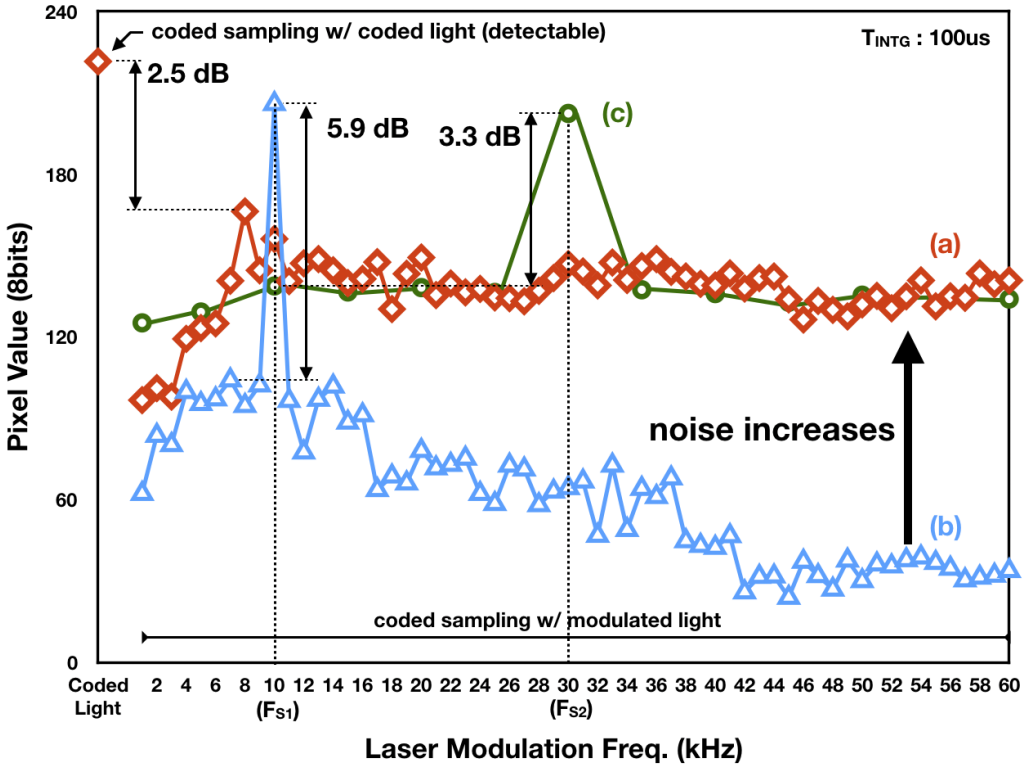

Figure 5.12 Signal selectivity: (a) coded sampling with coded light and modulated light (1 kHz ~ 60 kHz), (b) fixed sampling (F_{S1} = 10 kHz) with modulated light (1 kHz ~ 60 kHz) in Chapter 3.5.2, (c) fixed sampling (F_{S2} = 30 kHz) with modulated light (1,5,10,15,20,25,30,35,40,45,50,55,60 kHz).

5.3.3 Comparison and Discussion

Fig. 5.12 (a) shows signal selectivity that is pixel values on the coded sampling with the coded light and the modulated lights modulated by various frequencies (1 kHz ~ 60 kHz). And the SNR of the coded sampling is 2.5 dB. Fig. 5.12 (b) shows signal selectivity that is pixel values on the fixed sampling (F_{S1} = 10 kHz) with the modulated lights modulated by various frequencies (1 kHz ~ 60 kHz). And the SNR of the fixed sampling is 5.9 dB. Fig. 5.12 (c) shows signal selectivity that is pixel values on the fixed sampling (F_{S2} = 30 kHz) with the modulated lights modulated by various frequencies (1,5,10,15,20,25,30,35,40,45,50,55,60 kHz). And the SNR of the fixed sampling is 3.3 dB. In measurements of Fig. 5.12 (a), (b),

and (c), the integration time T_{INTG} is $100us$. Compare with Fig. 5.12 (b), the overall noise increased. And SNR decreased by 57.6%. From the SNR and overall noise level of fixed sampling (F_{S2} = 30 kHz) shown in Fig. 5.12 (c), the coded light based on modulated light modulated by modulation frequency 10 kHz has similar results of SNR and overall noise level. Therefore, the affect to an image sensor from the coded light is similar to the case using higher modulation frequency than base modulation frequency that is used to generate the coded light.

5.4 Summary

Instrumental security on the stage of collecting information using an image sensor is required in active optical sensing. Active optical sensing with the coded light is proposed. The requirements for the image sensor with coded light are mentioned: (1) constant integration time and (2) unpredictability. The method of bit conversion for making coded light is proposed. Active optical sensing with coded light is evaluated and the signal selectivity with coded light is confirmed in same integration time at the case with modulation light. However, the SNR of signal-selectivity decreases by 57.6% from case with modulated light. It is confirmed that the affect to an image sensor from the coded light is similar to the case using higher modulation frequency than base modulation frequency that is used to generate the coded light.

Chapter 6

Conclusion

This thesis focused on the image sensors for with in-pixel selective-signal detection and background light suppression. we have proposed the two types of image sensors, and evaluated the selectivity and the dynamic range with modulated and coded light. The followings are conclusions through this thesis.

Chapter 2: Instrumental security is a new challenge in active optical sensing such as 3-D range-finding system. Attacks against active optical sensing has been reported in conventional stereo matching, ToF, etc. Software- or system-level countermeasures are reported, but are insufficient. New active optical sensing scheme using a specific image sensor is proposed for the instrumental security. The only reflected light is accepted from incident light that consists of reflected light, disguised light, background light. The specific image sensor in proposed active optical sensing also requires functions not only detecting modulated light but detecting coded light with wide modulation frequency range and wide dynamic range.

Chapter 3: A optical sensing system, which is based on light-section method with the modulated light and the image sensor that can detect the selective-signal light modulated by specific frequency, has been proposed. For selective-signal detection, the demodulation pixel are employed in pixel circuit. To avoid saturation for wide dynamic range, Adaptive charge

unit (ACU) in each pixel is introduced. And the image sensor has been designed, fabricated and successfully measured. The signal selectivity of the image sensor is confirmed from the measurement. The minimum SBR, the dynamic range, and the maximum modulation frequency of the image sensor are -18.8 dB, 89.3 dB, 50 kHz respectively in measurement. The image sensor achieved wider modulation frequency range with wide dynamic range than previous works.

Chapter 4: active optical sensing system using the image sensor with selective-signal detection and background light suppression is proposed. Basic pixel circuit using current mirror with background light compensation is proposed toward high-resolution applications under strong background light. Two types of current-duplication-error-reduced pixel circuit are proposed further. The signal to background light ratio (SBR) of dummy-added type and V_B-separated type are -38.8 dB and -30.7 dB respectively with dynamic range 94.6 dB and 92.4 dB in the measurement. The number of transistors in a pixel of dummy-added type and V_B-separated type are 19 and 15 respectively. All type of pixel circuits achieved better SBR and DR with less the number of transistors in a pixel circuit than previous works.

Chapter 5: A new active sensing scheme, which is based on the coded light and the image sensor that can detect selective-signal, has been proposed. The bit conversion in generating the coded light is employed to avoid the increase of the integration time. The evaluations are performed in the measurement system based on the image sensor introduced in Chapter 3. And it is confirmed that the new active sensing scheme is worked on the measurement system with the SNR 2.5 dB. However, the SNR of signal-selectivity decreases by 57.6% from case with modulated light. It is confirmed that the affect to an image sensor from the coded light

is similar to the case using higher modulation frequency than base modulation frequency that is used to generate the coded light.

As can be seen from the above results, the image sensors and active optical sensing schemes with modulated light and coded light realize higher modulation frequency range, wide dynamic range toward robust active optical sensing. Chapter 1 and Chapter 2 illustrates the active optical sensing environment with the attacker under strong background light. The incident light into the image sensor consists of the reflected light from the object, disguised light from the attacker, and strong background light from the measurement environment.The active sensing scheme needs the only the reflected light from the object, and avoids the disguised light and background light from the incident light into the an image sensor. Against the strong background light, in Chapter 3 and Chapter 4, the image sensors with demodulation pixel and background light suppression circuit in its pixel are proposed and evaluated for wide dynamic range with the fixed sampling frequency. Against the disguised light, in Chapter 3 and Chapter 4, the proposed images sensors are evaluated with selective-signal detection based on modulated light and the fixed sampling frequency. It showed that the overcoming against the disguised light modulated with the fixed frequency is performed based on sampling with the different frequency to modulated light. In Chapter 5, the proposed active sensing scheme are evaluated with selective-signal detection based on coded light and coded sampling with the image sensor of Chapter 3. It showed that the overcoming against the disguised light modulated with the fixed frequency is performed based on coded sampling with the coded light.

We are sure that these results in this thesis, such as two type of image sensors and active op-

tical sensing with modulated light and coded light, can be used for the instrumental security, and contribute to the active optical sensing performance and reliability improvements.

Bibliography

[1] I. Daftardar, "How does the cruise control system in cars work?," *www.scienceabc.com*.

[2] M. Gupta, Q. Yin, and S. . K. . Nayar, "Structured Light in Sunlight," in *Computer Vision (ICCV), 2013 IEEE International Conference on*, pp. 545–552, 2013.

[3] H. Nohira, Y. Iwata, N. Yoshida, D. Fujimoto, and T. Matsumoto, "Consideration on Instrumentation Security of Stereo Vision Camera," *Symposium on Cryptography and Information Security*, Jan. 2018.

[4] J. Petit, B. Stottelaar, M. Feiri, and F. Kargl, "Remote attacks on automated vehicles sensors: Experiments on camera and lidar," *Black Hat Europe*, 2015.

[5] S. Sakurazawa, D. Fujimoto, and T. Matsumoto, "A Method for Evaluating Instrumentation Security of ToF Depth-Image Camera," *Symposium on Cryptography and Information Security*, pp. 1–8, Jan. 2018.

[6] C. Yan, W. Xu, and J. Liu, "Can you trust autonomous vehicles: Contactless attacks against sensors of self-driving vehicle," *co.tt*, 2016.

[7] H. Shin, D. Kim, Y. Kwon, and Y. Kim, "Illusion and Dazzle: Adversarial Optical Channel Exploits Against Lidars for Automotive Applications," in *Cryptographic Hardware*

and Embedded Systems – CHES 2017, pp. 445–467, Cham: Springer International Publishing, Aug. 2017.

[8] S. Sakurazawa, D. Fujimoto, and T. Matsumoto, "Demonstrating Pulse-Light Spoofing for a ToF Depth-Image Camera," *Symposium on Cryptography and Information Security*, pp. 1–7, Jan. 2017.

[9] S. Mandai, "3-D Range-Finding Image Sensor based on Triangulation and Time-of-Flight," *master thesis*, pp. 1–82, Feb. 2010.

[10] B. Jahne, H. Haußecker, and P. Geißler, *Handbook of Computer Vision and Applications, Volume 1*. Academic Press, May 1999.

[11] J. Cho, J. Choi, S.-J. Kim, S. Park, J. Shin, J. D. . K. . Kim, and E. Yoon, "A 3-D Camera With Adaptable Background Light Suppression Using Pixel-Binning and Super-Resolution," *IEEE Journal of Solid-State Circuits*, vol. 49, pp. 2319–2332, Oct. 2014.

[12] S. Ando and A. Kimachi, "Correlation image sensor: two-dimensional matched detection of amplitude-modulated light," *IEEE Transactions on Electron Devices*, vol. 50, pp. 2059–2066, Oct. 2003.

[13] U. KIM and M. Ikeda, "A 64×64 image sensor with the capability of selective light detection and background suppression," in *2017 IEEE SENSORS*, IEEE.

[14] Y. Oike, M. Ikeda, and K. Asada, "A 120 x 110 Position Sensor With the Capability of Sensitive and Selective Light Detection in Wide Dynamic Range for Robust Active Range Finding," *IEEE Journal of Solid-State Circuits*, vol. 39, pp. 246–251, Jan. 2004.

[15] W. Latimer, "3D Machine Vision Using Laser Triangulation," *www.techbriefs.com*.

[16] L. Marcu, P. M. W. French, and D. S. Elson, *Fluorescence Lifetime Spectroscopy and Imaging*. Principles and Applications in Biomedical Diagnostics, CRC Press, July 2014.

[17] M. Y. Berezin and S. Achilefu, "Fluorescence Lifetime Measurements and Biological Imaging," *Chemical Reviews*, vol. 110, pp. 2641–2684, May 2010.

[18] F. Menna, F. Remondino, R. Battisti, and E. Nocerino, "Geometric investigation of a gaming active device," in *Proceedings of the SPIE* (F. Remondino and M. R. Shortis, eds.), p. 80850G, Fondazione Bruno Kessler, Italy, SPIE, July 2011.

[19] K. Khoshelham and S. O. Elberink, "Accuracy and Resolution of Kinect Depth Data for Indoor Mapping Applications," *Sensors*, vol. 12, pp. 1437–1454, Feb. 2012.

[20] E. Özbay and A. Çinar, "A voxelize structured refinement method for registration of point clouds from Kinect sensors," *Engineering Science and Technology, an International Journal*, Oct. 2018.

[21] S. Kleinfelder, S. Lim, X. Liu, and A. El Gamal, "A 10000 frames/s CMOS digital pixel sensor," *IEEE Journal of Solid-State Circuits*, vol. 36, no. 12, pp. 2049–2059, 2001.

[22] J. Choi, S.-W. Han, S.-J. Kim, S.-I. Chang, and E. Yoon, "A Spatial-Temporal Multiresolution CMOS Image Sensor With Adaptive Frame Rates for Tracking the Moving

Objects in Region-of-Interest and Suppressing Motion Blur," *IEEE Journal of Solid-State Circuits*, vol. 42, pp. 2978–2989, Nov. 2007.

[23] M. Furuta, Y. Nishikawa, T. Inoue, and S. Kawahito, "A High-Speed, High-Sensitivity Digital CMOS Image Sensor With a Global Shutter and 12-bit Column-Parallel Cyclic A/D Converters," *IEEE Journal of Solid-State Circuits*, vol. 42, pp. 766–774, Mar. 2007.

[24] A. I. Krymski and N. Tu, "A 9-V/Lux-s 5000-frames/s 512 x 512 CMOS sensor," *IEEE Transactions on Electron Devices*, vol. 50, pp. 136–143, Jan. 2003.

[25] C. Shi, J. Yang, Y. Han, Z. Cao, Q. Qin, L. Liu, N.-J. Wu, and Z. Wang, "A 1000 fps Vision Chip Based on a Dynamically Reconfigurable Hybrid Architecture Comprising a PE Array Processor and Self-Organizing Map Neural Network," *IEEE Journal of Solid-State Circuits*, vol. 49, pp. 2067–2082, Aug. 2014.

[26] C. S. . Bamji, S. Mehta, B. Thompson, T. Elkhatib, S. Wurster, O. Akkaya, A. Payne, J. Godbaz, M. Fenton, V. Rajasekaran, L. Prather, S. Nagaraja, V. Mogallapu, D. Snow, R. McCauley, M. Mukadam, I. Agi, S. McCarthy, Z. Xu, T. Perry, W. Qian, V.-H. Chan, P. Adepu, G. Ali, M. Ahmed, A. Mukherjee, S. Nayak, D. Gampell, S. Acharya, L. Kordus, and P. O'Connor, "1Mpixel 65nm BSI 320MHz demodulated TOF Image sensor with 3μm global shutter pixels and analog binning," in *2018 IEEE International Solid-State Circuits Conference (ISSCC)*, pp. 94–96, IEEE, Mar. 2018.

[27] S. Kurtti, J. Nissinen, and J. Kostamovaara, "A Wide Dynamic Range CMOS Laser Radar Receiver With a Time-Domain Walk Error Compensation Scheme," *IEEE Transactions on Circuits and Systems I: Regular Papers*, vol. 64, no. 3, pp. 550–561.

[28] H. Zheng, R. Ma, M. Liu, and Z. Zhu, "High Sensitivity and Wide Dynamic Range Analog Front-End Circuits for Pulsed TOF 4-D Imaging LADAR Receiver," *Sensors Journal*, vol. 18, pp. 3114–3124, Mar. 2018.

[29] Y. Nakazawa, M. Nakano, J. Shiozaki, T. Kubota, M. Shirahata, T. Huzino, K. Sugawara, D. Suzuki, and N. Kobayashi, "車載距離センサに対するセキュリティ評価 (in Japanese）," in *SCIS*, pp. 4F1–1, 2016.

[30] R. G. Dutta, X. Guo, T. Zhang, K. A. Kwiat, C. A. Kamhoua, L. Njilla, and Y. Jin, "Estimation of Safe Sensor Measurements of Autonomous System Under Attack.," *DAC*, 2017.

[31] P. Guo, H. Kim, N. Virani, J. Xu, M. Zhu, and P. Liu, "RoboADS: Anomaly Detection Against Sensor and Actuator Misbehaviors in Mobile Robots," in *2018 48th Annual IEEE/IFIP International Conference on Dependable Systems and Networks (DSN)*, pp. 574–585, IEEE.

[32] K. Ambrosch, W. Kubinger, M. Humenberger, and A. Steininger, "Hardware implementation of an SAD based stereo vision algorithm.," *CVPR*, pp. 1–6, 2007.

[33] M. Hariyama, K. Tanji, and M. Kameyama, "FPGA Implementation of a High-Speed Stereo Matching Processor Based on Recursive Computation.," *ERSA*, 2009.

[34] K. Ambrosch and W. Kubinger, "Accurate hardware-based stereo vision ," *Computer Vision and Image Understanding*, vol. 114, pp. 1303–1316, Nov. 2010.

[35] S. Hiura and T. Matsuyama, "Depth measurement by the multi-focus camera," in *Proceedings. 1998 IEEE Computer Society Conference on Computer Vision and Pattern Recognition (Cat. No.98CB36231)*, pp. 953–959, IEEE Comput. Soc.

[36] Y. Takeda, S. Hiura, and K. Sato, "Fusing Depth from Defocus and Stereo with Coded Apertures," in *2013 IEEE Conference on Computer Vision and Pattern Recognition (CVPR)*, pp. 209–216, IEEE.

[37] K. Kim, Y. Lee, H. S. Park, and C.-M. Kyung, "Depth extraction using adaptive blur channel selection for dual aperture camera.," *APCCAS*, pp. 198–201, 2016.

[38] E. Zimmermann, Y. Salvadé, and R. Dändliker, "Stabilized three-wavelength source calibrated by electronic means for high-accuracy absolute distance measurement," *Optics Letters*, vol. 21, pp. 531–533, Apr. 1996.

[39] S. Le Floch, Y. Salvadé, R. Mitouassiwou, and P. Favre, "Radio frequency controlled synthetic wavelength sweep for absolute distance measurement by optical interferometry," *Applied Optics IP*, vol. 47, pp. 3027–3031, May 2008.

[40] Y. Kuramoto and H. Okuda, "High-accuracy absolute distance measurement by two-wavelength double heterodyne interferometry with variable synthetic wavelengths," *International Workshop on Future Linear Colliders LCWS*, Feb. 2014.

[41] W. Gao, S. W. Kim, H. Bosse, H. Haitjema, Y. L. Chen, X. D. Lu, W. Knapp, A. Weckenmann, W. T. Estler, and H. Kunzmann, "Measurement technologies for precision positioning," *CIRP Annals*, vol. 64, pp. 773–796, Jan. 2015.

[42] S. Wei, X. Zhang, and X. Tang, "Bistatic forward-looking SAR interferometry," in *2016 IEEE International Geoscience and Remote Sensing Symposium (IGARSS)*, pp. 6488–6491, IEEE, 2016.

[43] L.-w. Xu, H. Chen, X.-m. Zhang, and X.-m. Wang, "Inter-source passive body-wave interferometry by multidimensional deconvolution (MDD)," in *2016 Symposium on Piezoelectricity, Acoustic Waves, and Device Applications (SPAWDA)*, pp. 349–353, IEEE, 2016.

[44] A. Budillon, M. Crosetto, G. Ferraioli, A. C. Johnsy, O. Monserrat, and G. Schirinzi, "Scatterer detection in urban environment using persistent scatterer interferometry and SAR tomography.," *IGARSS*, 2017.

[45] C. Pernechele, D. Fantinel, D. Magrin, L. Lessio, and G. Rodeghiero, "Low coherence interferometry-based meter-distance range finder," in *2017 IEEE International Workshop on Metrology for AeroSpace (MetroAeroSpace)*, pp. 126–130, IEEE, 2017.

[46] D. Stoppa, N. Massari, L. Pancheri, M. Malfatti, M. Perenzoni, and L. Gonzo, "A Range Image Sensor Based on 10-um Lock-In Pixels in 0.18-um CMOS Imaging Technology," *IEEE Journal of Solid-State Circuits*, vol. 46, pp. 248–258, Dec. 2010.

[47] E. Charbon, "Introduction to time-of-flight imaging," in *IEEE SENSORS 2014 Proceedings*, pp. 610–613, IEEE, 2014.

[48] G. Zach, M. Davidovic, and H. Zimmermann, "A 16 x 16 Pixel Distance Sensor With In-Pixel Circuitry That Tolerates 150 klx of Ambient Light," *IEEE Journal of Solid-State Circuits*, vol. 45, pp. 1345–1353, July 2010.

[49] O. Sgrott, D. Mosconi, M. Perenzoni, G. Pedretti, L. Gonzo, and D. Stoppa, "A 134-Pixel CMOS Sensor for Combined Time-of-Flight and Optical Triangulation 3-D Imaging," *IEEE Journal of Solid-State Circuits*, vol. 45, pp. 1354–1364, June 2010.

[50] S. Chan, R. E. Warburton, G. Gariepy, Y. Altmann, S. McLaughlin, J. Leach, and D. Faccio, "Fast tracking of hidden objects with single-pixel detectors," *Electronics Letters*, vol. 53, pp. 1005–1008, July 2017.

[51] M. Beer, B. J. . Hosticka, O. M. Schrey, W. Brockherde, and R. Kokozinski, "Range accuracy of SPAD-based time-of-flight sensors.," *ECCTD*, pp. 1–4, 2017.

[52] Y. Oike, M. Ikeda, and K. Asada, "Design and implementation of real-time 3-D image sensor with 640×480 pixel resolution," *Solid-State Circuits, IEEE Journal of*, vol. 39, no. 4, pp. 622–628, 2004.

[53] J. Im, H. Fujii, A. Yamashita, and H. Asama, "Multi-modal diagnostic method for detection of concrete crack direction using light-section method and hammering test.," *URAI*, pp. 922–927, 2017.

[54] L. Lindgren, J. Melander, R. Johansson, and B. Moller, "A multiresolution 100-GOPS 4-Gpixels/s programmable smart vision sensor for multisense imaging," *IEEE Journal of Solid-State Circuits*, vol. 40, pp. 1350–1359, June 2005.

[55] S. Mandai, M. Ikeda, and K. Asada, "A 256×256 14k range maps/s 3-D range-finding image sensor using row-parallel embedded binary," in *2010 IEEE International Solid-State Circuits Conference - (ISSCC)*, pp. 404–405, IEEE, 2010.

[56] Y. Oike, M. Ikeda, and K. Asada, "640 × 480 Real-time range finder using high-speed readout scheme and column-parallel position detector," in *2003 Symposium on VLSI Circuits. Digest of Technical Papers (IEEE Cat. No.03CH37408)*, pp. 153–156, Japan Soc. Appl. Phys, 2003.

[57] Y. Oike, M. Ikeda, and K. Asada, "A 375×365 high-speed 3-D range-finding image sensor using row-parallel search architecture and multisampling technique," *IEEE Journal of Solid-State Circuits*, vol. 40, pp. 444–453, Jan. 2005.

[58] Y. Oike, H. Shintaku, S. Takayama, M. Ikeda, and K. Asada, "Real-time and high-resolution 3-D imaging system using light-section method and smart cmos sensor," in *Proceedings of IEEE Sensors 2003 (IEEE Cat. No.03CH37498)*, pp. 502–507, IEEE, 2003.

[59] Leica, "Topographic LiDAR Sensors SPL100," *www.leica-geosystems.com*.

[60] K. MINOLTA, "3D-LiDAR," *www.konicaminolta.com*.

[61] J. Ohta, K. Yamamoto, T. Hirai, K. Kagawa, M. . Nunoshita, M. Yamada, Y. Yamasaki, S. Sugishita, and K. . Watanabe, "An image sensor with an in-pixel demodulation function for detecting the intensity of a modulated light signal," *IEEE Transactions on Electron Devices*, vol. 50, pp. 166–172, Jan. 2003.

[62] M. F. Mushtaq, S. Jamel, A. H. Disina, Z. A. Pindar, N. S. A. Shakir, and M. M. Deris, "A Survey on the Cryptographic Encryption Algorithms," *International Journal of Advanced Computer Science and Applications (ijacsa)*, vol. 8, no. 11, 2017.

[63] D. D. Padilla, P. A. Davidson Jr, J. J. Carlson, and D. K. Novick, "Advancements in Sensing and Perception using Structured Lighting Techniques: An LDRD Final Report," *prod.sandia.gov*, 2005.

[64] J. Shin, B. Kang, K. Lee, and J. D. . K. . Kim, "A 3D image sensor with adaptable charge subtraction scheme for background light suppression," *Sensors*, vol. 8659, p. 865907, Feb. 2013.

[65] M. Perenzoni, N. Massari, D. Stoppa, L. Pancheri, M. Malfatti, and L. Gonzo, "A 160x120-Pixels Range Camera With In-Pixel Correlated Double Sampling and Fixed-Pattern Noise Correction," *IEEE Journal of Solid-State Circuits*, vol. 46, pp. 1672–1681, June 2011.

[66] T. Oggier, R. Kaufmann, M. Lehmann, B. Buttgen, S. Neukom, M. Richter, M. Schweizer, P. Metzler, F. Lustenberger, and N. Blanc, "Novel pixel architecture with inherent background suppression for 3D time-of-flight imaging," in *Proceedings of the SPIE*, pp. 1–8, Ctr. Suisse d'Electronique et de Microtechnique SA, Switzerland, Jan. 2005.

[67] G. Zach and H. Zimmermann, "A 2x32 range-finding sensor array with pixel-inherent suppression of ambient light up to 120klx," in *2009 IEEE International Solid-State Circuits Conference (ISSCC 2009)*, pp. 352–353,353a, IEEE.

[68] M. Davidovic, G. Zach, K. Schneider-Hornstein, and H. Zimmermann, "Range finding sensor in 90nm CMOS with bridge correlator based background light suppression," in *ESSCIRC, 2010 Proceedings of the*, pp. 298–301, IEEE, 2010.

[69] T. Ringbeck, T. Möller, and B. Hagebeuker, "Multidimensional measurement by using 3-D PMD sensors," *Advances in Radio Science*, 2007.

[70] S.-M. Han, T. Takasawa, K. Yasutomi, S. Aoyama, K. Kagawa, and S. Kawahito, "A Time-of-Flight Range Image Sensor With Background Canceling Lock-in Pixels Based on Lateral Electric Field Charge Modulation," *IEEE J. Electron Devices Soc.*, vol. 3, no. 3, pp. 267–275, 2015.

[71] A. Payne, A. Daniel, A. Mehta, B. Thompson, C. S. . Bamji, D. Snow, H. Oshima, L. Prather, M. Fenton, L. Kordus, P. O' 'Connor, R. McCauley, S. Nayak, S. Acharya, S. Mehta, T. Elkhatib, T. Meyer, T. O' 'Dwyer, T. Perry, V.-H. Chan, V. Wong, V. Mogallapu, W. Qian, and Z. Xu, "A 512x424 CMOS 3D Time-of-Flight image sensor with multi-frequency photo-demodulation up to 130MHz and 2GS/s ADC," in *2014 IEEE International Solid- State Circuits Conference (ISSCC)*, pp. 134–135, IEEE, Feb. 2014.

[72] C. Niclass and et al, "A 100-m Range 10-Frame/s 340 96-Pixel Time-of-Flight Depth Sensor in 0.18- CMOS," *Solid-State Circuits, IEEE Journal of*, vol. 48, no. 2, pp. 559–572, 2013.

[73] B. Büttgen and P. Seitz, "Robust Optical Time-of-Flight Range Imaging Based on Smart Pixel Structures," *IEEE Transactions on Circuits and Systems I: Regular Papers*, vol. 55, no. 6, pp. 1512–1525, 2008.

[74] Y. M. Wang, I. Ovsiannikov, S. J. Byun, and T. Y. Lee, "Compact ambient light cancellation design and optimization for 3D time-of-flight image sensors," *Proc Int Image ...*, 2013.

[75] M. Habibi and S. M. Sayedi, "An electronic marker tag detection smart camera for object localization," *Microelectronics (ICM)*, pp. 374–377, 2009.

[76] M. Habibi, "A high sensitivity correlation image sensor," in *Sensors Applications Symposium (SAS), 2011 IEEE*, pp. 197–202, IEEE, 2011.

[77] M. Habibi, "Analysis, enhancement, and sensitivity improvement of the correlation image sensor," *IEEE Transactions on Instrumentation and . . .*, 2012.

[78] S. Ando, T. Nara, N. Ono, and T. Kurihara, "Real-Time Orientation-Sensitive Magnetooptic Imager for Leakage Flux Inspection," *IEEE Transactions on Magnetics*, vol. 43, pp. 1044–1051, Mar. 2007.

[79] T. Spirig, P. Seitz, O. Vietze, and F. Heitger, "The lock-in CCD-two-dimensional synchronous detection of light," *IEEE Journal of Quantum Electronics*, vol. 31, no. 9, pp. 1705–1708, 1995.

[80] K. Yamamoto, Y. Oya, K. Kagawa, M. Nunoshita, J. Ohta, and K. Watanabe, "A 128 x 128 Pixel Complementary Metal Oxide Semiconductor Image Sensor with an Improved Pixel Architecture for Detecting Modulated Light Signals," *Optical Review*, vol. 13, no. 2, pp. 64–68, 2006.

[81] J. Cheon, Y. Chae, D. Kim, S. Lim, I. Lee, H.-K. Lee, D. J. Kim, and G. Han, "Smart CMOS Image Sensor With High SBR and Subpixel Resolution for Light-Section-Based Range Finding," *IEEE Transactions on Electron Devices*, vol. 56, pp. 2546–2555, Oct. 2009.

[82] S. Vappangi and V. Mani, "Concurrent illumination and communication: A survey on Visible Light Communication," *Physical Communication*, vol. 33, pp. 90 – 114, 2019.

[83] T.-H. Do and M. Yoo, "Visible Light Communication based Vehicle-to-Vehicle Tracking using CMOS Camera," *IEEE Access*, 2019.

[84] T. Yamazato, I. Takai, H. Okada, T. Fujii, T. Yendo, S. Arai, M. Andoh, T. Harada, K. Yasutomi, K. Kagawa, and S. Kawahito, "Image-sensor-based visible light communication for automotive applications," *IEEE Communications Magazine*, vol. 52, no. 7, pp. 88–97, 2014.

[85] I. Takai, T. Harada, M. Andoh, K. Yasutomi, K. Kagawa, and S. Kawahito, "Optical Vehicle-to-Vehicle Communication System Using LED Transmitter and Camera Receiver," *IEEE Photonics Journal*, vol. 6, no. 5, pp. 1–14, 2014.

[86] M. Novak, O. Wilfert, and T. Simicek, "Visible light communication beacon system for internet of things," in *2017 Conference on Microwave Techniques (COMITE*, 2017.

[87] U. KIM and M. Ikeda, "An Image Sensor with In-pixel Selective-Charge-Subtraction Circuits for Selective Light Detection," 2019.

[88] M. Montilla, S. A. Orjuela-Vargas, and W. Philips, "State of the art of 3D scanning systems and inspection of textile surfaces," in *Proceedings of the SPIE*, p. 90180A, Univ. Antonio Nariño (Colombia), Feb. 2014.

[89] J. Geng, "Structured-light 3D surface imaging: a tutorial," *Advances in Optics and Photonics*, vol. 3, pp. 128–, June 2011.

[90] S. Malassiotis and M. G. Strintzis, "Stereo vision system for precision dimensional inspection of 3D holes," *Machine Vision and Applications*, vol. 15, pp. 101–113, Dec. 2003.

[91] P. Bergström, M. Fergusson, P. Folkesson, A. Runnemalm, M. Ottosson, A. Andersson, and M. Sjödahl, "Automatic in-line inspection of shape based on photogrammetry," 2016.

[92] X. Wen, K. Song, M. Niu, Z. Dong, and Y. Yan, "3D inspection technology combining passive stereo matching and active structured light for steel plate surface sample," *International Journal of Surface Science and Engineering*, vol. 11, no. 4, p. 299, 2017.

[93] R. Forster, "Manchester encoding: opposing definitions resolved," *Engineering Science & Education Journal*, vol. 9, no. 6, pp. 278–280, 2000.

List of Publications

Journal Papers

1. U. Kim and M. Ikeda, "An Image Sensor with In-pixel Selective-Charge-Subtraction Circuits for Selective Light Detection," *IEICE Electronic Express*, 2019.

2. U. Kim and M. Ikeda, "An image sensor with in-pixel current-mode subtraction for selective light detection," *IEICE Electronic Express*, 2019. (summited)

International Conference Papers

1. U. Kim and M. Ikeda, "A Design of Image Sensor for In-pixel Background Suppression and Frequency Detection," in *3rd International Workshop on Image Sensors and imaging Systems (IWISS2016)*, Nov. 2016.

2. U. Kim and M. Ikeda, "A 64 × 64 image sensor with the capability of selective light detection and background suppression," in *Proceedings of the IEEE Sensors Conference*, Nov. 2017.

3. U. Kim and M. Ikeda, "A study on pixel circuit with compensation of background light using current mirror," in *Proceedings of the IEEE Sensors Conference*, Nov. 2018.

4. U. Kim and M. Ikeda, "Active optical sensing with randomized coded light for intentional interference tolerance," in *Proceedings of International Image Sensor Workshop*, Jun. 2019.

Domestic Conference Papers

1. U. Kim and M. Ikeda, “ピクセル内背景光抑圧機能を有する検波型イメージセンサの設計,” in *Proceedings of IEICE Society Conference*, C-12-14, Sep. 2016. (*in Japanese*)

2. U. Kim and M. Ikeda, “背景光補償型画素回路の検討,” 映像情報メディア学会, pp.31-34, Sep. 2017. (*in Japanese*)

3. U. Kim and M. Ikeda, “A Study on Pixel Circuit with Duplication Circuit of Background Light,” in *Workshop of LSI and System*, 2018 (*Poster*).